# FURTHER DEVELOPMENT OF THE MINIATURIZED DISK BEND TEST APPROACH FOR POST-IRRADIATION MECHANICAL PROPERTY TESTING

by

DONG-SEONG SOHN

B.S., SEOUL NATIONAL UNIVERSITY
(1974)

M.S., KOREA ADVANCED INSTITUTE OF SCIENCE AND TECHNOLOGY
(1977)

SUBMITTED TO THE DEPARTMENT OF NUCLEAR ENGINEERING IN PARTIAL FULFILLMENT OF THE REQUIREMENTS FOR THE DEGREE OF

DOCTOR OF PHILOSOPHY

at the

MASSACHUSETTS INSTITUTE OF TECHNOLOGY

AUGUST 1984



Signature of Author Signature redacted
Department of NUCLEAR ENGINEERING
AUGUST , 1984

Certified by Signature redacted
Otto K. Harling
Thesis Supervisor

Accepted by Signature redacted
Alan F. Henry
Chairman, Departmental Committee on Graduate Students

# FURTHER DEVELOPMENT OF THE MINIATURIZED DISK BEND TEST APPROACH FOR POST-IRRADIATION MECHANICAL PROPERTY TESTING

by

DONG-SEONG SOHN

Submitted to the Department of NUCLEAR ENGINEERING on AUGUST , 1984 in partial fulfillment of the requirements for the degree of DOCTOR OF PHILOSOPHY.

ABSTRACT

The major objectives of this research are;

1. to develop analysis methods in order to extract post-irradiation tensile properties
2. to verify these analysis methods by applying these to various alloys of known mechanical properties
3. to explore the possibility of measuring changes in ductile-brittle transition temperature after irradiation using the MDBT approach.

The load at the deviation point from linearity in the MDBT load/deflection curve (defined as the yield load (YL)) is correlated with the yield strength (YS) of the material. An iterative method, using the results of computer analysis of the MDBT by a finite element computer code ABAQUS, was developed for the estimation of YS. A simple analytic expression was used to calculate the ductility of brittle specimens from the deflection at maximum load in the load/deflection curve. The MDBT analysis methods developed for YS and ductility in this research were successfully applied to the analysis of test data for several kinds of modified type 316 stainless steel (SS) irradiated to doses up to 34 dpa.

In reference tests to verify the analysis methods, the YS and ductility measured by the MDBT method showed good agreement with the reference values measured in conventional uniaxial tests. The effect of different plastic behavior on the specimen load/deflection response in the initial linear region was found to be insignificant. A set of computer analysis results, which is sufficient for the estimation of YS from measured YL for any material whose measured YL and elastic modulus are between approximately 42 to 14 N and 200 to 80 GPa, respectively, was produced. These computer generated results are shown in Fig. 4.3. This can be applied to the testing of other irradiated materials.

MDBT tests using impact loading have been shown to have potential for measuring changes in ductile-brittle transition temperature (DBTT). Dramatic changes in the characteristic load/deflection curve are used as an indicator in such tests. Further work is necessary to minimize and characterize the DBTT shift with respect to full sized specimens.

The MIT MDBT method with the association of the analysis methods developed in this thesis has shown its capability to measure tensile properties. Also the potential of the MDBT method to measure changes in the DBTT has been shown.

Thesis Supervisor: Dr. Otto K. Harling
Title: Professor of Nuclear Engineering

ACKNOWDGEMENT

I gratefully acknowledge the advice, encouragement and patience of my advisor, Professor O. K. Harling. I would also like to express special thanks to my thesis reader, Professor N. J. Grant and to Professor D. M. Parks for their advice and guidance.

Doctors G. Kohse and M. Lee were both generous in consulting and advising at many stages of the work. Doctors S. H. Kang and E. Y. Ting and Mr. E. J. Lavernia provided valuable samples. Dr. C. W. Lau was most helpful during my introduction to the computer code ABAQUS. Mr. M. Richardson of the Instron company helped me in the analysis of noise in the feedback signals.

All the staff at the Nuclear Reactor Laboratory were helpful and friendly. I extend my gratitude to all of them. J. Bernard, W. Woodworth, G. Pollard and M. Anderson deserve particular mention.

I am grateful to the US DOE for their sponsorship of this research (Contract number DE-AC02-78ER-10107).

I would like to express gratitude to my loving wife, Young-Mee, for her constant patience, support and encouragement. Finally, I would like to express great thanks to my parents, Moon-Joon and Jung-Ryun Sohn, for their support through unending prayer and encouragement.

TABLE OF CONTENTS

## LIST OF FIGURES

## LIST OF TABLES

# CHAPTER 1 INTRODUCTION

## 1.1 Objective and Scope

Development of materials for use under intense irradiation environment requires that many candidate materials be tested after irradiation in various facilities. Conventional test specimens are bulky and sometimes prohibitive for irradiation testing considering the number of candidate materials and the irradiation space. Reduction of the required irradiation space by the use of miniaturized test specimen and by the standardization of specimen size would be very beneficial for the efficient use of the limited and costly irradiation space. To this end, a simply supported bend test for disk shaped specimens no larger than those used for transmission electron microscopy (TEM), 3 mm diameter X 0.25 mm thick, is being developed in this work. In the developmental process as reported in references 1.1 through 1.7, the MIT miniaturized disk bend test (MDBT) method has shown promise for obtaining mechanical properties, including tensile, ductile - brittle transition and fatigue properties. The specimen used in the MIT MDBT is 20 to 500 times smaller in volume than most of the more conventional uniaxial tensile specimens currently being used for irradiation testing. The damage gradient over the irradiated specimen which is possible in some conventional specimens as discussed in reference 1.8 can be avoided by the use of a miniaturized specimen. Also, MDBT specimens can be used directly for TEM examination.

The primary objective of this research was to develop the analysis

methods to extract post-irradiation tensile properties such as yield strength and ductility from the MDBT data. A secondary objective of this research was to find possible methods to measure the change of the ductile - brittle transition temperature after irradiation by the use of the MIT MDBT approach. In order to achieve the research objectives the following subtasks have been accomplished:

1. study the specimen behavior during the test and find possible parameters that can be correlated with the tensile properties of the material.

2. develop analysis methods to extract tensile properties from these parameters.

3. verify the analysis methods by applying these to the tests of specimen disks with known material properties.

4. apply the methods to irradiation testing of various alloys and fine tune the methods if necessary.

5. perform impact tests using the MDBT approach and find possible methods to obtain the ductile - brittle transition properties of the material.

## 1.2 Background

The MIT MDBT system was first developed by Manahan, Argon and Harling and was extensively described in references 1.1 and 1.2. Various kinds of miniaturized specimens and testing methods have been adopted by researchers for irradiation testing. Most of these specimens

are tested so as to approximate the conventional uniaxial testing condition. Two such miniaturized tensile specimens, wire and sheet types, were developed by Panayotou and Opperman as described in reference 1.8. Both types of specimen are approximately 13 mm in overall length with gage section lengths of about 6 mm. The diameter of the wire type specimen's reduced section is 0.25 mm and the sheet specimen's reduced section is 1 mm by 0.25 mm. Two types of sheet tensile specimens with slightly different dimensions have been used in irradiation tests by Grossbeck and Thoms as described in reference 1.9. The smaller specimen, ORNL SS - 2, has a gauge section of 12.7 mm long, 1.02 mm wide and 0.25 mm thick. The larger specimen has a similar shape but somewhat larger dimensions. Test results using these miniaturized specimen were reported to show relatively good agreement with conventional data in most cases. There also have been attempts to adopt bending of a disk specimen in irradiation testing. Huang, Hamilton and Wire in reference 1.10 used TEM specimen size disks in bend testing to determine post-irradiation ductility for screening purposes. Miniature Charpy V - notch (CVN) specimens about one third the size of standard CVN specimens were used in instrumented drop tower impact tests by Hu and Panayotou (reference 1.11). The results of above mentioned miniature tests are reported to have shown good agreement with reference values obtained from conventional standard tests.

The TEM disk specimen is the smallest which has so far being used for mechanical property testing, minimizing both irradiation volume requirements and post-irradition specimen activity. MIT's MDBT method extract tensile properties, and potentially other mechanical properties,

from these specimens. Furthermore, the MIT approach has been distinct from that of other groups in that finite element modeling has been used to extract material properties from the experimental load/deflection curves.

## 1.3 Outline

The work reported herein is organized as follows:

Chapter 2 provides descriptions, characterizations and calibrations of the test equipment used in the MDBT. Also included is a brief description of modifications and improvements to the testing system.

Chapter 3 presents the MDBT analysis methods and a series of reference tests to verify the analysis method. Preliminary results of the development for the ductile - brittle transition test are also descibed.

Chapter 4 describes actual application of the MDBT method to the testing of irradiated developmental alloys. Brief descriptions of the composition, design objectives and processing methods of the materials irradiation tested in this research are also provided.

Chapter 5 presents a brief summary of the thesis along with recommendations for future research.

Appendices present design drawings for added test components and a set of input and output data for the computer analysis of the MDBT using a finite element code ABAQUS.

## References for Chapter 1


1.1 M.P. Manahan, "The Development of A Miniaturized Disk Bend Test For The Determination of Post-Irradiation Mechanical Behavior", Sc.D Thesis, Dept. of Nucl. Eng., MIT, (May, 1982)

1.2 M.P. Manahan, A.S. Argon and O.K. Harling, J. Nucl. Matr., 103 & 104, (1981), pp 1545-1550

1.3 O.K. Harling, M. Lee, D-S Sohn, G. Kohse and C.W. Lau, "The MIT Miniaturized Disk Bend Test", presented at the ASTM Symposium on the Use of Nonstandard Subsized Specimens for Irradiation Testing, Albuquerque, N.M., (Sept. 1983), to be published in an ASTM STP.

1.4 M. Lee, D-S Sohn, N.J. Grant and O.K. Harling, "Minaiturized Disk Bend Tests of Neutron Irradiated Path A Type Alloys", J. Nucl. Matr., 122 & 123, (1984), pp 146-151

1.5 M.P. Manahan and A.S. Argon, "Design of Mechanical Property Tests and Establishment of Associated Testing Systems", MITNRL-006 and DOE/ER-10107-1, (Dec. 1980)

1.6 O.K. Harling, M. Lee, D-S Sohn, G. Kohse and N.J. Grant, "Neutron Irradiated Mechanical Properties of Some Rapidly Solidified Austenitic Stainless Steels", submitted to the Twelfth Symposium on The Effects of Radiation on Materials, Williamsburgh, Va., (Jun. 1984), to be published in an ASTM STP.

1.7 G.E. Kohse, "Ion Bombardment Effects on The Fatigue Life of Stainless Steel under Simulated Fusion First Wall Conditions.", Ph.D. Thesis, Dept. of Nucl. Eng., MIT, (Feb. 1983)

1.8 N.F. Panayotou and E.K. Opperman, "Specimen Size Effect and Fusion Materials Research", DOE/ER-0045/8, pp 25-65

1.9 M.L. Grossbeck and K.R. Thoms, "ORR-MFE-4 : A Spectral Tailoring Experiment to Simulate The He/dpa Ratio of A Fusion Reactor in Austenitic Stainless Steel", DOE/ER-0045/3, pp 10-23

1.10 F.H. Huang, M.L. Hamilton and G.L. Wire, "Bend Testing for Miniature Disks", Nucl. Techn., Vol. 57, (May, 1982), pp 234-242.

1.11 W.L. Hu and N.F. Panayotou, "Miniature Charpy Specimen Test Device Development and Impact Test Results for The Ferritic Alloy HT-9", DOE/ER-0045/7, pp 235-251

# CHAPTER 2 EXPERIMENTAL SYSTEMS AND THEIR DESCRIPTIONS

## 2.1 System Description

In the miniaturized disk bend test (MDBT), a central load is applied by a punch to a specimen disk simply supported by a hollow cylindrical die. This punch and support is connected to the Instron 1331 servo-hydraulic testing machine and is mounted in an environmental chamber. M.P. Manahan and A.S.Argon and O.K.Harling first developed the testing system and it is extensively described in references 1.1 and 1.2. The testing system is installed in a hot cell and is shown in Fig. 2.1.

The testing system uses a load cell designed for low load measurment (0 - 667 N full range). The disk deflection can be measured by a linear variable displacement transformer (LVDT) and/or an extensometer. The test environment is controlled using an environmental chamber. A specimen can be tested at elevated temperature using resistance heating either in inert gas atmosphere or in vacuum. The induction heating method used by Manahan et al has been changed to resistance heating to prevent noise generation from the R.F. generator of the induction heating unit. In high temperature testing the specimen is heated to test temperature, tested and cooled down in a helium atmosphere in order to avoid oxidation of the fracture surface. After being tested at elevated temperatures, disk specimens sometimes clung to the punch and were hard to remove. In order to solve this problem a specimen remover was designed. The design drawing for this specimen remover is presented in

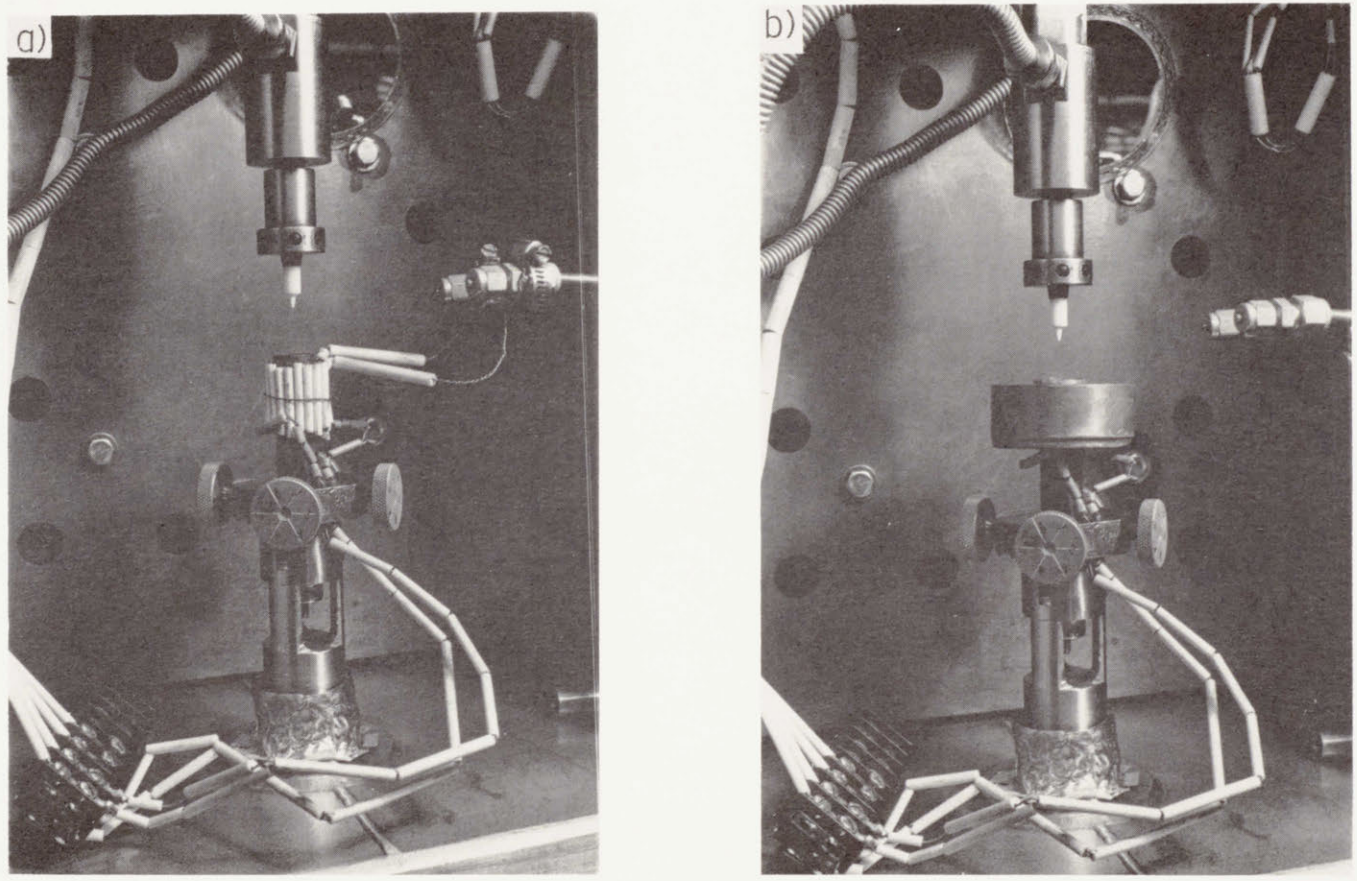


Figure 2.1-1 Miniaturized disk bend test system, showing the load train inside the environmental chamber, a) assembled for high temperature testing and b) assembled for low temperature testing.

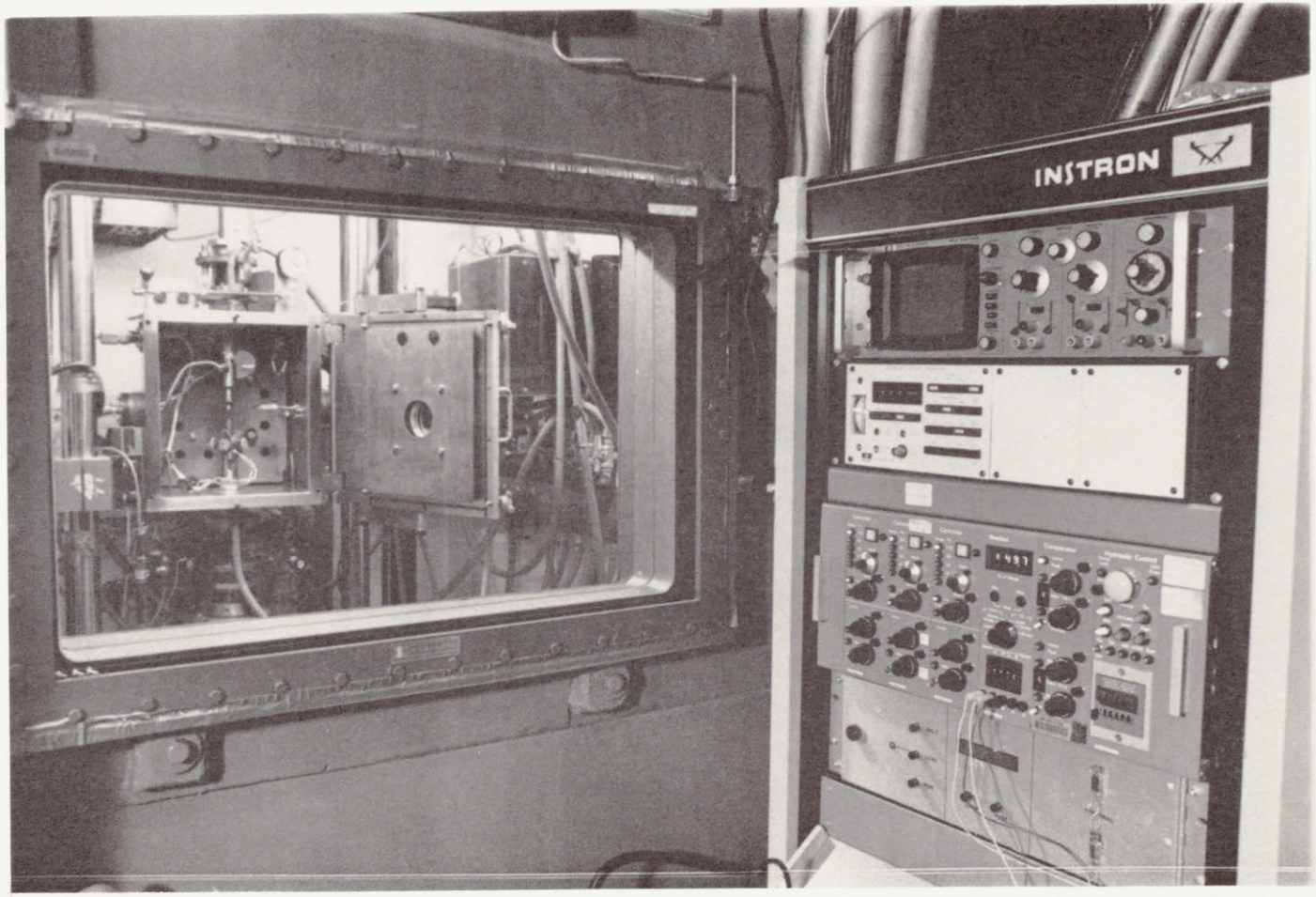


Figure 2.1-2 Miniaturized disk bend test system, showing the hydraulic testing apparatus installed in a hot cell (left) and the electronic control system on the reactor building floor (right).

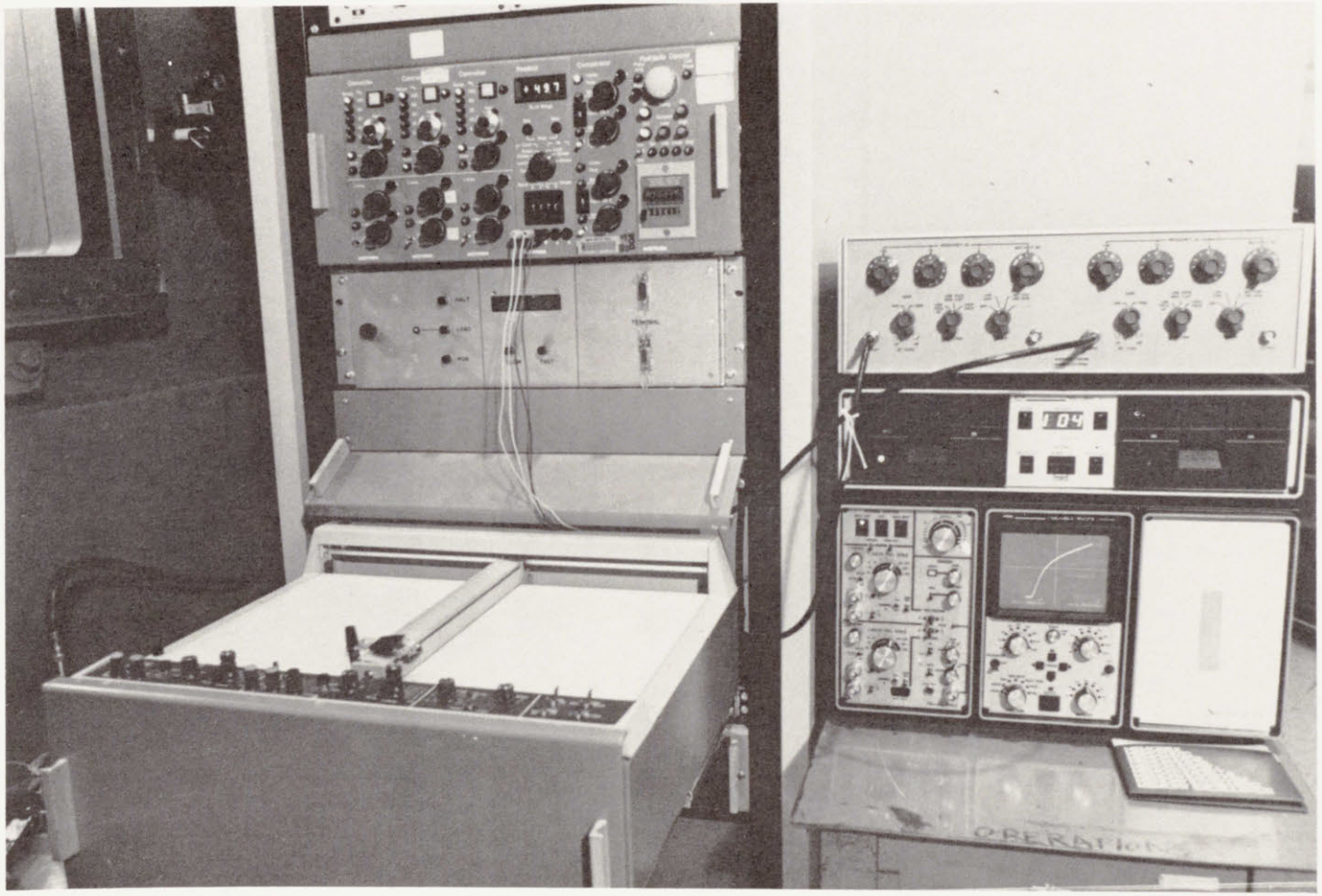

Figure 2.1-3 Miniaturized disk bend test system, showing the Instron controller (left) and the digital data acquisition system consisting of an electronic filter and a Nicolet digital oscilloscope.

Appendix A. As shown in a schematic illustration of the load train in Fig. 2.2, it is installed between the punch and the positioning washer before elevated temperature testing. The major advantage of this design is that it makes it possible to remove the specimen from the punch while the disk is at elevated temperature so that the specimen can be removed with minimal force. This simple design worked quite well and specimen removal after high temperature testing has not caused any trouble. A copper cooling cup and insulating pads were used for low temperature testing. They are installed outside of the upper disk structure as shown in Fig. 2.2. When used with liquid nitrogen, this apparatus can maintain disk specimen temperature as low as 128 K. The design drawing for the cooling cup is presented in Appendix A.

In the analysis of MDBT data, the initial linear region of the load/deflection curve is important. Because the load level in this portion is low (in most cases less than 44 N) noise from various sources is of concern. Noise reduction is also required to make it easier to pinpoint the deviation point from linearity in the load/deflection curve obtained in MDBT. Since the signals from the MDBT - load and deflection - have a frequency distribution in a fairly low range, an electronic filter was used in low pass mode to filter out high frequency noise. The test is single shot in nature and thus its signals are essentially direct current (0 Hz). In order to further facilitate accurate data accumulation, a twelve bit digitizer with 0.02 % full scale resolution along with a magnetic disk recorder and a microprocessor was incorporated for data readout. The introduction of the electronic filter and the digitizer made significant improvements in noise

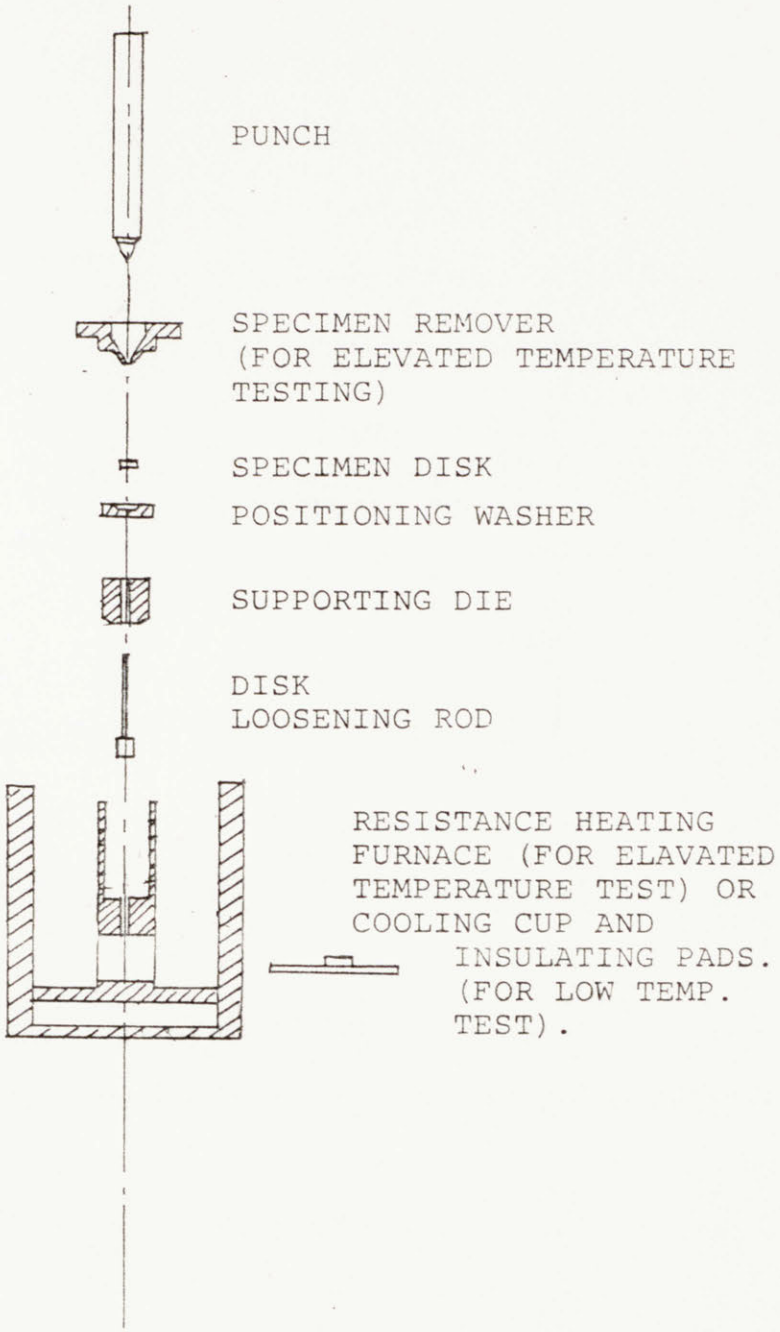


Figure 2.2 Schematic illustration of test components used in the MIT MDBT.

reduction and accurate readout of the data. This will be further discussed in Section 2.3. The filter used is a Kronhite model 3342 dual channel filter with variable cutoff frequency capability. The digitizer system is a Nicolet 4094 digital oscilloscope with 12 bit resolution and 16K word buffer memory. A photograph of the filter and the digital oscilloscope connected to the Instron controller and an X - Y plotter is shown in Fig. 2.1.

## 2.2 System Characterization and Calibration

In the MDBT various gauges, transducers and measuring systems are used to generate test data. In order to assure the proper functioning of the testing system and the precision of test data, it is necessary to characterize and calibrate the system.

2.2.1 Load Cell The load cell used in the MDBT has a full load range of 667 N (150 lb). It was calibrated against an Instron load cell in full load range and using a compression spring and measuring weights in the 0 - 44.5 N range. The Instron load cell in its 5 % range has a full load range of 0 - 2224 N with -0.38 % maximum error. When the MDBT load cell was calibrated against the Instron load cell in the 5 % range, the maximum error in the 0 - 667 N range was 6.7 N. In order to calibrate the load cell in the 0 - 44.5 N range, a compression spring and several weights with better than 0.6 % precision were used. The spring was first calibrated by measuring the spring deflection under a given load applied by a known weight. Spring deflection was measured with a dial gauge of 0.0025 mm (0.0001 in) precision and was quite reproducible

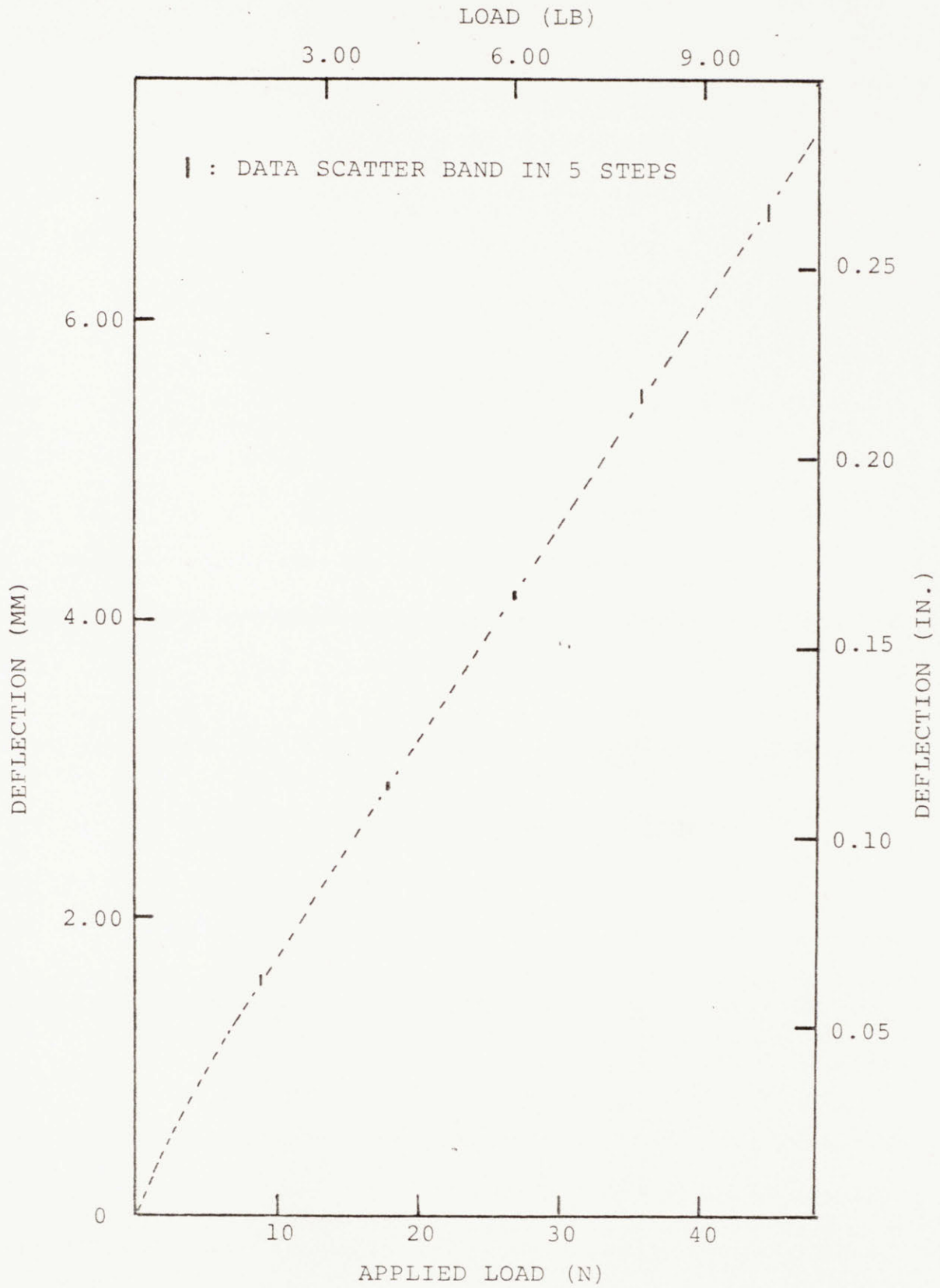


Figure 2.3 Result of compression spring calibration, measuring weight with better than 0.6% precision were used in this calibration.

as shown in Fig. 2.3. Because the deflection was measured at each known load, the only major requirement for the spring in this load cell calibration was reproducibility. The result of five repetative measurements is shown in Fig. 2.3. with the data scatter band indicated. The maximum data scatter was $\pm$ 0.051 mm out of 6.761 mm deflection at 35.6 N load. As one can see from the figure, the spring deflection is linearly proportional to the load except in the very early region. The nonlinearity in the initial region is probably due to the fact that the spring is not quite square. The spring was 25 mm in diameter and top and bottom ends were ground to make the faces flat and perpendicular to the spring axis. Small amount of non-perpendicularity can produce non-linearity (more deflection compared with that in linear region) in the load/deflection response until the spring is seated perpendicularly and the applied load is distributed evenly. As discussed above, non-linearity does not affect the calibration result provided that the same amount of preload is applied in load cell calibration so that the spring is used in the same range in both tests. In the calibration of the MDBT load cell, the spring was installed in the load train and the same amount of preload was applied before testing. The load and deflection were then measured continuously using the MDBT load cell and an extensometer described in Subsection 2.2.2. Measured load at predetermined deflection from the spring calibration results was read from the load/deflection curve and compared with the reference load. The results of five measurements is presented in Table 2.1 and in Fig. 2.4. The maximum deviation is 0.71 N at 44.5 N and -3.2 % at 17.8 N.

In the test of ductile-brittle transition temperature using MDBT

Table 2.1 Result of MDBT Load Cell Calibration*

| Calibration Load (lb) | Measured Load+ (lb) |
|---|---|
| 2 | 2.02 - 2.06 |
| 4 | 3.88 - 3.93 |
| 6 | 5.96 - 6.00 |
| 8 | 7.98 - 8.04 |
| 10 | 10.06 -10.16 |

* The excitation voltage supplied to the load cell was 7.86 V.

+ Shows data scatter band in 5 measurements.

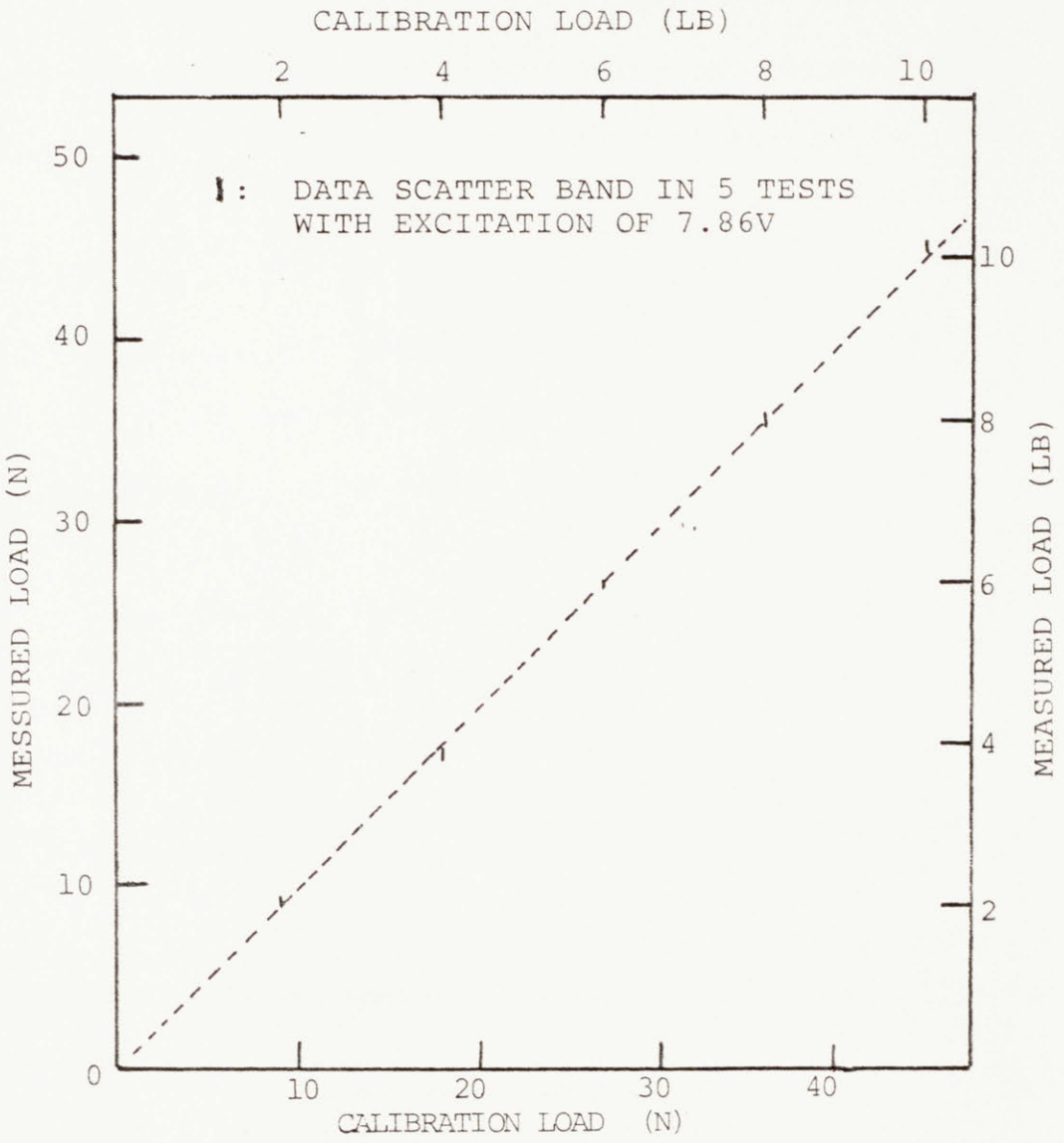


Figure 2.4 Result of calibration of the MDBT load cell, a calibrated spring was used in this calibration.

approach, an impact load is usually applied and adequate dynamic load following capability of the load cell is therefore needed. The digitizer discussed above has a maximum digitizing rate of two million points per second (0.5 micro-sec./point) with aperture uncertainty of 50 pico-sec. and is used in these measurements. Shock load was applied by tapping the load train close to the load cell with a pair of forceps. It was found that the MDBT load cell could follow impact loads faster than 1.9 MN/s. The maximum impact load rate measured in actual test of ductile-brittle transition using the MDBT approach was 1.1 MN/s . Therefore, the load cell seems to have enough dynamic load following capability for the type of DBTT tests developed here.

2.2.2 Extensometer The deflection of a specimen disk in the MDBT is measured with an MTS model 632.12B-20 extensometer in most cases. In a comparison test with the LVDT which was factory installed in the actuator of the Instron mainframe, it was found that the extensometer output had lower noise and higher precision. The extensometer was calibrated using an Instron model A18-3A High Precision Extensometer Calibrator of $\pm$ 0.00038 mm (0.000015 in) precision in compression. The results are presented in Table 2.2 and in Fig. 2.5. The calibration for the extensometer was 1.797 V/mm (45.64 mV/mil) in the 0 - 2.54 mm range. Note that the accuracy is highest in the - 0.254 to - 1.270 mm range. Therefore, in actual testing, the extensometer is set to about - 0.508 mm so that testing is performed in the most accurate range. The maximum deflection measured in most MDBT tests is less than 1.0 mm and the deviation from linearity in the load/deflection curve occurs at deflections less than 0.25 mm in all tests. Thus, the calibration for the initial

Table 2.2 Result of Extensometer Calibration, Showing Calibration of 45.64 mV/0.025 mm for the Whole Range and 45.72 mV/0.025 mm for the Most Accurate Range (-0.254 to -1.270 mm).

| Extensometer Calibrator* Deflection, mm(in) | Voltage Output from+ Extensometer, mV | Voltage Difference in 0.254 mm Deflection mV |
|---|---|---|
| -0.000(0.00000) | $0.0\pm^{0.12}_{0.18}$ | ——— |
| -0.254(0.01000) | 454.5±0.4 | 454.5 |
| -0.508(0.02000) | 911.5±0.1 | 457.0 |
| -0.762(0.03000) | 1368.7±0.2 | 457.2 |
| -1.016(0.04000) | 1825.8±0.4 | 457.1 |
| -1.270(0.05000) | 2283.1±0.2 | 457.3 |
| -1.524(0.06000) | 2737.9±0.4 | 454.8 |
| -1.778(0.07000) | $3193.7\pm^{1.1}_{0.6}$ | 455.8 |
| -2.032(0.08000) | 3654.8±0.2 | 461.1 |
| -2.286(0.09000) | 4108.9±0.4 | 454.1 |
| -2.540(0.10000) | 4558.3±0.9 | 449.4 |

* The precision of this calibrator is 0.00038 mm (0.000015 in).

+ Average value with data band. Result of 3 measurements.

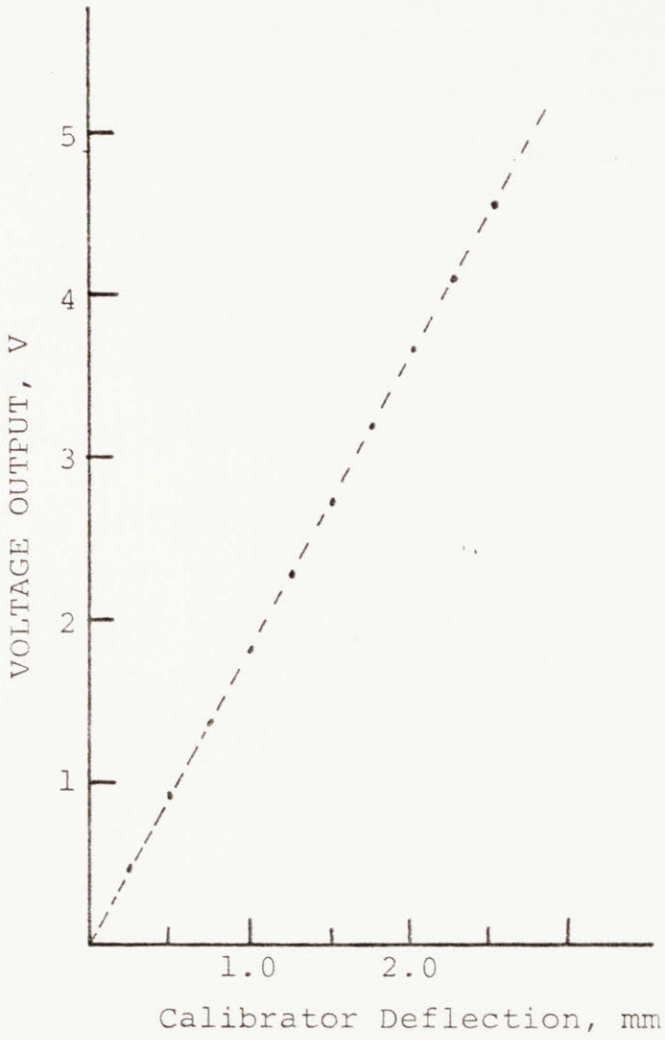


Figure 2.5 Result of calibration of extensometer used in the MDBT, showing good linearity with the slope of 1.797 v/mm.

linear regions is 1.800 V/mm (45.72 mV/mil) with ± 0.002 V/mm precision or errors less than ± 0.1 %.

2.2.3 Linear Variable Displacement Transducer The LVDT installed in the Instron actuator is used mainly for the control of lower load train stroke in the MDBT. The full travel range of the stroke in the 5 % range setting is 2.54 mm. It was calibrated against the extensometer and was found to have a precision of ± 0.033 mm in the MDBT stroke range.

2.2.4 Temperature Test temperature is monitored using a thermocouple (TC) permanently embedded in the wall of the upper disk supporting structure. The temperature difference between the temperature at the TC and that of a disk specimen was measured with a TC soldered to a disk specimen and put into the testing position. In calibration the disk specimen with TC was loaded with 67 N in order to simulate the testing condition. Elevated temperature calibration was done in helium gas atmosphere and low temperature calibration in room air. The result is presented in Table 2.3.

2.2.5 Punch Tip and Supporting Die The radius of the punch tip is one of the major variables in the MDBT. Larger punch tip radius will make the disk response stiffer and smaller radius will make it less stiff. Punch tip radius was measured with a Nikon optical comparator of 50X magnification equipped with a pair of digital micrometers. The precision of this system is ± 0.0013 mm. The punch tip profile was measured at three different angles and the results showed good agreement with each other to within ± 0.02 mm and thus fairly good angular symmetry. The results are shown in Fig. 2.6. The design value for the

Table 2.3 Result of Temperature Calibration+

| Disk TC (°C)* | 300 | 400 | 500 | 600 | |
|---|---|---|---|---|---|
| Embedded TC (°C) | 304±2 | 407±2 | 512±2 | 616±3 | |
| Disk TC (°C)* | -40 | -80 | -120 | -140 | -150 |
| Embedded TC (°C) | -44±1 | -84±1 | -124±1 | -142±1 | -152±1 |

+ Calibration was done in helium gas atmosphere at 0.11 MPa for elevated temperature calibration and in open air for low temperature calibration.

* The disk specimen with a TC soldered was loaded with 67N load to simulate actual testing condition.

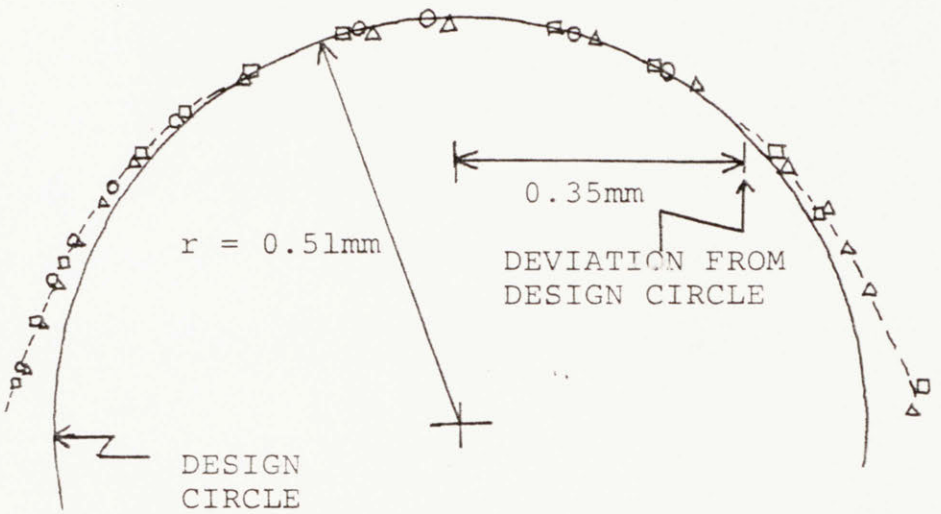


□,△,○ : INDICATE THREE MEASUREMENTS AT THREE DIFFERENT ANGLES.

Figure 2.6 Result of punch tip radius measurement, showing good conformity with design circle to about 0.35mm radius: results of three measurements at three different angles.

punch tip radius is 0.51 mm (0.020 in). The measured profile conformed well to the design circle in the tip portion but deviated from it away from the tip, at about 0.35 mm radius as indicated in the figure. Considering the fact that deviation from linearity in MDBT load/deflection curve occurs when the radius of the contacting region between the punch tip and a disk specimen is about 0.076 mm in most cases, the unconformity found in this measurement would not affect the linear region in the load/deflection curve.

The radius of the disk supporting region of the supporting die was measured with the optical comparator used in punch tip profile measurement. The design value for this radius is 1.23 mm (0.0485 in). The radius was calculated from the result of circle measurement and found to be $1.24 \pm 0.01$ mm.

2.2.6 Load Train Stiffness The stiffness of the whole load train was measured using a rod and a cylinder of high density alumina installed in place of the punch and the supporting die, respectively. The result for the whole load range is presented in Fig. 2.7 and an expanded view for the 0 - 44.5 N range in Fig. 2.8. As one can see from the result, the curve is not very linear in the very early region usually used in the MDBT and the slope increases with increasing loads. The slope was $6.6 \times 10^4$ N/mm ($3.8 \times 10^5$ lb/in) at about 650 N load and $0.84 \times 10^4$ N/mm ($0.48 \times 10^5$ lb/in) at about 25 N load.

## 2.3 Signal Noise Analysis and Filtering

In the MDBT, all testing is done in the stroke control mode. The

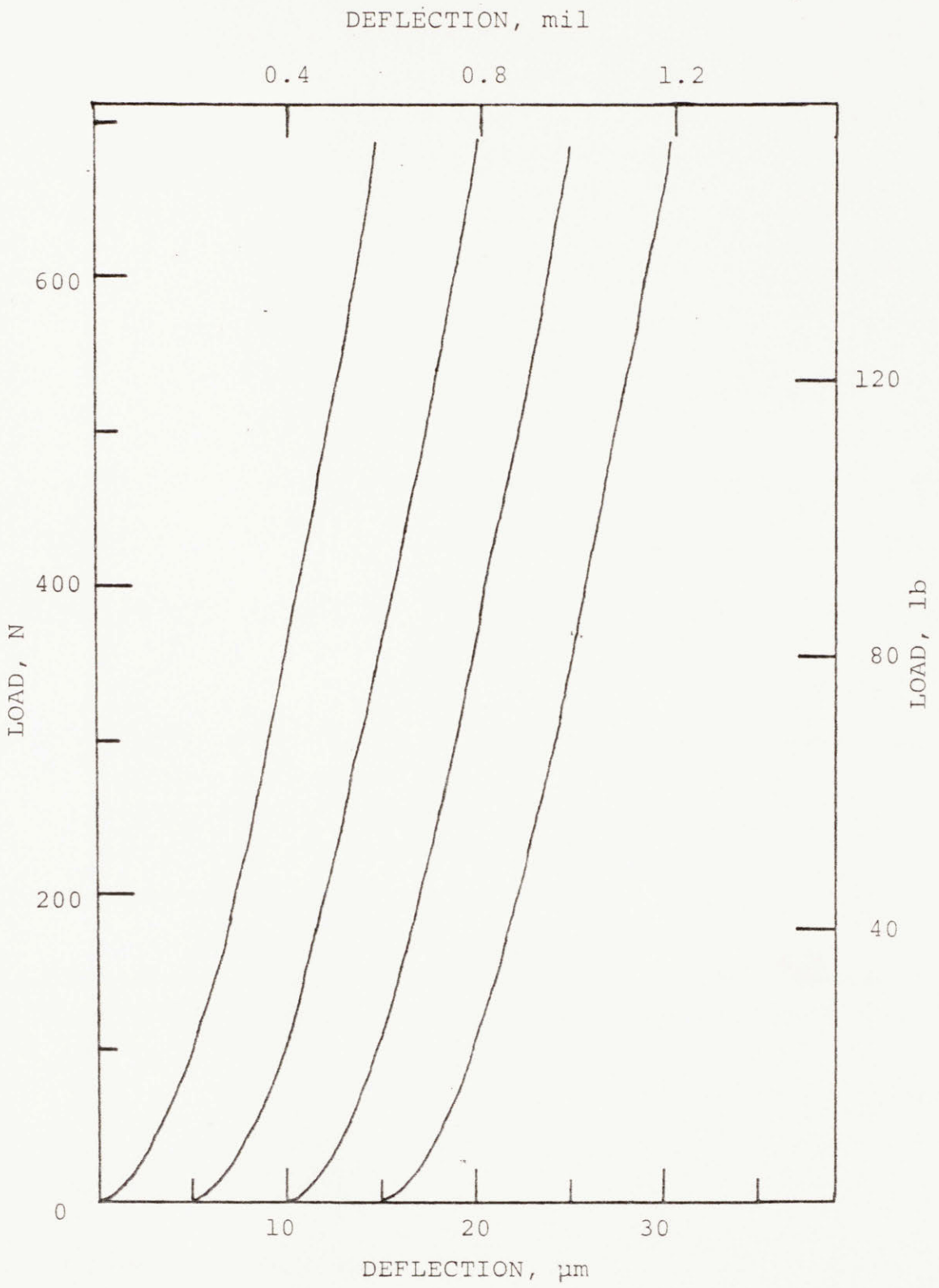


Figure 2.7 Result of load train compliance measurement, full load range. Non-linearity can be seen in initial region where most of the MDBT are done. Each curve represents a test.

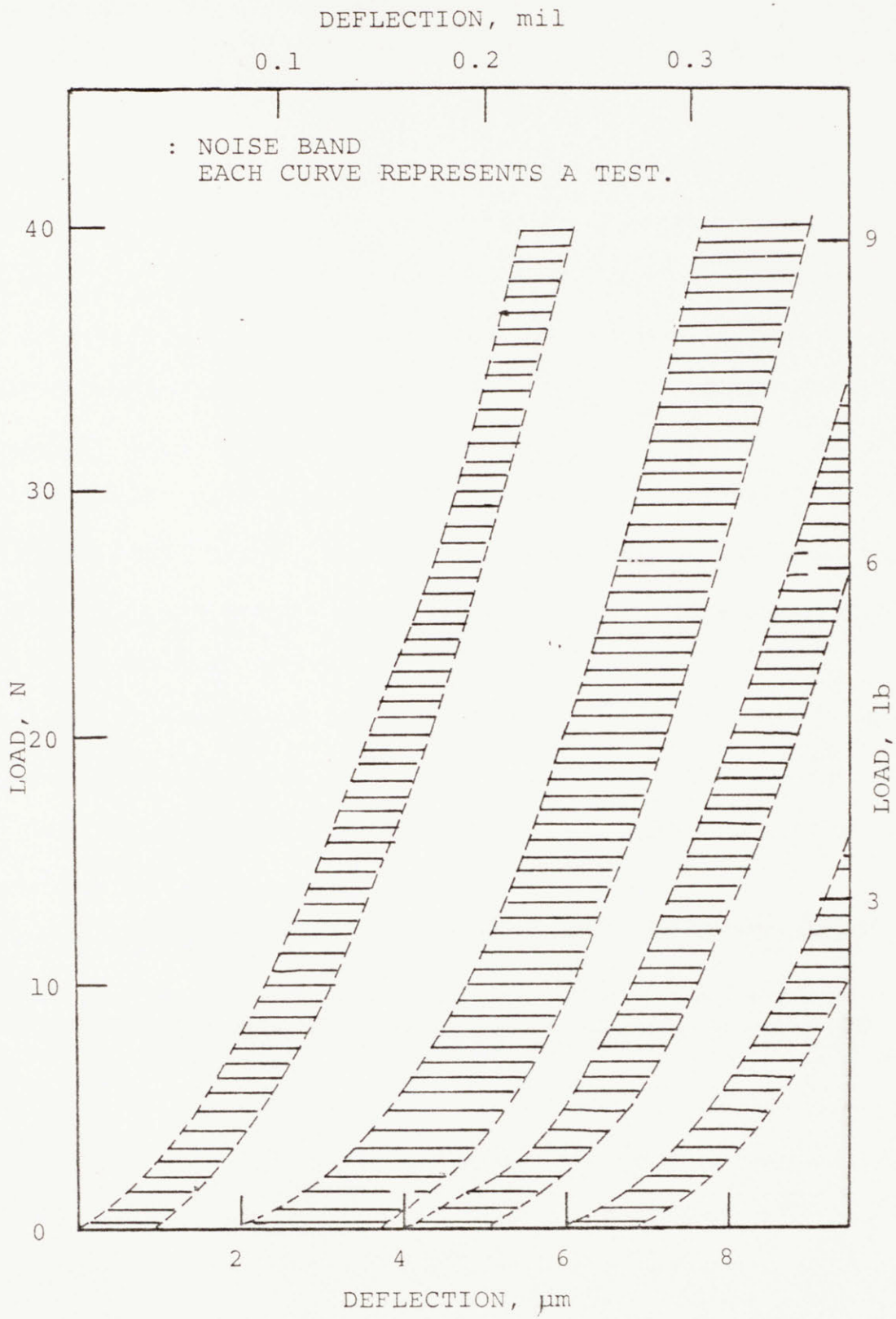


Figure 2.8 Expanded view of the initial region (0-42N range) in load train compliance measurement.

Instron uses a stroke controller to control the motion of the lower load train. The stroke controller is driven by a master control signal from a function generator with feedback from the LVDT in the actuator. The control signal is applied to a fluid control manifold so that appropriate hydraulic power is supplied to the actuator as shown in the simplified block diagram for stroke control in Fig. 2.9. The actuator generates the stroke of the lower load train and thus load is applied and the specimen disk is deformed. Therefore the stroke signal has great effect on measured extensometer signal and load signal. The LVDT is operated with excitation of 5K Hz alternating current from the Instron stroke controller. Although the feedback signal from the LVDT is filtered by a lowpass filter at 1500 Hz and rectified before being fed to stroke feedback signal output terminal, the signal from the output terminal can have 5K Hz and other frequency noise components. Similarly, the extensometer and load signals can have various noise components. The signals from the output terminals were found to have a significant amount of noise which was analysed to optimize filtration.

2.3.1 Noise Analysis A signal with various frequency components can be transformed to the amplitude-frequency domain using Fourier transform. In this noise analysis, the signal was first digitized with the Nicolet 4094 digital oscilloscope and then Fourier transformed with the fast fourier transform (FFT) in the Nicolet 4094 system waveform analysis package. In order to avoid distortion of the frequency and amplitude information in the Fourier transformation due to discrete sampling, the signals were sampled at three different frequencies : 200K Hz, 20K Hz and 2K Hz. A low pass filter with cutoff frequency of half the sam-

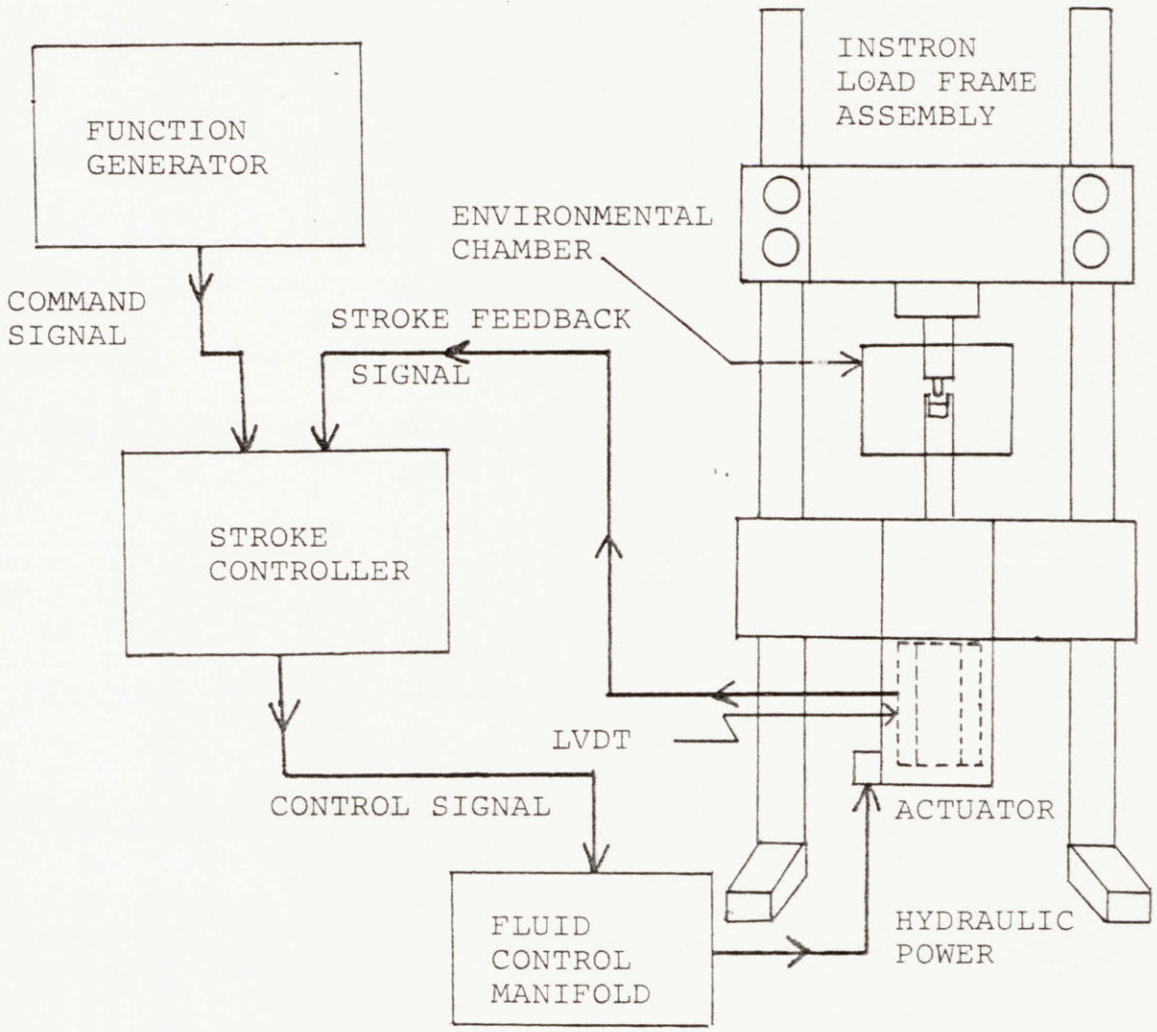


Figure 2.9 Simplified block diagram for Instron stroke control.

pling frequency was used to minimize distortion of the frequency spectrum due to aliasing. Aliasing can be illustrated in the following example. If an 83.3 Hz sine wave is sampled at 100 Hz, the apparent frequency in the sampled signal will be 16.7 Hz as shown in Fig. 2.10. This phenomenon is called aliasing and it usually happens when a wave form is sampled at less than twice its frequency. In the frequency domain, aliasing causes a folding back of frequencies and distorts both the amplitude and the phase informations of the Fourier transform and this effect can be estimated using a folding diagram as shown in Fig. 2.11. Therefore it is a recommended practice in sampling a waveform for Fourier transform to filter the signal with a low pass filter at half the sampling frequency. The FFT analysis results showed the followings:

1) All the three signals (load, stroke and extensometer feedback) are essentially dc. The extensometer feedback signals show two peaks at 0 Hz and 1 Hz.

2) The load feedback signal has a noise component of -18 dB at about 445 Hz. Other noise components are lower than -25 dB.

3) All the noise components in the extensometer feedback signal are lower than -35 dB.

4) The LVDT feedback signal seems to have a noise component of -27 dB at 4.99K Hz. Others are lower than -31 dB.

2.3.2 Filtering of Noise As described earlier, the result of FFT analysis verified that the load and the deflection signals are essentially dc. Therefore, in theory, as low a frequency as obtainable

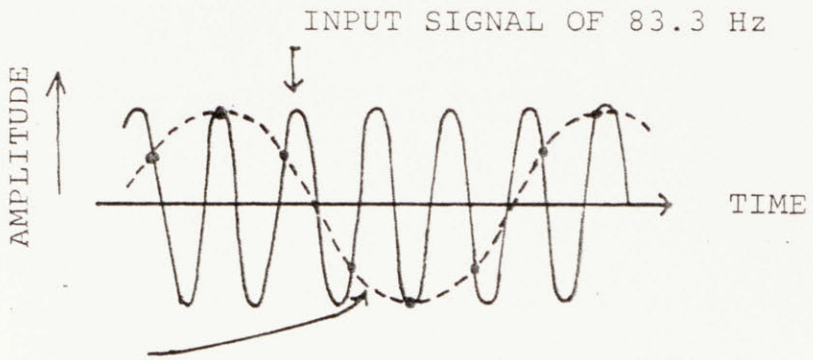


Figure 2.10 An illustration of aliasing, 83.3 Hz sine wave sampled at 100 Hz.

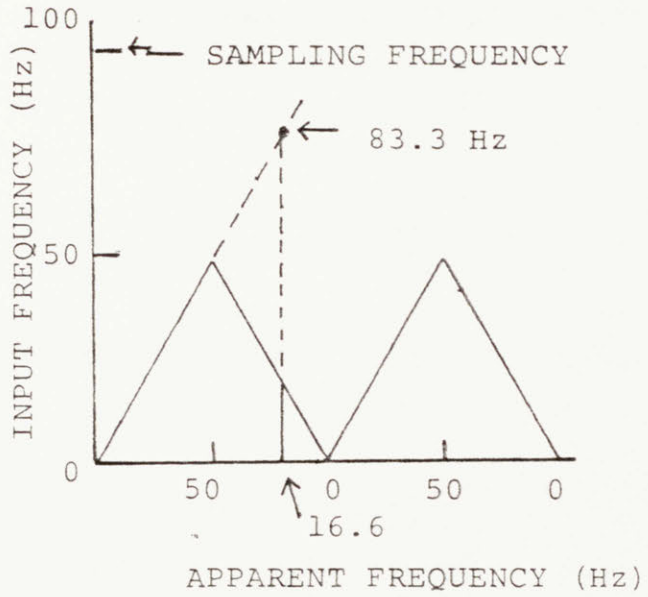


Figure 2.11 Folding diagram for sampling frequency of 100 Hz.

can be used to filter out the noise from the signal. However, actual filters have a tendency to attenuate frequencies slightly below the cutoff frequency. Thus the cutoff frequency should be chosen after checking this effect on an actual signal. A Kronhite 3342 dual channel filter with variable cutoff frequency capability is used in filtering. Various cutoff frequencies were tried and the results are presented in Fig.'s 2.12 and 2.13. Fig. 2.12 shows that noise is reduced as cutoff frequency is decreased and noise is almost indiscernible at cutoff frequencies less than 400 Hz. The effect of filtering on the load/deflection curve can be seen in Fig. 2.13. Filtering seems not to affect the curve until the cutoff frequency is reduced to 400 Hz. When filtered at 200 Hz, the slope of the curve becomes slightly reduced. However the whole curve is within the noise band of the unfiltered curve. The curve filtered at 30 Hz shows slight deviation from the noise band of the unfiltered curve after the initial linear region. A cutoff frequency of 400 Hz was chosen based on these results and is used in MDBT testing.

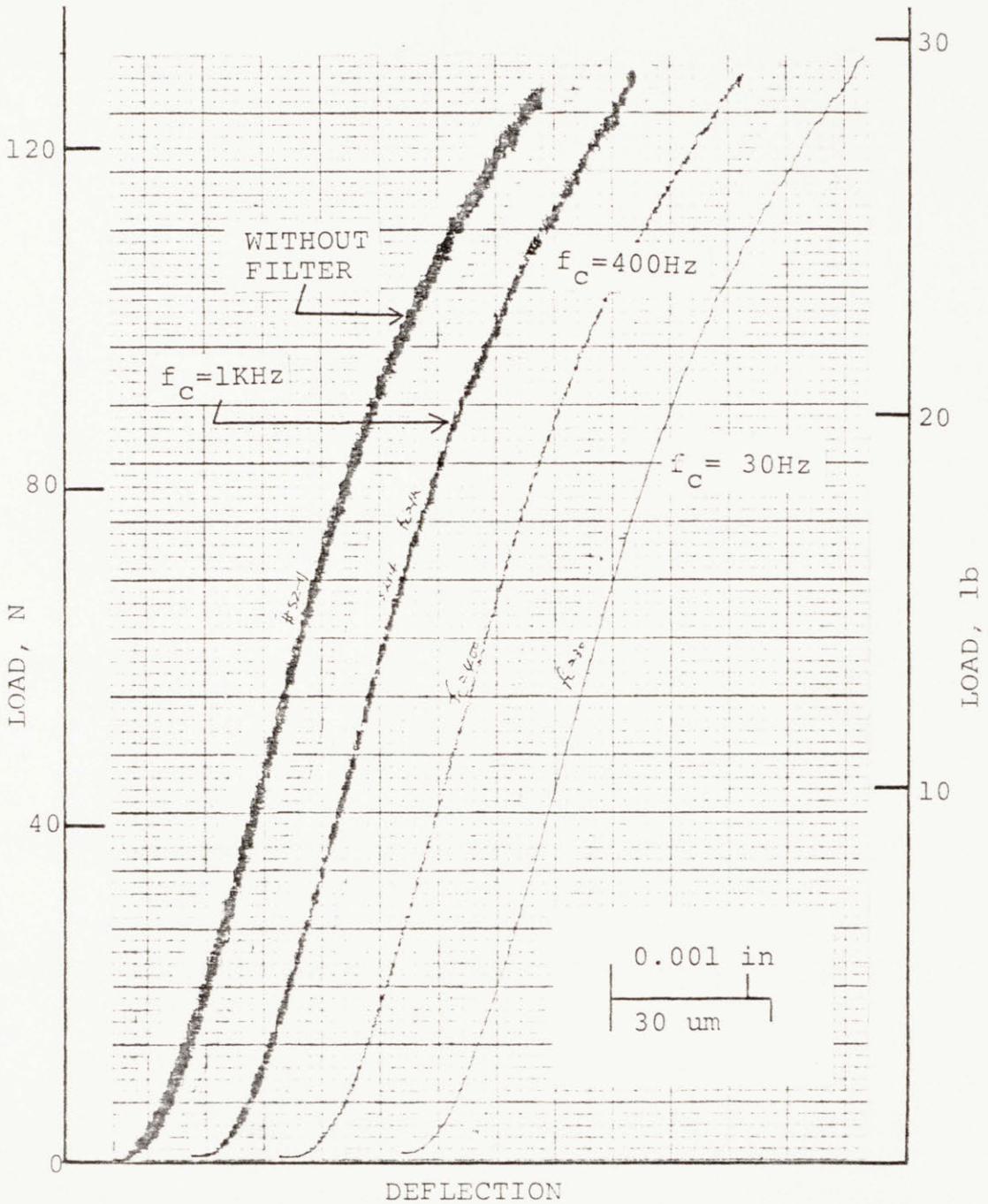


Figure 2.12 Effect of filtering on the MDBT load/deflection curve, showing reduction of noise as cut off frequency is decreased.

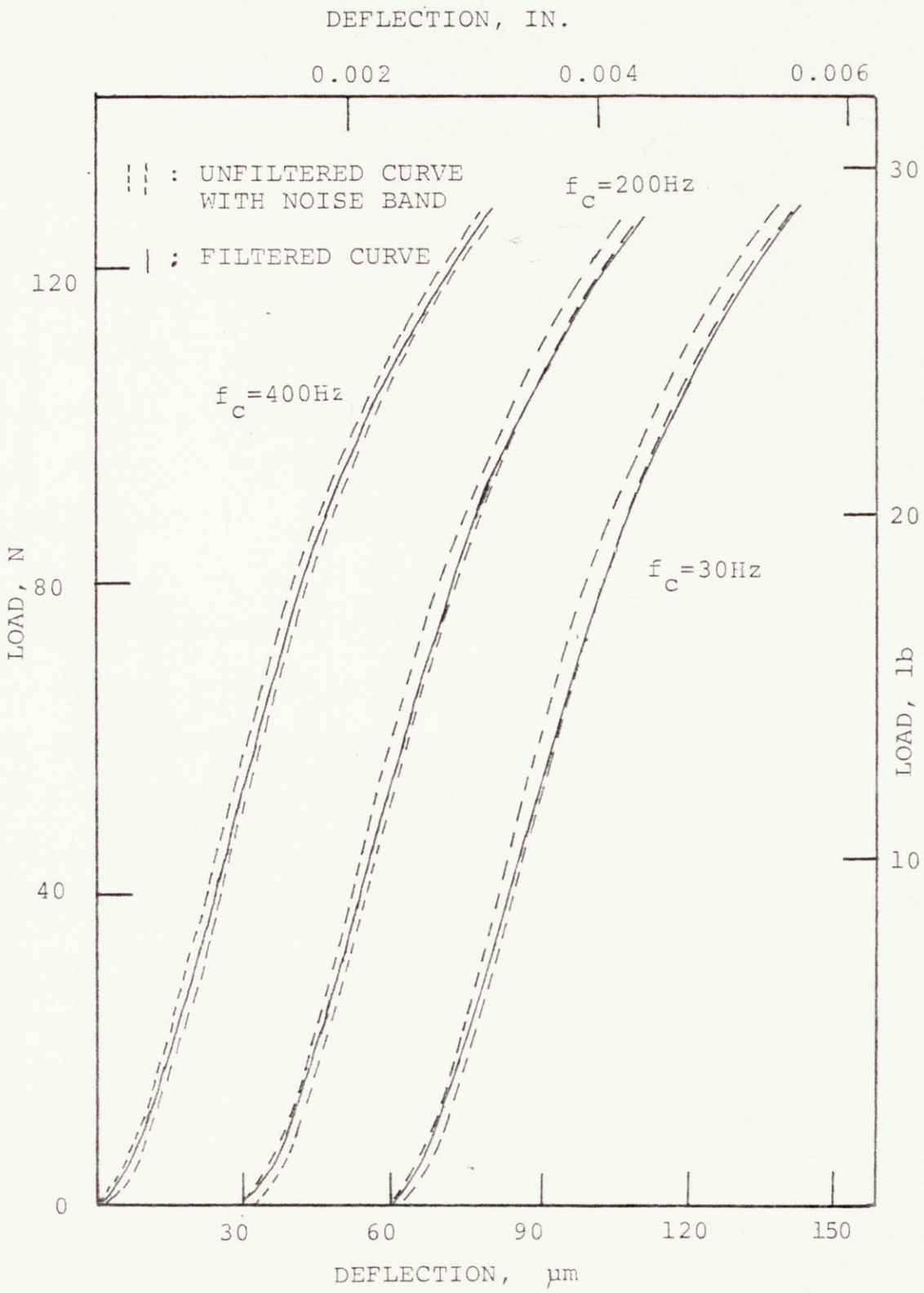


Figure 2.13 Effect of different cut off frequency on filtered MDBT curves, showing no effect at 400 Hz, but noticeable effect at 30 Hz.

# CHAPTER 3 MINIATURIZED DISK BEND TEST

Testing of irraditated material poses several additional difficulties not encountered in unirradiated material testing. Irradiation of specimens to dose levels comparable to lifetime doses of expected applications and handling of radioactive specimens are among the major difficulties in irradiated material testing. Irradiation of specimens to expected lifetime dose sometimes requires several years of irradiation even in the highest flux test reactors available now. Proper irradiation space is costly and very limited compared with the need. Furthermore, the damage gradient over the specimen can be significant in some conventional size specimen as discussed in reference 3.1. Those difficulties can be alleviated by the use of miniaturized specimens. Miniaturization of mechanical property testing by the adoption of simply supported bending of very small specimen disk in a punch and die arrangement especially with finite element analysis of the test offers the possibility of obtaining a wide range of useful mechanical properties such as strength, ductility, ductile-brittle transition temperature, fatigue properties, etc. from very small specimens. The MIT miniaturized disk bend test (MDBT) which uses disk specimens of standard transmission electron microscopy disk size, i.e., 3 mm in diameter and 0.25 mm in thickness, has shown promising possibilities of obtaining mechanical properties as discussed in references 3.2 through 3.6.

In the usual mode of the MIT test, the disk specimen is simply supported along the circumference, on a die, while a punch presses the

center of the disk into the cavity of the die. The applied load and the central deflection of the specimen are monitored with the load cell and the extensometer described in Chapter 2. Typical load/deflection curves for ductile and brittle specimens are shown in Fig. 3.1. A disk specimen experiences simple bending in the early region of the test. As the load increases,the punch forces the specimen material deeper into the die and the predominant stress mode changes from bending to membrane stretching. Ducitle disk specimens are thought to fail during the later part the membrane stretching regime. Post test examination of failed ductile specimens showed circular cracks along a circle of about 0.8 mm diameter. Fig. 3.2 presents a typical crack found in ductile failure. Brittle disk specimens fail in the bending regime. Failed brittle disks showed linear cracks initiated at the center of the bottom surface. A typical example of brittle cracks is presented in Fig. 3.3.

The load range typically obtained in the MDBT is 0-670 N (0-150 lb) and the load range of the initial linear region is 0-45 N. The maximum deflection to failure is typically 1.0 mm (0.040 in). Maximum errors in load measurement are 7 N from 0-670 N and 0.71 N from 0-44.5 N. The precision of the deflection measurement is better than $\pm$0.1 % of the measured value. Test specimens are prepared by wet grinding with 600 grid abrasive paper to 0.254$\pm$0.0025 mm (0.0100$\pm$0.0001 in). The reproducibility of the MDBT has been found to be excellant and is shown in Fig. 3.4. Presented in the figure are MDBT curves from cold worked 302 stainless steel (SS) at 773 K. These were independent measurements made over a period of time to act as checks that the test system performance had not shifted.

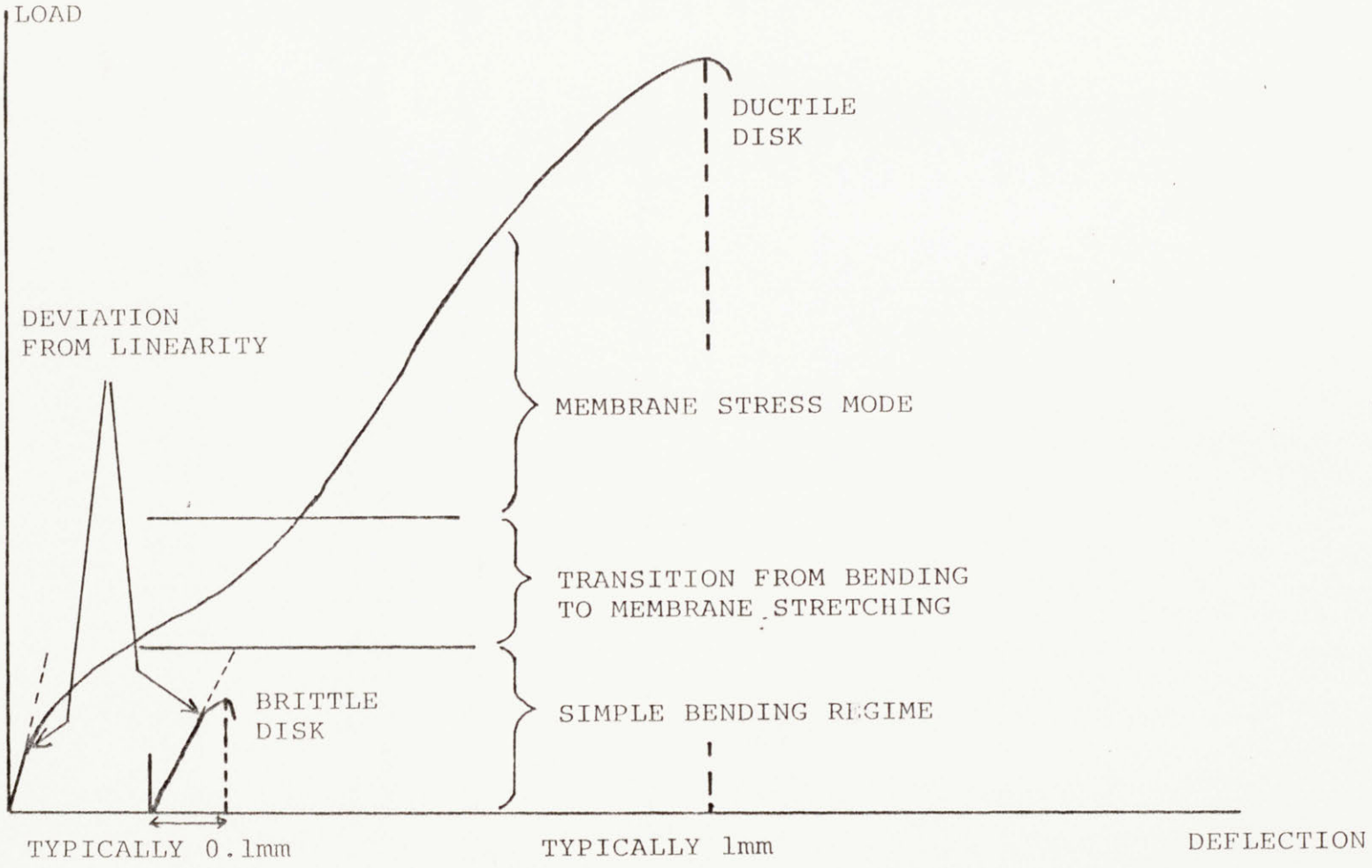


Figure 3.1 Typical applied load/central deflection curves for ductile and brittle disks - brittle disks, with ductility less than about 5%, show drastic reduction in the deflection at maximum load and in the maximum load.


Figure 3.2 Typical ductile fracture surface showing a circular crack along a circle of about 0.8 mm diameter with through thickness thinning.

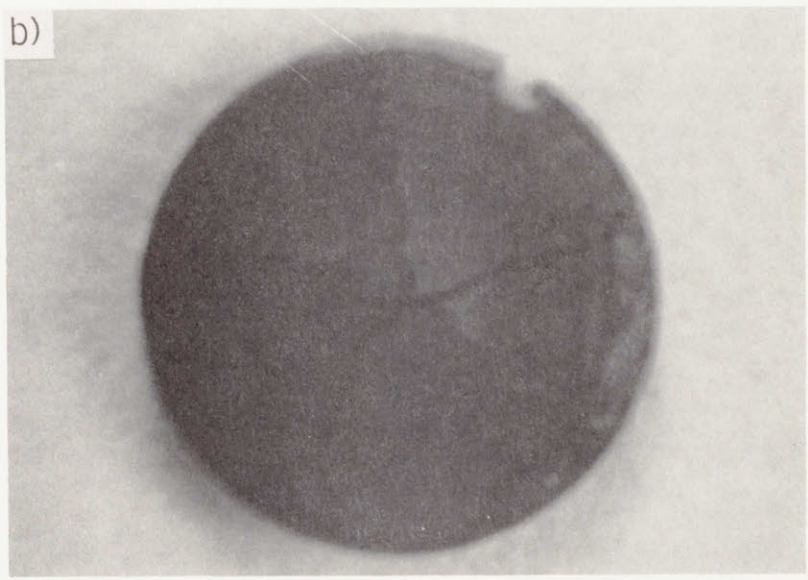


Figure 3.3 Typical brittle fracture surface at about 22 X showing radial cracks initiated at the disk center.

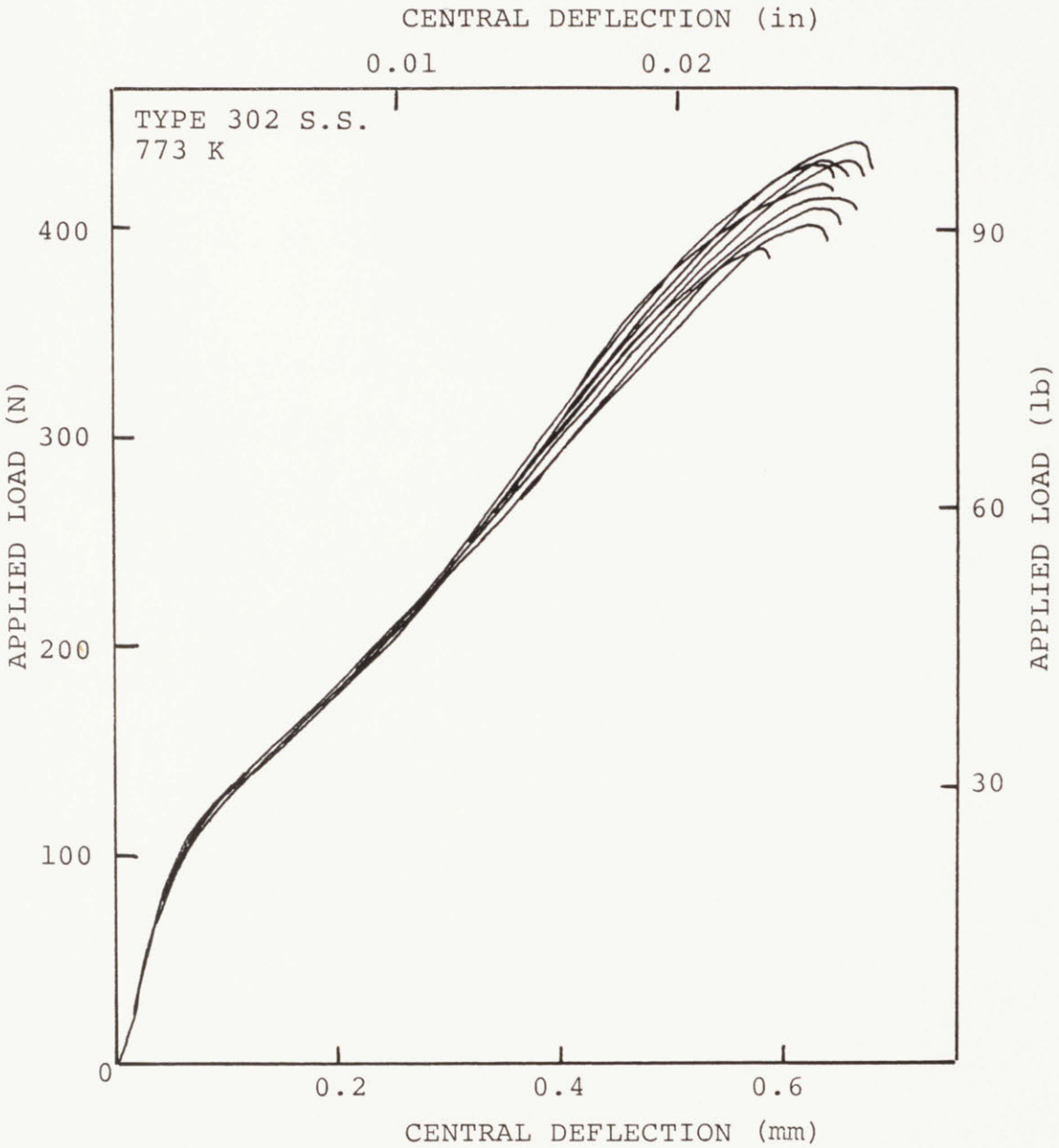


Figure 3.4 Reproducibility in miniaturized disk bend test, data obtained from a series of nine tests of SS302 disk samples at 773K.

3.1 Tensile Test using MDBT approach

The load/deflection curves obtained from the MDBT usually show linear response in the initial region. This portion of the curve was found to be controlled mainly by the yield strength and the elastic modulus. This dependence on the material properties was verified in experimental data and in parametric studies using a finite element computer code ABAQUS (reference 3.7) and is discussed in Subsection 3.1.2 and 3.1.4. Based on these findings, the load at the deviation point from linearity in the MDBT load/deflection curve, defined as the yield load, was correlated with the yield strength of the material. The experimental data for several different kinds of alloys indicated a strong monotonic dependence of the yield load on the yield strength of the material. An iterative procedure for the yield load using the ABAQUS finite element code was used to determine the yield strength of the material. In a series of reference tests to check the validity of this analysis method, the predicted yield strengths from MDBT data agreed well with the reference values from conventional uniaxial tests.

The load/deflection curves for very brittle specimens had shown an abrupt load drop after the linear portion and this was found to be due to the onset of failure in the specimen. The deflection at the sudden load drop was correlated with total elongation and the ductility of the specimen was estimated from this deflection using an analytic formula derived under the assumption of spherical cap geometry during

deformation. The spherical cap geometry assumption is commonly used in the analysis of circular disk deformation at small deflection.

3.1.1 Computer Modeling of the MDBT In the MIT MDBT, a central load is applied by a hemispherically tipped punch onto the center of a circular disk specimen simply supported by a cylindrical die. A schematic illustration of the testing is shown in Fig. 3.5. The components are usually aligned to better than 0.04 mm. Considering the disk specimen radius of 1.52 mm, the test condition can be thought as axi-symmetric. Using this axi-symmetry, only half of the disk cross section, as shown in Fig. 3.6, was used in computer modeling. The half disk cross section is divided into 63 elements. Each element is modeled to have eight nodal points - four at the corners and four at the middle of the edges. Computer calculation is done using the information at the nodal points. Detailed information on element and nodal point numbering and the coordinates of each nodal point can be found in Appendices B and C. The boundries between the punch and the disk and between the support and the disk were modeled through the use of the multi-point constraint (MPC) subroutine option and the gap option in the ABAQUS code. The MPC subroutine for the MDBT was written by Manahan (reference 3.2) and used in the current calculations. The MPC subroutine uses a shadow node concept to model the moving boundary condition encountered in the MDBT. In current calculations, the shadow nodes are defined as follows. Nodes which have the potential to make contact with the punch or the support are identified before calculation. The relative motion of the identified physical node P with respect to the punch or the support is then mapped into the Cartesian coordinate system by the relative motion of a

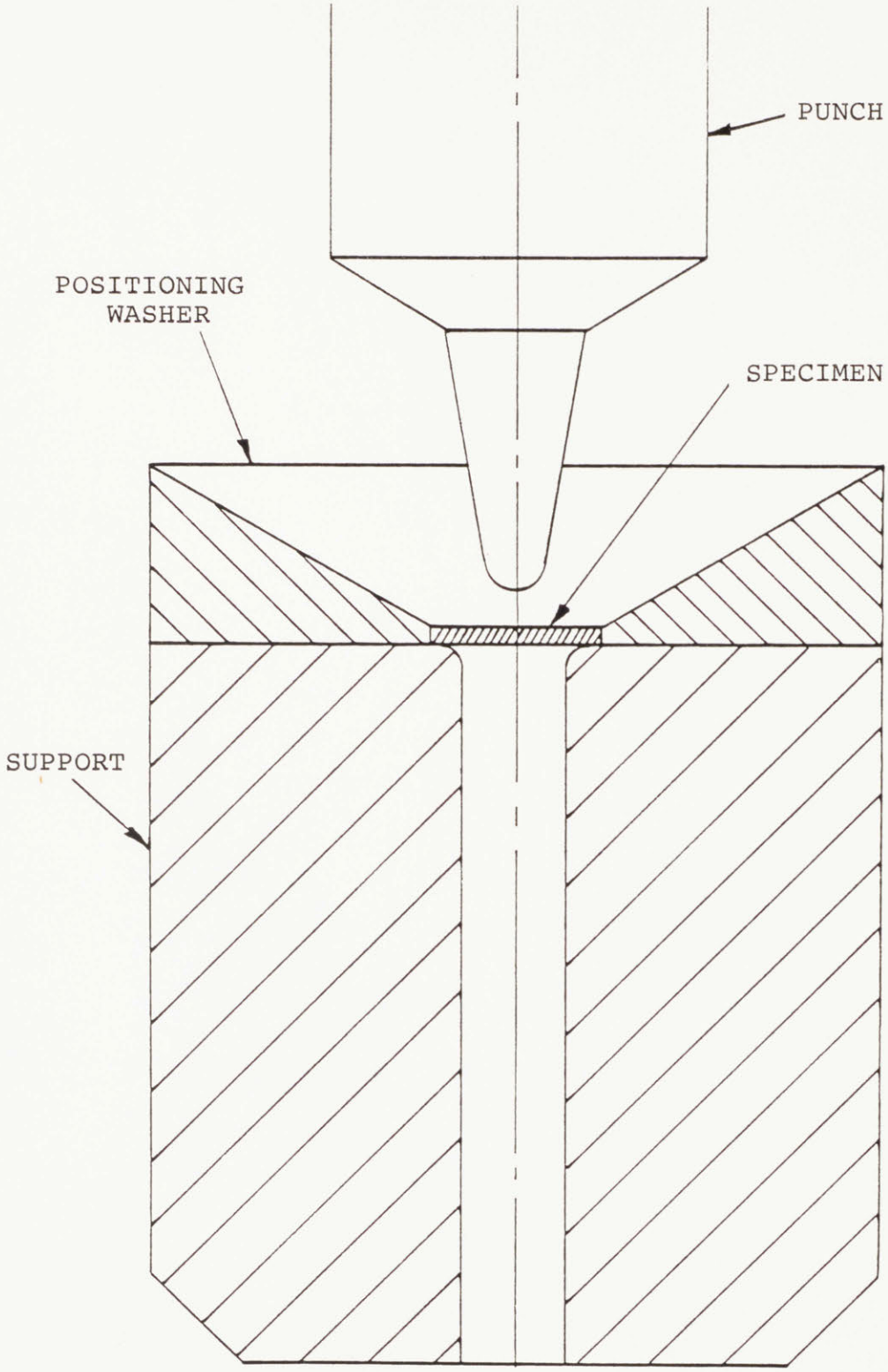


Figure 3.5 Schematic illustration of Miniaturized Disk Bend Test, showing simply supported central loading.

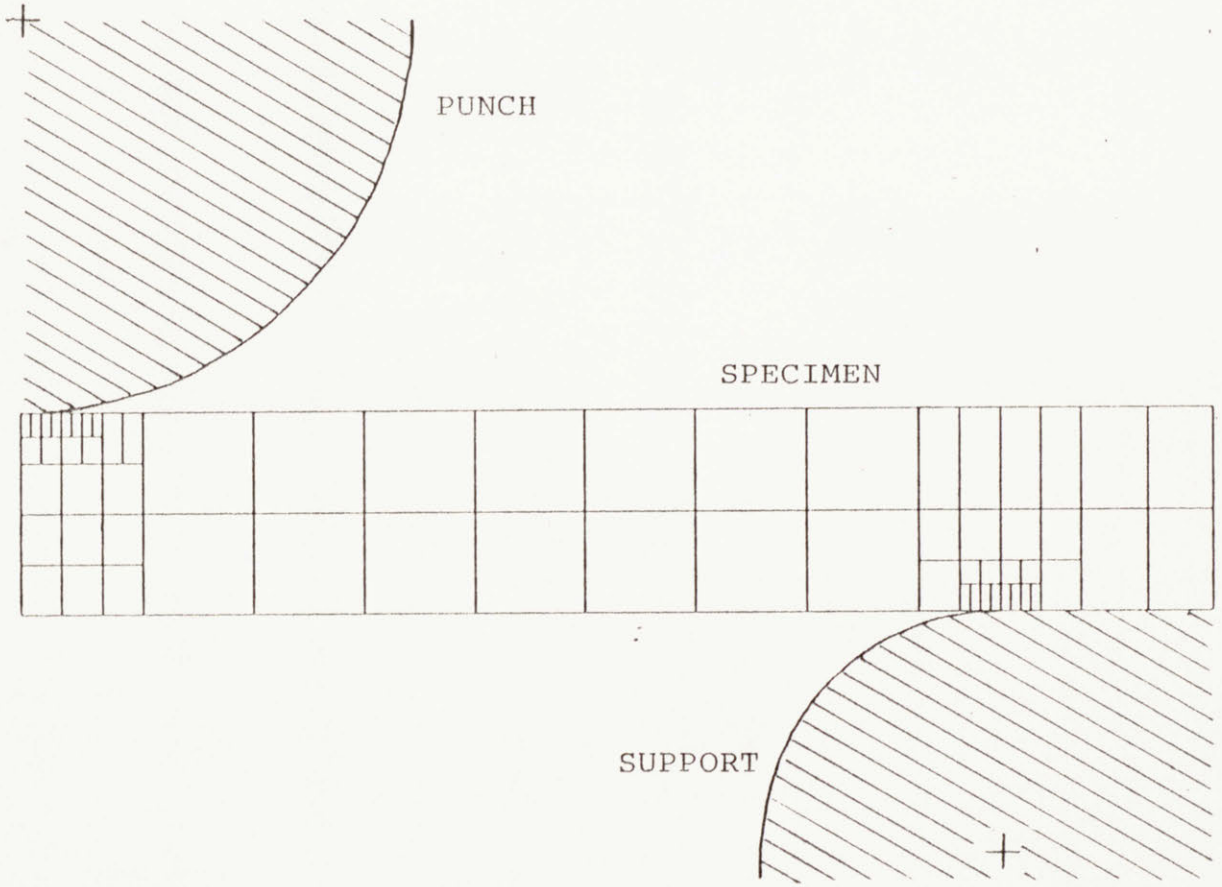


Figure 3.6 Cross sectional view of half of test components, showing element mesh data used in computer calculation.

shadow node Q with respect to a fixed shadow node R so that the displacement vectors of the shadow node Q in X and Y coordinates indicate the change in separation distance and the radially projected lateral displacement onto the surface of the support or the punch of the node P, respectively. This mapping is illustrated in Fig.'s 3.7 and 3.8, prime mark indicates a position or value after deformation. The normal vector $\underline{n}$ is defined as a unit vector pointing from Q to R in the Cartesian coordinate system. Fig. 3.7 shows the modeling of the support boundary. The scalar product of the normal vector $\underline{n}$ and the X displacement vector of Q, $\underline{U}_x \underline{n}$, indicates the change in separation distance between a nodal point P and the support before and after deformation (d'-d). The Y displacement vector of Q, $U_y$, shows the radially projected lateral displacement of P, L in the figure, onto the support. Fig. 3.8 presents a similar illustration for the punch boundary. In this case, Q is located on the negative X axis because the disk is located on the negative side from the punch and thus the normal vector is in the positive X direction. The MPC subroutine transforms the nodal displacement information in the (R,Z) coordinate system into the (X,Y) coordinate system so that the main program can monitor the gap between a nodal point on the disk and the punch or the support and calculate the frictional forces when a gap is closed.

Previously, a 20 element mesh with element size of 1.50mm X 1.27mm in the punch contact region was used for computer calculations. When these ABAQUS calculation results were compared with experimental load/deflection curves, the calculations were found to predict stiffer

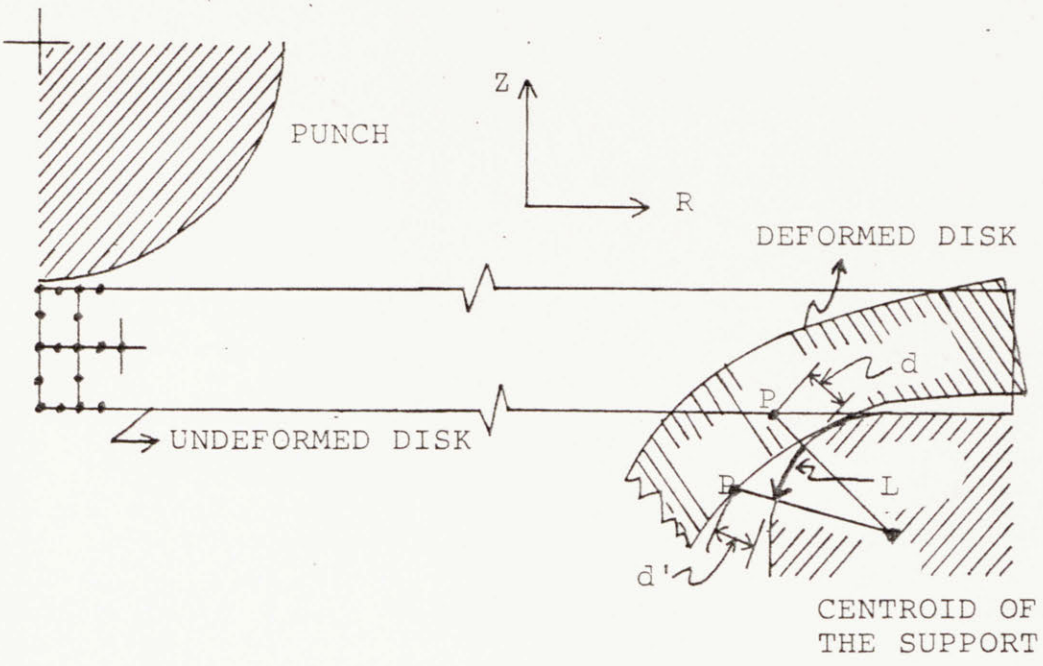


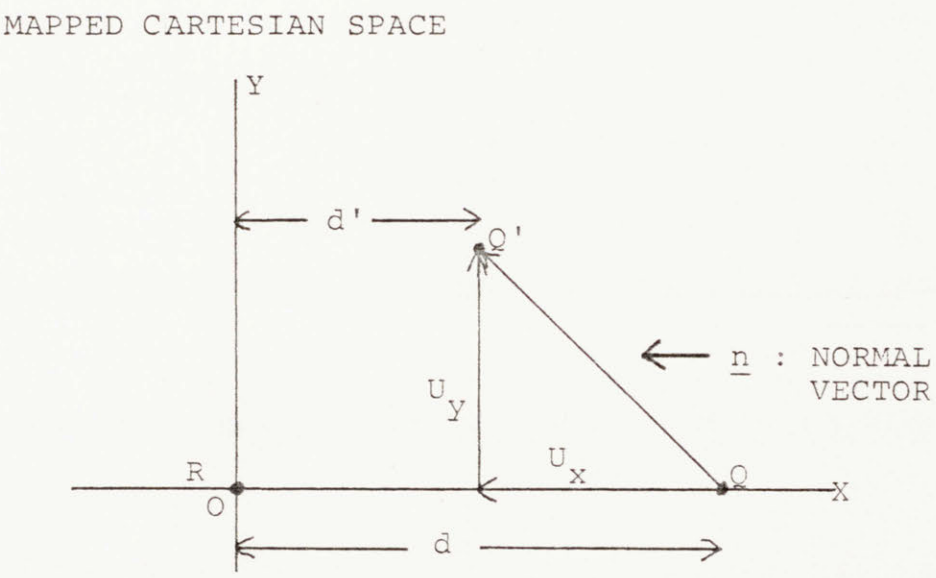


Figure 3.7 Modeling of the support boundary using the shadow node concept. The relative motion of a physical node P with respect to the support is mapped into the Cartesian coordinate system by the relative motion of a shadow node Q with respect to a fixed shadow node R. The prime mark indicates the position or the value after deformation.

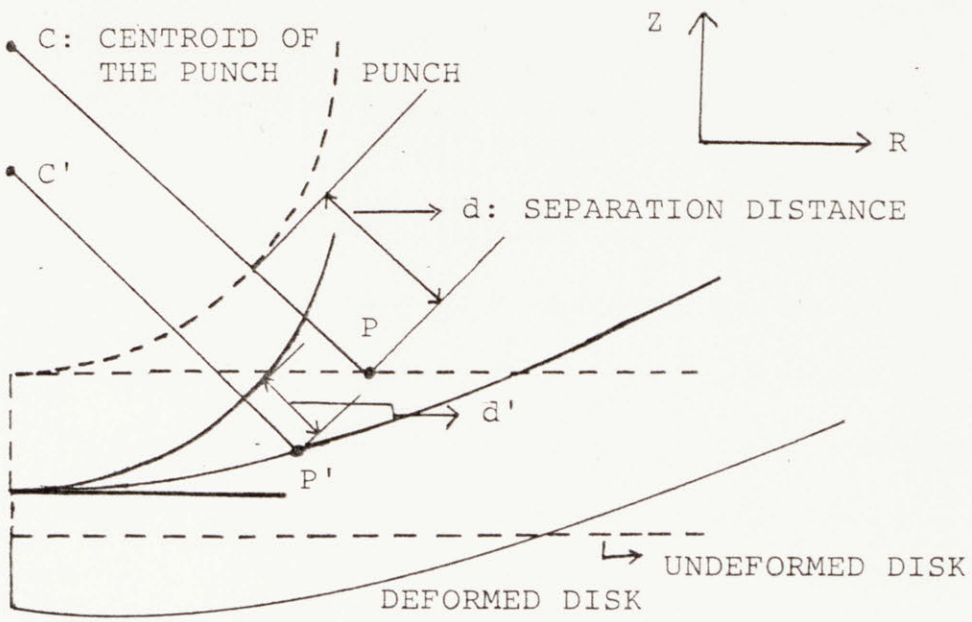


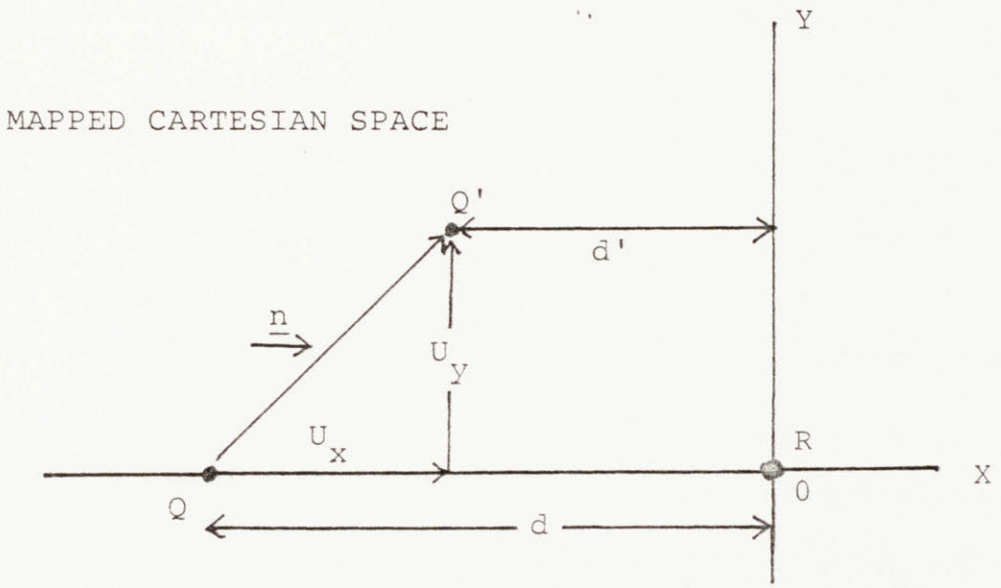


Figure 3.8 Modeling of the punch boundary using the shadow node concept. The relative motion of a physical node P with respect to the punch is mapped into cartesian coordinate system by the relative motion of A shadow node Q with respect to a fixed shadow node R. The prime mark indicates the position or the value after deformation.

disk responses in the linear region and also lower yield loads than the experimental curves. This was found to be due to the fact that no more than two nodal points made contact with the punch by the end of the linear response regime and applied the whole load to the disk specimen. In the actual test the load and punch/disk contract area increase continuously, producing a continuous enlargement of the strain-hardened portion of the disk. However, in the computer calculation using the 20 element mesh, load and contacting area increase stepwise in two steps. Eight to ten contacting nodal points are generally thought to be needed to model the actual loading conditions adequately. In the subsequent finite element analysis using various element meshes, it was recognized that the portions which made contact with the punch or the support were important in determining the disk response in the initial linear region. This seems to reflect the fact that significant changes in the element state occur only in the contacting portions and the rest of the elements stay in the elasticity range during the deformation in the linear region. Therefore the contacting portions were finely meshed to 0.013mm X 0.032mm so that about 12 nodal points contacted with the punch at the deviation from linearity. The resultant 63 element mesh data is schematically presented in Fig. 3.6 and detailed mesh nodal/element numbering of the disk and its coordinates are available in Appendices B and C.

The results of ABAQUS calculations with the 63 element mesh showed good simulation of experimental load/deflection curves up to the point of deviation from linearity. A typical result is shown in Fig. 3.9

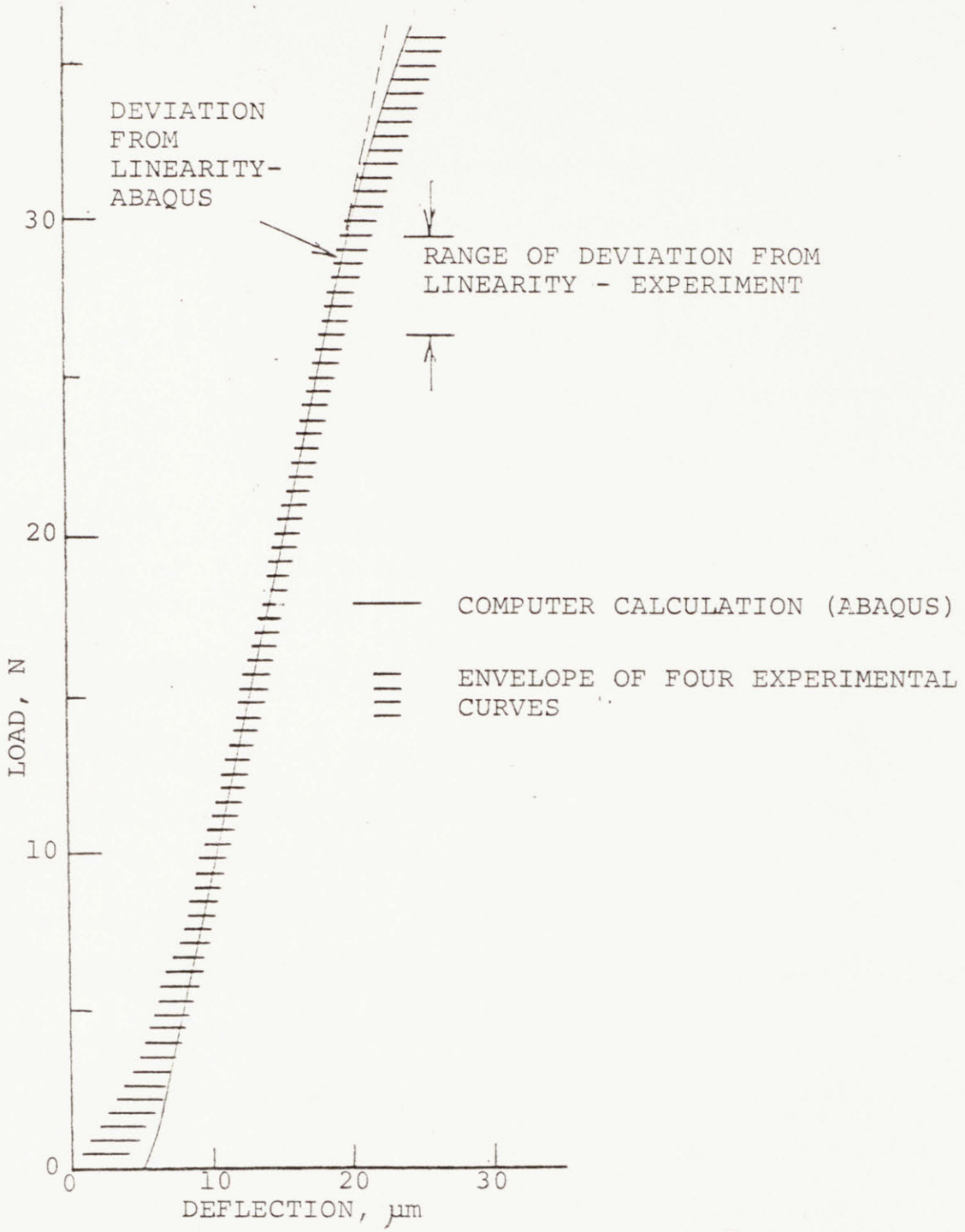


Figure 3.9 Comparison of computer simulation result with experimental data band for a cupro-nickel alloy, showing good agreement up to the point of deviation from linearity

for a cupro-nickel alloy used in the reference tests to verify the method used in the analysis of MDBT results. The load/deflection response was calculated using known mechanical properties. The mismatch between ABAQUS and experimental results in the very early part of the curve seems to be due mainly to the insufficient number of nodal points contacting the punch in this region. In most cases the calculation and experiment showed good agreement after eight nodal points made contact with the punch in the ABAQUS finite element calculation. Computer generated load/deflection curves showed stiffer response than experimental curves when less than eight nodal points contacted the punch. In the early part of the load/deflection curves, the fewer the number of contacting nodal points, the greater the mismatch. Although the calculational result exhibited good simulation of experimental results, it was not clear whether the critical element size was small enough. In order to check this, the contacting elements were further refined to 0.0064mm X 0.0159mm. Detailed node/element drawings are presented in Appendix C. The result of the computer calculation using this ultrafine mesh is compared in Table 3.1 with the result using 63 element mesh. The difference between the two results was less than 2.6 % of the 63 element result and this was judged to be insignificant. Therefore the 63 element mesh has been used in subsequent computer analysis of the MDBT.

3.1.2 Analysis for Strength Measured MDBT load/ deflection curves usually show a linear disk response in the initial region. The strong dependence of this linear region on yield strength and elastic modulus

Table 3.1 Result of load/deflection calculations using the 63 element mesh and an ultra-fine mesh with critical element size of 0.0064 mm × 0.0159 mm.

| Deflection mm | Load | |
|---|---|---|
| | 63 el. mesh N | Ultrafine mesh N |
| 0.0013 | 1.75 | 1.77 |
| 0.0025 | 3.96 | 3.94 |
| 0.0051 | 8.42 | 8.64 |
| 0.0076 | 13.35 | 13.56 |
| 0.0102 | 18.29 | 18.61 |
| 0.0127 | 23.30 | 23.76 |
| 0.0152 | 28.43 | 28.79 |
| 0.0178 | 33.19 | 33.96 |
| 0.0191 | 35.94 | 36.27 |
| 0.0203 | 38.38 | 38.54 |
| 0.0216 | 40.38 | 40.80 |
| 0.0229 | 42.50 | 42.83 |

* Detailed element mesh informations are presented in Appendices B and C.

of the material can be seen in the expanded view of the initial region as presented in Fig.'s 3.10 and 3.11. Fig. 3.10 illustrates the effects of different elastic moduli on this region for different kinds of alloys with two comparable yield strengths. The effect of yield strength is shown in Fig. 3.11 for a series of aluminum alloys with different thermo-mechanical treatments. The materials used in these tests are described in Subsection 3.1.4.

As expected disk specimens with higher elastic moduli exhibit steeper slopes in Fig. 3.10. The slope of the load/deflection curve for small deflections can be calculated using analytical formula available in standard texts. For a rigid circular disk under point load, Roarke and Young (reference 3.8) give the following equation:

$$\frac{P}{W} = -\frac{4\pi E m^2 t^3}{3(m-1)(3m+1)a^2} \qquad 3.1$$

where P : applied load

W : central deflection of the disk specimen

E : modulus of elasticity

m : reciprocal of $\nu$, Poisson's ratio

t : thickness of the disk specimen, typically 0.25 mm

a : radius of the support, 1.23 mm in the MIT MDBT.

Measured slopes from the linear region in the MDBT load/deflection curves are always less than those predicted by Eq. 3.1. This was found to be due mainly to the contribution from local plastic indentation of

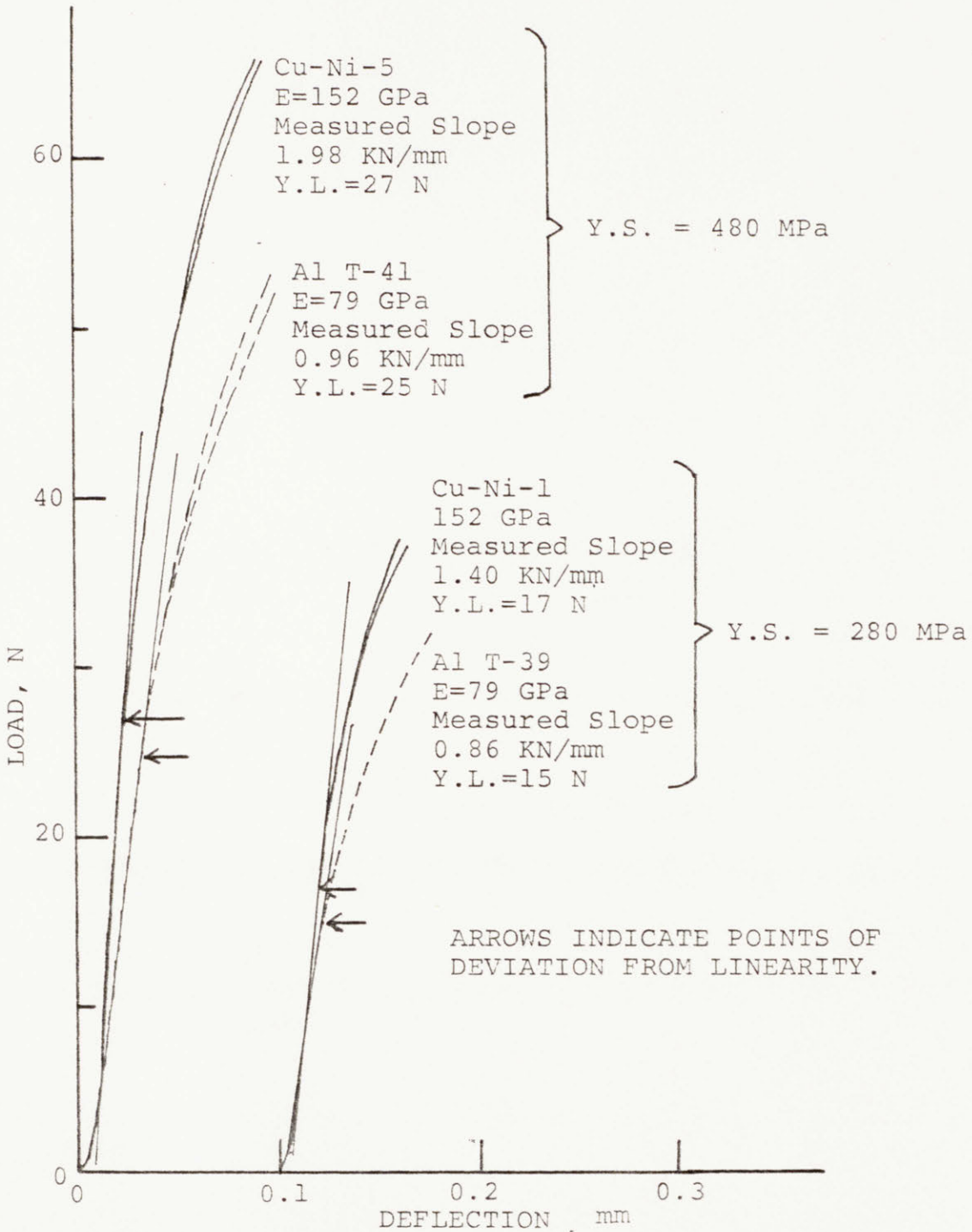


Figure 3.10 Expanded view of the initial linear regions of MDBT load/deflection curves, showing the strong effect of the elastic modulus on the slope.

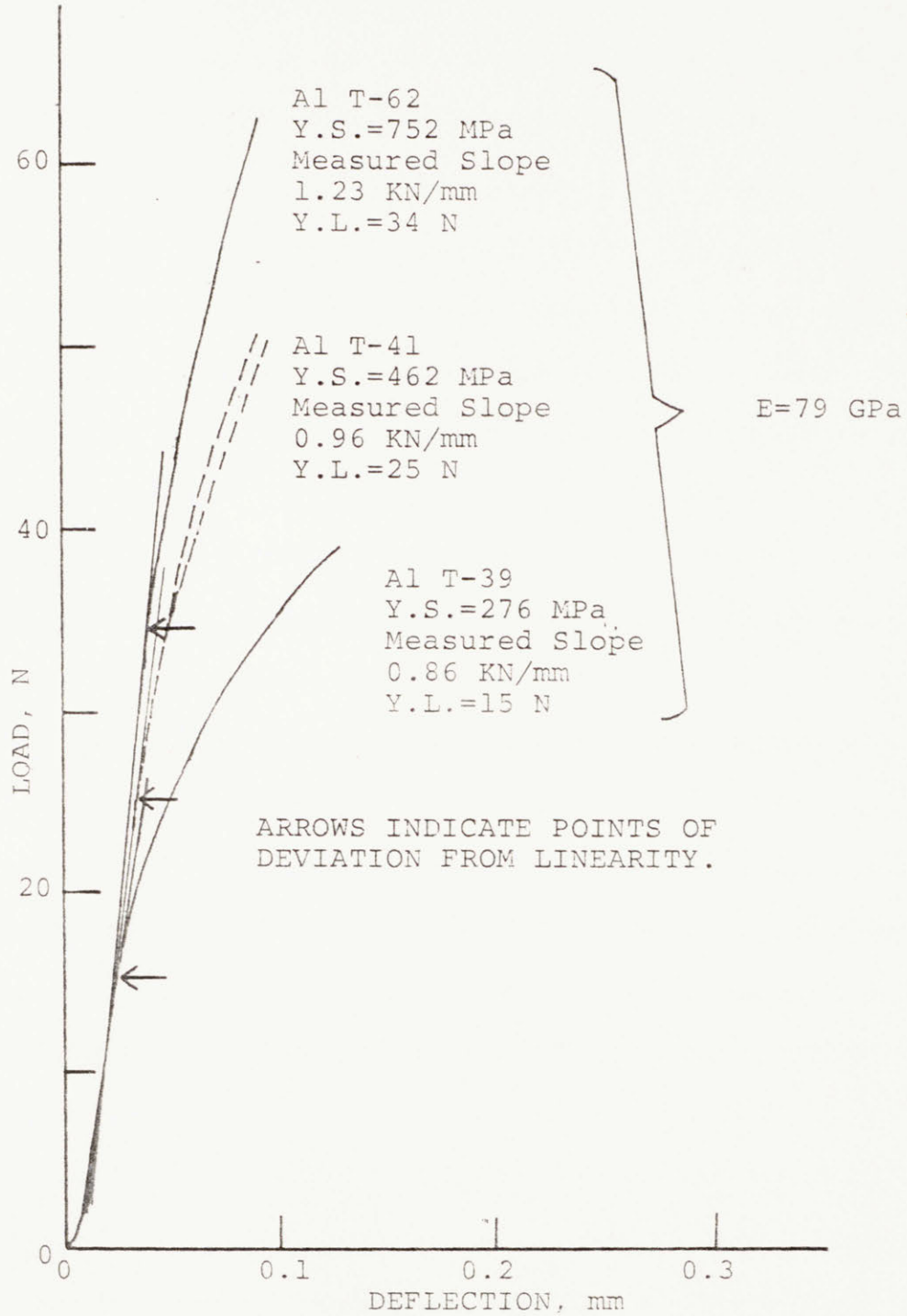


Figure 3.11 Expanded view of the initial linear regions of MDBT load/deflection curves, showing monotonic correlation between the yield strength and the yield load.

the disk by the punch tip. Usually a small indentation mark was found at the center of the disk even after loading to load levels less than the yield load, indicating local yielding and plastic indentation by the punch. Disk yielding at the punch contact point is found to occur as soon as contact is made, because the stress at that portion is very high due to the fact that a very tiny area carries all the applied load. This local plastic indentation would make the actual punch travel distance greater than the central deflection of the bulk disk. The deflection recorded in the MDBT is the actual punch travel distance and the one calculated by Eq. 3.1 is the disk deflection. As the applied load increases, the yielded region and the depth of local plastic indentation increase. This effect would appear as a smaller slope in measured load/deflection curves than the calculated slope because of the additional deflection due to local indentation. This interpretation explains the observed smaller slopes (smaller than predicted by Eq. 3.1.) in Fig. 3.10 and were verified in the finite element calculations for the MDBT. The results from ABAQUS showed local plastic indentation, as presented in the deformed configuration of the disk, see Appendix D, and the predicted slope matched well with experimental data as illustrated in Fig. 3.9.

The linear regions in Fig. 3.11 show different slopes for the same kind of alloy - thus for the same elastic modulus. This result seems mainly due to different local plastic indentation behavior of different yield strength materials. Disks with higher yield strength would resist plastic indentation more than those with lower yield strength. Higher

resistance to plastic indentation would cause less intrusion of the punch tip into the disk and thus a steeper slope. Therefore disks with higher yield strength would exhibit steeper slopes. This was verified by computer analysis. The ABAQUS code predicted shallower indentation at the same load level and steeper slope for higher yield strength material even when the elastic modulus was the same.

Fig. 3.11 also shows that the yield load is strongly dependant on the yield strength and is higher for higher yield strength material. This relationship between the yield load and the yield strength has been consistantly found in all the materials tested so far. In the computer study of the disk response in this region, the yielded region was found to initiate at the punch contacting region and propagate through the thickness and radially as shown in Appendix D. However the bulk of the disk was in the elastic regime and overall response of the disk was elastic. The disk response seemed to deviate from linearity when significant portions of the disk had yielded. The fraction of the yielded region at the observed deviation from linearity was about 10 % in most cases. Based on the results discussed above, it could be said that the deviation from linearity in the MDBT load/deflection curve was mainly related to the yielding of the material and thus the yield load is correlated with the yield strength of the material.

In order to estimate the yield strength from the measured yield load in the MDBT, an iterative procedure for yield load through the use of the ABAQUS finite element code was employed as follows:

1) Estimate the expected mechanical properties of the material and calculate disk response with the ABAQUS code using estimated mechenical properties.

2) Obtain the yield load from the ABAQUS load/deflection curve and compare it with experimental yield load.

3) If the yield loads are the same, the estimated yield strength is the yield strength measured in MDBT. If not, repeat steps one and two until both yield loads are matched.

In the testing of irradiated materials, which is the main purpose of this research, unirradiated material properties are usually available and relatively good estimations of irradiated mechanical properties are often possible by comparing MDBT curves before and after irradiation. Therefore the iterative procedure does not usually require many iterations.

ABAQUS finite element calculations require the plastic behavior data of the material as input and this data is hard to get in most cases. One possible way to provide this data from simple tensile data such as yield strength, ultimate strength , and ductility is to use the power law assumption for the material and fit the strength data to the power law. The power law can be expressed as $\sigma = K \varepsilon^n$ for true stress and true strain. The coefficients K and n are called as the strength coefficient and the strain-hardening exponent, respectively. Using the relationships among true stress/strain and engineering stress/strain, one can write as follows:

$$S_y = K*0.002^n \qquad 3.2$$

$$K*n^n = S_u*(1+n+n^2/2+\cdots) \qquad 3.3$$

where

$S_y$ = engineering yield stress

$S_u$ = ultimate tensile strength

When $n<0.05$, Eq. 3.3 can be approximated with errors less than about 5 % by

$$K*n^n = S_u \qquad 3.4$$

When $0.05<n<0.1$, Eq. 3.3 can be approximated with errors less than 0.5 % by

$$K*n^n = S_u*(1+n) \qquad 3.5$$

The coefficients K and n can be easily determined from yield strength and ultimate strength data using Eq.'s 3.2 and 3.4 or Eq.'s 3.2 and 3.5 depending on the estimated value of n. In cases where the calculated n was unreasonably low ( n is expected to be greater than uniform engineering strain), n was increased by 0.02 or 0.01. This adjustment seems not to affect the calculated disk response in the initial linear region as discussed in the following paragraph.

In order to check the effect of different strain hardening exponents on the calculated disk response, a parametric study was done using the finite element computer code ABAQUS. The input data used in this

study are shown in Table 3.2. The case U5 was calculated as the upper boundary for modified 316 type developmental alloys after iraadiation at 773 K. The strain hardening exponent for this irradiated material at 773 K was estimated as 0.04 and used in case U5 calculation. As one can see in the table, n was increased to 0.08 in case U58 in order to see the effect of different strain hardening exponent on the calculated disk response. Other input data were the same for both case calculations. Calculated disk responses in the initial linear region are presented in Table 3.3. Considering the convergence limit of 1.4 Newton on the load used in these calculations, the differences are negligible and the results are almost identical. Therefore, the result of this parametric study seems to show the negligible effect of 0.04 or 100 % change in strain hardening exponent on the linear region disk response and the insignificant effect of minor adjustment in strain hardening exponent.

Use of the power law assumption for a material which does not follow the power law may produce significantly different plastic behavior data even if correct strength and ductility data were used in the calculation. However, the possible error introduced by the use of the power law assumption in determining the plastic behavior of the material seems to be insignificant based on the following observations. As can be seen from the strain contour plot of the specimen at the point of deviation from linearity, presented in Fig. 3.12, most of the disk volume (>90 %) stays in the elastic range and only 0.8 % of the disk volume experiences strains higher than 5 %. Generally the difference between the flow stress calculated using the power law assumption and that of actual material would be significant in the 30-60 % true strain range and the

Table 3.2 Mechanical property data used in a parametric study of the effect of different plastic behavior on disk response.

Elastic Properties:

Elastic Modulus: $159 \times 10^9$ Pa.

Poison's Ratio : 0.3

Yield Strength : 752 MPa.

Plastic Behavior

| Plastic Strain | Flow Stress, MPa | |
|---|---|---|
| | Case U5 | Case U58 |
| 0.000 | 752 | 752 |
| 0.006 | 794 | 840 |
| 0.010 | 809 | 869 |
| 0.018 | 824 | 903 |
| 0.048 | 856 | 974 |
| 0.098 | 879 | 1028 |
| 0.248 | 913 | 1107 |
| 0.998 | 965 | 1236 |

Table 3.3 Effect of strain hardening exponent change (0.04 or 100% change) on the initial load/deflection response of the disk specimen, showing relative insensitivity of the initial disk response to the change of plastic behavior.*

| Defelction, mm | Load, Newton | |
|---|---|---|
| | Case U5 n=0.04 | Case U58 n=0.08 |
| 0.0025 | 7.598 | 7.598 |
| 0.0051 | 16.60 | 16.60 |
| 0.0076 | 24.15 | 24.60 |
| 0.0102 | 39.54 | 39.71 |
| 0.0127 | 44.82 | 46.00 |
| 0.0152 | 54.08 | 55.25 |
| 0.0178 | 63.17 | 64.71 |
| 0.0191 | 67.73 | 68.92 |
| 0.0203 | 70.12 | 72.19 |
| 0.0216 | 73.71 | NA |
| 0.0229 | 77.71 | 78.81 |

* 1. Input data are presented in Table 3.2.

2. Convergence limit used was 1.4 N.

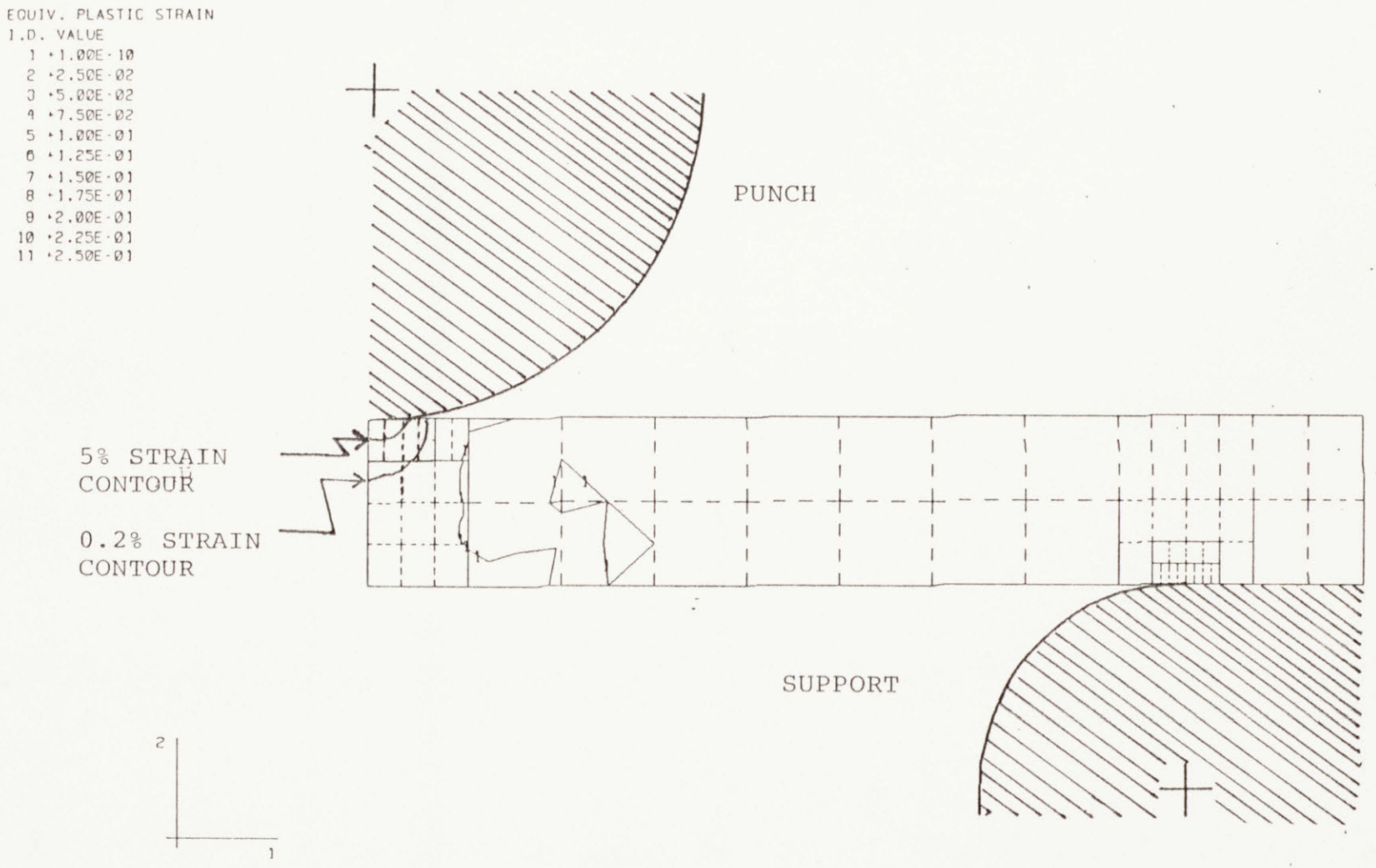


Figure 3.12 Typical strain contours at the deviation point from linearity, showing greater than 90% of the disk volume stays in elasticity range and only 0.8% of the disk volume experiences strains higher than 5%.

maximum of such difference would not exceed 30 % of the power law flow stress at that strain. Therefore, the effect of about 30 % difference in flow stress would be confined to about 0.8 % of the total volume and almost all of the disk volume would not be affected even if the power law assumption is used for some material which does not follow the power law plastic behavior. This would appear as a negligible difference on the calculated load/deflection response in the initial linear region. Furthermore, in irradiated material, irradiation increases the yield strength and reduces the difference between the yield strength and the ultimate strength so that the possible difference between the power law flow stress and the actual material flow stress is decreased. The parametric study discussed above supports this explanation. The input data presented in Table 3.2 shows about 21 % difference in flow stress at 25 % strain for two cases and the result shows the negligible effect of such difference on calculated disk response, in the linear region, as can be seen in Table 3.3. Therefore it can be concluded that the use of the power law assumption for the plastic behavior of a material which does not follow the power law would not introduce significant error.

In order to check the validity of the proposed iterative method, ABAQUS calculations were done for various materials with known material properties. ABAQUS yield loads obtained from calculated curves are compared with experimental yield loads in Fig. 3.13. The result shows good agreement, within experimental error, between these two yield load values and thus indicates that the MDBT combined with the proposed analysis method can estimate the yield strength with reasonable accuracy. More detailed descriptions are presented in Subsection 3.1.4.

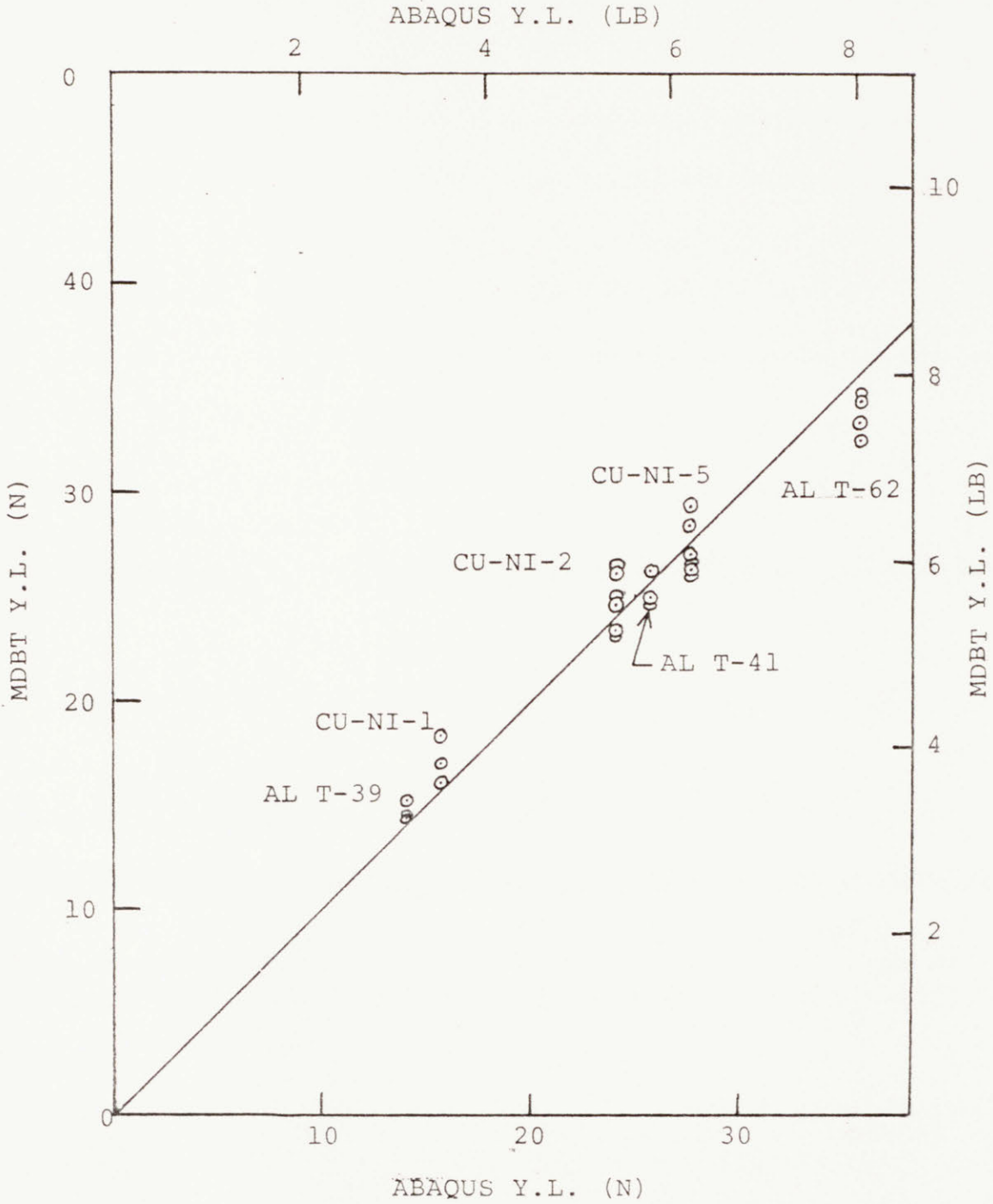


Figure 3.13 Comparison of yield loads obtained from MDBT and from computer calculated load/ defection curves for several cupro-nickel and aluminum alloys, showing good agreement between the two yield load values.

3.1.3 Ductility Calculation MDBT load/deflection curves of brittle disk specimens show a sudden drop of load after the initial linear region as can be seen in the typical curve in Fig. 3.1. Post-test examination indicated that such disks failed along radial cracks initiated at the disk center where the tensile strain is maximum during the bending mode of deformation. For small deflection in the bending of a circular disk, the spherical cap geometry assumption is usually adopted. A schematic drawing of a spherically bent disk specimen is presented in Fig. 3.14. From the figure, the radius of curvature is

$$\rho = (a^2+w^2)/(2*w) \qquad 3.6$$

where $\rho$ : radius of curvature of the bent disk

$a$ : radius of the support

$w$ : central deflection of the disk

and thus the strain is

$$\varepsilon = t/(2*\rho) = t*w/(a^2+w^2) \qquad 3.7$$

where $t$ : thickness of the disk

An equation of the same form was derived by Huang, Hamilton and Wire (reference 3.9). In their derivation, they used the radius of the disk specimen in place of the the radius of the support probably due to the fact that their disk specimens and support have about the same radii. This approach for estimating the ductility of the specimen was verified by comparing the tensile ductility with bend ductility of the disk

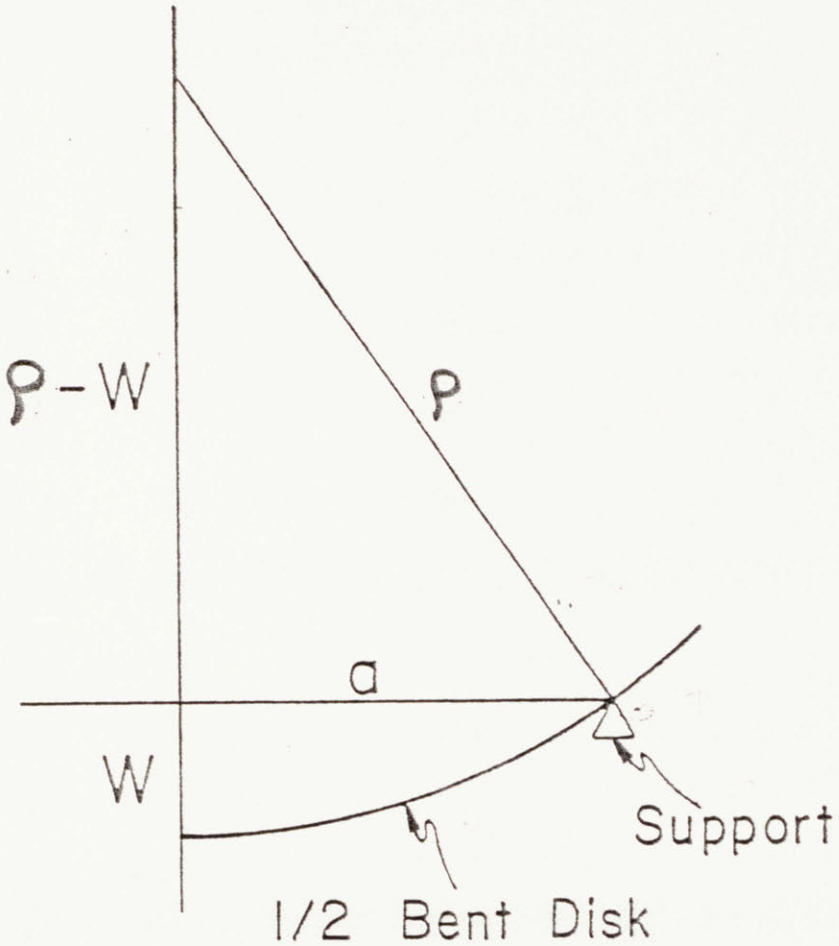


Figure 3.14 Geometry of a spherically deformed disk specimen.

specimens machined from the grip ends of the same conventional tensile specimen. Their data showed good agreement between bend ductilities and tensile ductilities for several kinds of irradiated developmental alloys. The differeneces between the MIT MDBT and Huang, et al.'s test geometries are the smaller radius of the support (1.23 mm vs. 1.50 mm) and of the punch tip (0.51 mm vs. 1.59 mm) used in the MIT Test (reference 3.10). The size of the disk specimen is the same in both cases. The larger radius of the punch tip, larger than that of the support in Huang, et al.'s geometry limits the testing to the bending mode regime. The use of the smaller radius punch tip than that of the support in the MIT test permits larger deflection of the disk and a test which can provide load/deflection curves for ductile materials. On the other hand, the small radius punch tip in the MIT test will introduce more local plastic deformation and potential error in the measurement of bulk disk deflection. The difference in the support radius should not make a fundamental difference in the testing. The larger the support radius, the greater the specimen deflection for a given punch tip radius . If we confine our interest to the testing of brittle material which is the limitation for the application of Eq. 3.3, the differences in test geometry should not make much difference because the test is essentially in the simple bending mode in both cases and the effect of local plastic indentation in the MIT test is minimal at this small deflection. The validity of Eq. 3.3 for the MDBT in the MIT system was checked with two aluminum alloys with different ducitilities. The result is summarized in Table 3.4. The materials used in these tests

Table 3.4 Result of verification tests for ductility analysis method using two aluminum alloys.

| Material[1] | Ref. Duct. | MDBT Ductility, % | | Measured[2] Deflection mm (mil) | Estimated[3] Indent Depth mm (mil) |
|---|---|---|---|---|---|
| | | With Indent Depth Correction | Without Indent Depth Correction | | |
| Al T-Ingot. | 1.5% | 1.9 | 2.1 | 0.12(4.9) | 0.010(0.39) |
| | | 2.2 | 2.3 | 0.14(5.5) | 0.011(0.42) |
| Al T-62 | 4.0% | 5.1 | 5.4 | 0.33(12.9) | 0.018(0.70) |
| | | 4.4 | 4.7 | 0.27(10.8) | 0.019(0.76) |

N.B 1. Two specimens from each alloy were tested for ductility. Specimen disks were machined from the grip ends of a tested tensile specimen. Materials are described in Reference 3.10

2. Deflection was corrected for system stiffness.

3. Indent depth was estimated from the difference between measured slope and calculated slope using Eq. 3.1.

are described in reference 3.11 and the test is described in Subsection 3.1.4. The two ductility values show good agreement with reference values when measured deflections were corrected for the indent depth estimated from the difference between measured and calculated slopes using Eq. 3.1. If local indentation of the disk is a major contributor to the difference in the slopes, the indent depth would be the difference between the deflection expected from the measured slope and that from the calculated slope at a given load. This kind of correction can be applied on irradiated materials with ease. A larger number of test specimens would have been desirable for the verication of this technique. However, as discussed above, similar technique has been verified by Huang, et al. and differences between the two techniques should not make significant differences in the test results, the good agreement obtained from two alloys was thought to verify the technique used in the MIT MDBT. More tests with specimens of wider range of ductilities are suggested for future work.

3.1.4 Reference Test for Verification Final validation of the analysis method proposed in this chapter would be actual application of the method to materials with known properties. Five aluminum alloys, Al T-ingot, -62, -44, -41 (reference 3.11) and -39 (reference 3.12) and three cupro-nickel alloys, Cu-Ni-1, -2 and -5 (reference 3.13) and a modified 9Cr-1Mo alloy (reference 3.14) had been used for this purpose. All the aluminum alloys and cupro-nickel alloys except Al T-ingot were rapid solidification processed and were given different thermo-mechanical treatments to achieve different mechanical properties. Al T-ingot

was used in the ingot state. A summary of their mechanical properties is presented in Table 3.5. In the case of aluminum and cupro-nickel alloys, disk specimens were machined as shown in Fig. 3.15 from the grip ends of a tensile specimen that had been conventionally tested. For the modified 9Cr-1Mo alloy, specimens were taken from the same lot as reported in reference 3.13. Disks of 3 mm diameter and 0.41 mm thickness were cut out and wet ground on both sides to 0.254$\pm$ 0.0025 mm (0.0100$\pm$0.0001 in) thickness with 600 grit abrasive paper. Specimen disks were bend tested in the testing system described in Chapter 2. Measured load/deflection curves for Al T-ingot and -62 show brittle type curves similar to the typical curve shown in Fig. 3.1 and bend ductilities were calculated using Eq. 3.7. The results are presented in Table 3.4 and show good agreement with the reference ductilities measured in conventional uniaxial tests. This good agreement and the discussions presented in Subsection 3.1.3 indicate that, for brittle material, ductilities can be measured in the MIT MDBT using Eq. 3.7.

All the other alloys showed ductile type MDBT load/deflection curves similar to the one presented in Fig. 3.1. Yield loads were obtained from these load/deflection curves. Computer analyses were done with the ABAQUS finite element code for all the cupro-nickel and aluminum alloys except Al T-ingot and -44 . ABAQUS yield loads were derived from calculated load/deflection curves and compared with the corresponding experimental yield loads. Mechanical properties of Al T-44 were in between those of Al T-62 and -41. Calculated load/deflection responses of the latter two alloys were close and

Table 3.5 Summary of mechanical properties of the materials used in reference tests for the verification of the technique for extracting yield strength using the MIT MDBT approach.

| Alloy | | Yield Strength MPa | Ultimate Tensile Strength MPa | Ductility % | Elastic Modulus GPa |
|---|---|---|---|---|---|
| Al alloy | T-62[1] | 752 | 779 | 4.0 | 78.6 |
| | T-44[1] | 600 | 724 | 8.6 | 78.6 |
| | T-41[1] | 462 | 600 | 16.4 | 78.6 |
| | T-39[2] | 276 | 372 | 8.0 | 78.6 |
| | T-Ingot[1] | 738 | 752 | 1.5 | 78.6 |
| Cu-Ni alloy | Cu-Ni-1[3] | 276 | 365 | 31 | 117.2 |
| | Cu-Ni-2[3] | 421 | 476 | 24 | 117.2 |
| | Cu-Ni-5[3] | 496 | 579 | 32 | 151.7 |
| Modified 9Cr-1Mo[4] | | 710 | 807 | 18.7 | 206.9 |

| Alloy | | Composition (wt.%) and Thermo-mechanical treatments |
|---|---|---|
| Al alloy | | All Al-alloys : TMT after extrusion(28/1) @ 400°C |
| | T-Ing. | 0.01Mn, 0.03Ti, 0.07Si, 0.13Fe, 0.21Cr, 0.76Zr, 1.00Ni, 1.70Cu, 3.05Mg, 6.27Zn, bal. Al sol. @ 460°C 1hr, water quench, age 24hr @ 120°C |
| | T-62 | The same composition as T-Ing. sol. @ 490°C, age 24hr @ 120°C |
| | T-44 | The same composition as T-Ing. sol. @ 490°C, age 24hr @ 120°C |
| | T-41 | The same composition as T-Ing. sol. @ 460°C, age 24hr @ 120°C |
| (A17075-39) | T-39 | The same composition as T-Ing. RSP, As extruded. |
| Cu-Ni alloy | Cu-Ni-1 | 10.1Ni, 2.15Fe, bal.Cu/Extrusion(25/1) @ 750°C |
| | Cu-Ni-2 | 10.7Ni, 8.23Fe, bal.Cu/Extrusion(25/1) @ 750°C |
| | Cu-Ni-5 | 30.4Ni, 2.74Cr, bal.Cu/Extrusion(25/1) @ 750°C |

N.B. 1. Reference 3.11
2. Reference 3.12
3. Reference 3.13
4. Reference 3.14

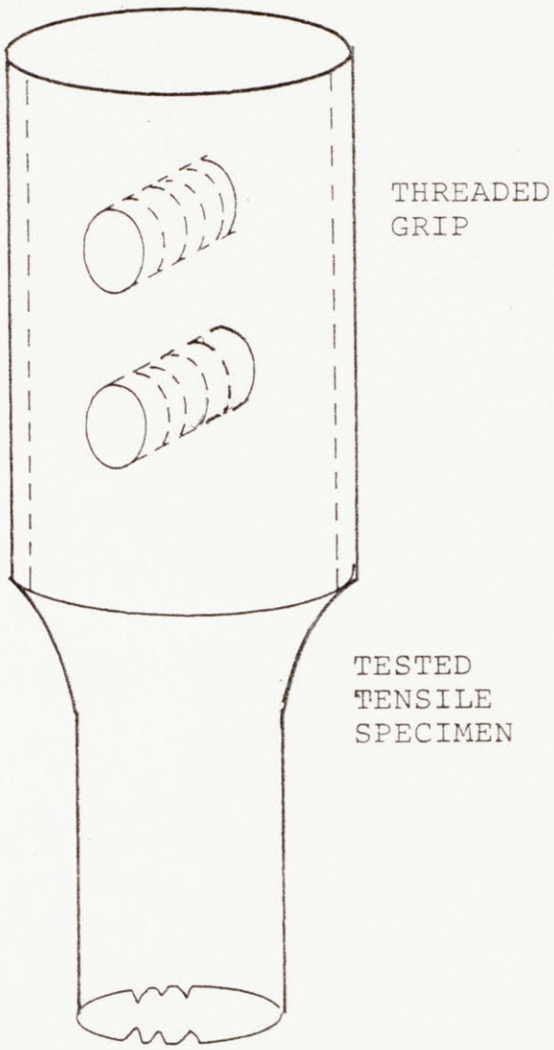


Figure 3.15 A tested tensile specimen showing the locations where disk specimens were machined for use in the MDBT.

the load/deflection response of Al T-44 was estimated from an interpolation of the calculated results for Al T-62 and -41.

All the load/deflection curves obtained from MDBT show linear response in the initial region. When the data for the initial linear regions of different alloys were fitted to straight lines, the correlation coefficients of the fittings were better than 0.998 in all the cases. The initial linear region of the MDBT load/deflection curve can be characterized by the yield load and the slope. The linear regions exhibited strong dependence on the yield strengths and the elastic moduli as illustrated in Fig.'s 3.16 and 3.17 as well as Fig.'s 3.10 and 3.11. Fig. 3.16 shows the strong effect of the yield strength on the yield load and the relatively weak effect of elastic modulus. As can be seen in Fig. 3.17, the slope of the linear region seems to be governed mainly by the elastic modulus and, to a much less extent, by the yield strength. The slope data presented were corrected for the load train compliance. Above observation seems to verify that the linear region in MDBT load/deflection curve is governed mainly by the elastic modulus and yield strength of the material and that the yield load has strong correlation with the yield strength.

The results of the finite element computer calculations demonstrate good simulation of the yield loads as illustrated in Fig. 3.13 and as summarized in Table 3.6. Because the first calculation showed good agreement with the experimental results, no further iterative calculations were done. However, the yield loads obtained from computer calculated load/deflection curves were not exactly the same as experimentaly measured yield loads. Therefore interpolation was used to

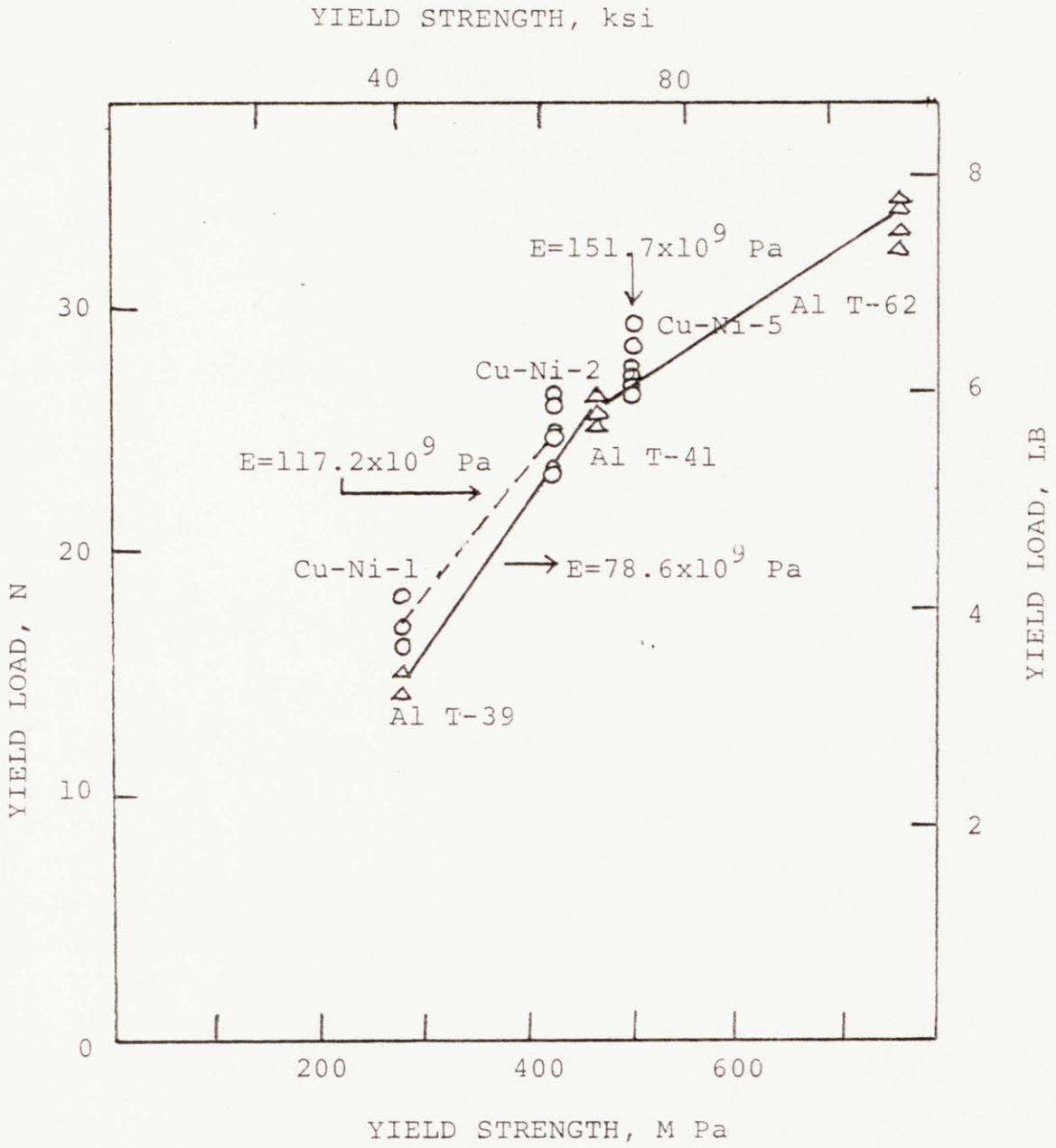


Figure 3.16 Effect of yield strength and elastic modulus on measured yield load, showing strong effect of yield strength on the yield load.

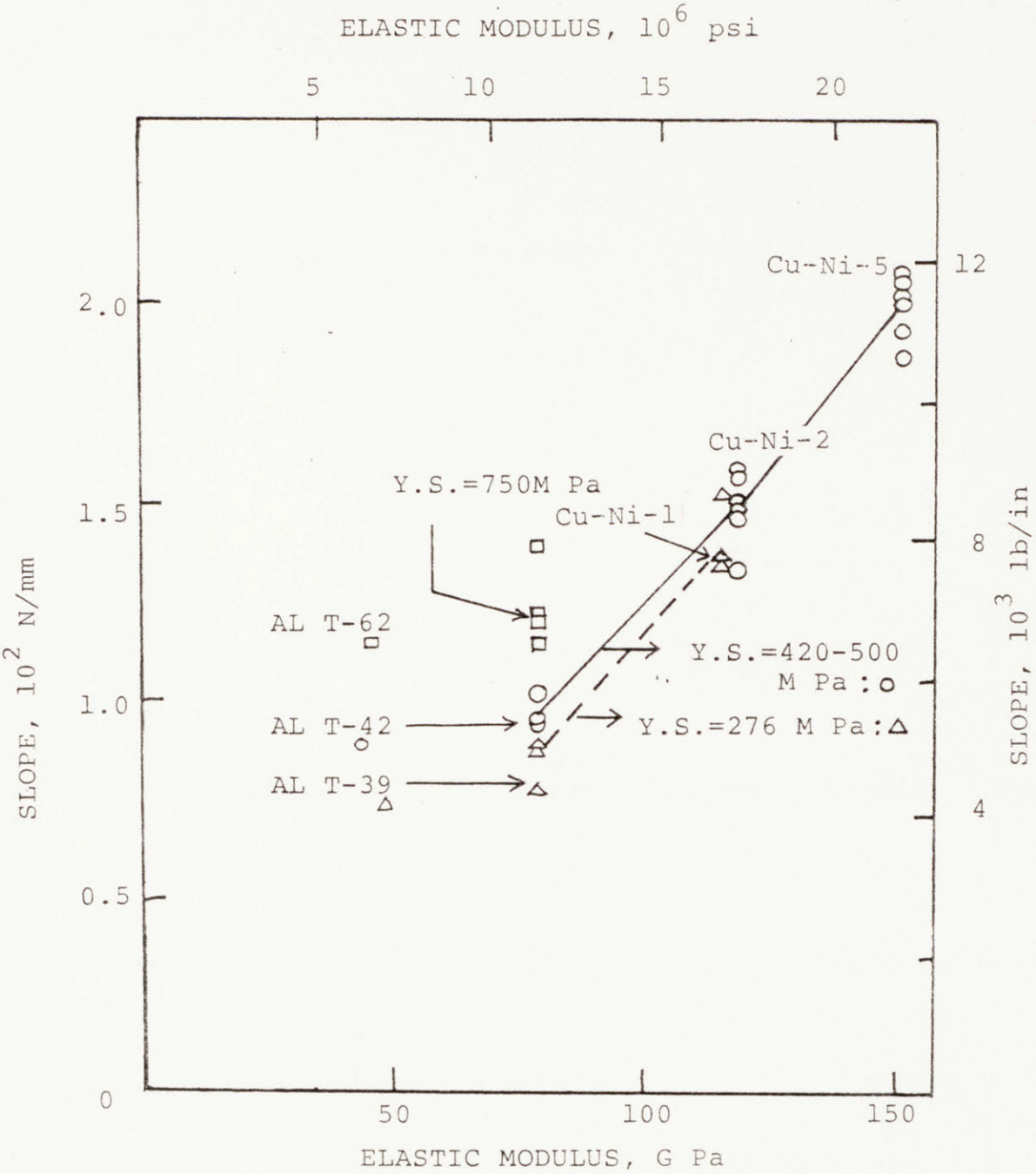


Figure 3.17 Effect of elastic modulus and yield strength on the slope of linear region in MDBT load/dfln curve.

Table 3.6 Summary comparison of the MDBT experimental results and the computer simulated (by the finite element code ABAQUS) yield loads, results of three to six measurements, showing good agreements.

| Material | MDBT[1] Y.L., N | ABAQUS Y.L., N | Material | MDBT[1] Y.L., N | ABAQUS Y.L., N |
|---|---|---|---|---|---|
| Al T-62[2] | 34.7<br>34.2<br>33<br>32.5 | 35.8 | Cu-Ni-1[3] | 16.0<br>16.9<br>18.2 | 15.6 |
| Al T-41[2] | 24.9<br>24.9<br>26.2 | 25.6 | Cu-Ni-2[3] | 23.4 26.4<br>24.5<br>23.3<br>24.4<br>26.1 | 24.0 |
| Al T-39[2] | 14.2<br>14.2<br>15.1 | 14.0 | Cu-Ni-5[3] | 27.1 28.5<br>26.2 26.2<br>26.7<br>29.4 | 27.6 |

N.B. 1. These tests are described in detail in Subsection 3.1.4.

2. Reference 3.11.

3. Reference 3.13

obtain yield strengths for all the materials. As shown in Table 3.7, interpolation was done as follows:

1) two ABAQUS results with close yield strength values and the same elastic modulus (the results for Al T-62 and -41 in the first interpolation in Table 3.7) were fitted to a linear equation, (Y.S. in MPa) = 28.43X(Y.L. in N) - 265.8, in this case.

2) yield strengths were calculated from measured yield loads using the above equation.

Computer calculation results for the irradiation test of modified type 316 stainless steel (SS) were used for the interpolations of Cu-Ni-5 alloy and modified 9Cr-1Mo alloy. The elastic modulus and the yield strength of the Cu-Ni-5 alloy at room temperture are about the same as the elastic modulus and the lower bound estimate for yield strength of irradiated type 316SS at 773 K. Therefore the computer calculation results for the upper bound case of irradiated 316SS at 773 K as well as for Cu-Ni-5 alloy were used in the interpolation for Cu-Ni-5 alloy. Similarly the computer calculation results of the upper and the lower bounds for irradiated 316SS at room temperture were used in the interpolation for modified 9Cr-1Mo alloy. The data used in these interpolations and the results are summarized in Table 3.7. The results from MDBT with finite element analysis are compared with the reference yield strengths obtained in conventional uniaxial tensile tests in Fig. 3.18. The MDBT results show good agreement with the conventional test results.

The plastic behavior of materials were fitted to a power law in all the input preparations for computer calculation. This procedure is

Table 3.7 Yield strength estimations from MDBT results, showing the computer calculation results used in the linear interpolation (a) and the estimated yield strengths from interpolation (b). Several MDBT measurements were made for each alloy and the experimental yield loads for each measurement are shown in the table below.

1. Estimations for Al T-62, -44 and -41.

a) Computer calculation results
- Al T-62 Y.S.=752 MPa, Y.L.=35.8 N
- Al T-41 Y.S.=462 MPa, Y.L.=25.6 N

b) Estimated results using above two results for a linear interpolation of Y.S.

| Material | Al T-62 | | | | Al T-44 | | Al T-41 | | |
|---|---|---|---|---|---|---|---|---|---|
| Measured Y.L.,N | 34.7 | 34.2 | 33.4 | 32.5 | 28.0 | 31.6 | 24.9 | 24.9 | 26.2 |
| Estimated Y.S., MPa | 719 | 705 | 682 | 657 | 530 | 631 | 442 | 442 | 479 |

2. Estimations for Al T-41 and -39.

a) Computer calculation results
- Al T-41 Y.S.=462 MPa, Y.L.=25.6 N
- Al T-39 Y.S.=276 MPa, Y.L.=14.0 N

b) Estimated results using above two results for a linear interpolation of Y.S.

| Material | Al T-41 | | | Al T-39 | | |
|---|---|---|---|---|---|---|
| Measured Y.L.,N | 24.9 | 24.9 | 26.2 | 14.2 | 14.2 | 15.1 |
| Estimated Y.S., MPa | 451 | 451 | 472 | 279 | 279 | 294 |

Table 3.7 Continued.

3. Estimations for Cu-Ni-1 and Cu-Ni-2.

a) Computer calculation results
- Cu-Ni-1 Y.S.=276 MPa, Y.L.=15.6 N
- Cu-Ni-2 Y.S.=421 MPa, Y.L.=24.0 N

b) Estimated results using above two results for a linear interpolation of Y.S.

| Material | Cu-Ni-1 | | | Cu-Ni-2 | | | | | |
|---|---|---|---|---|---|---|---|---|---|
| Measured Y.L.,N | 16.0 | 16.9 | 18.2 | 23.4 | 24.5 | 23.3 | 24.4 | 26.1 | 26.4 |
| Estimated Y.S., MPa | 283 | 298 | 321 | 411 | 430 | 409 | 428 | 457 | 462 |

4. Estimations for Cu-Ni-5.

a) Computer calculation results
- Cu-Ni-5 Y.S.=496 MPa, Y.L.=27.6 N
- U5[1] Y.S.=752 MPa, Y.L.=40.3 N

b) Estimated results using above two results for a linear interpolation of Y.S.

| Material | Cu-Ni-5 | | | | | |
|---|---|---|---|---|---|---|
| Measured Y.L., N | 27.1 | 26.2 | 26.7 | 29.4 | 28.5 | 26.2 |
| Estimated Y.S., MPa | 486 | 468 | 378 | 532 | 514 | 468 |

5. Estimations for modified 9Cr-1Mo.

a) Computer calculation results
- LR[2] Y.S.=496 MPa, Y.L.=28.0 N, $E=201.3\times10^9$ Pa
- UR[2] Y.S.=752 MPa, Y.L.=41.8 N, $E=201.3\times10^9$ Pa

b) Estimated results using above two results for a linear interpolation of Y.S.

Table 3.7 Continued.

| Material | Modified 9Cr-1Mo | | | | | |
|---|---|---|---|---|---|---|
| Measured Y.L., N | 39.5 | 41.1 | 39.7 | 40.1 | 42.5 | 41.4 |
| Estimated Y.S., MPa | 709 | 739 | 713 | 720 | 765 | 745 |

N.B. 1 The case for 773 K upper bound for the irradiation test of modified type 316 stainless steel alloys.

2 The upper (UR) and lower (LR) bound cases for modified type 316 stainless steel at room temperature.

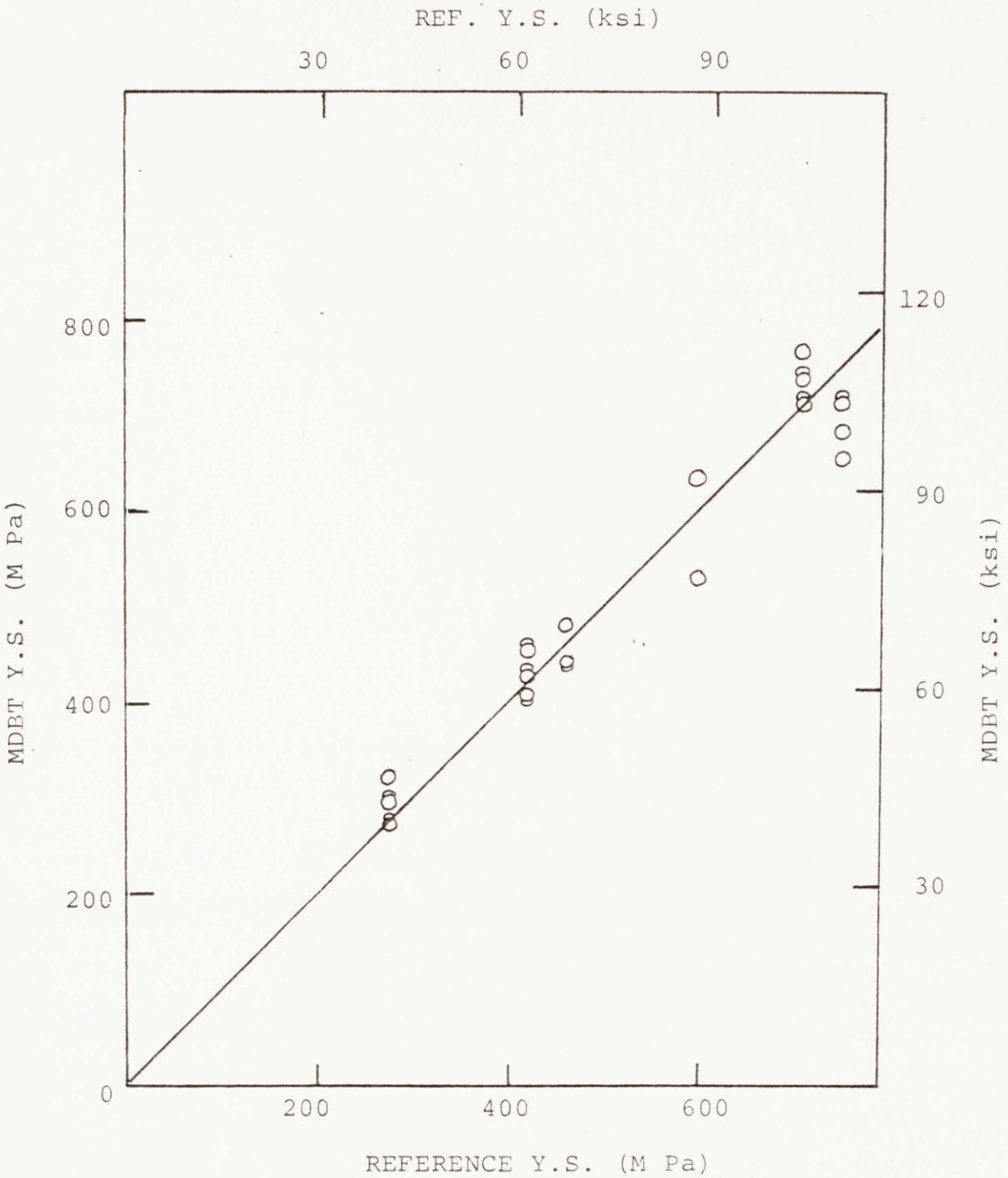


Figure 3.18 Comparison of yield strengths measured in MDBT with those measured in conventional tensile test. MDBT specimen disks were machined from the grip of a previously tested specimen.

described in Subsection 3.1.2. As discussed in that Subsection, the results for yield strength are not very sensitive to the assumed hardening behavior. The good agreement shown in the final results for the MDBT estimated YS and reference YS seems to verify this. Therefore the results obtained from ABAQUS analyses can be used in the estimation of yield strength for any material with yield strength and elastic modulus within or close to the material property matrix used in the computer analyses. All the computer analysis results done so far are presented in Fig. 4.3 along with the reference test results. This figure can be used for the estimation of yield strength for unknown material using the MDBT measured yield load and the known or estimated elastic modulus.

## 3.2 Ductile-Brittle Transition Test using the MDBT Approach

The possibility of ductile-brittle transition testing using the MDBT approach was explored using maximum loading speed of the Instron 1332 dynamic testing machine. The loading speed obtained was 2.5 m/s corresponding to strain rates of the same order as those expected in conventional Charpy V-notch impact testing. Some initial results for ferritic 410SS are presented in Fig. 3.19. These show MDBT load/deflection curves carried out to fracture for temperatures ranging from room temperature (RT) to 133 K. The curves at RT and the band containing nine tests at 183 K represent predominantly ductile fracture. The curves obtained at 173 K and lower exhibit a clear change in the characteristic shape of the load/deflection curve, i.e., a sudden

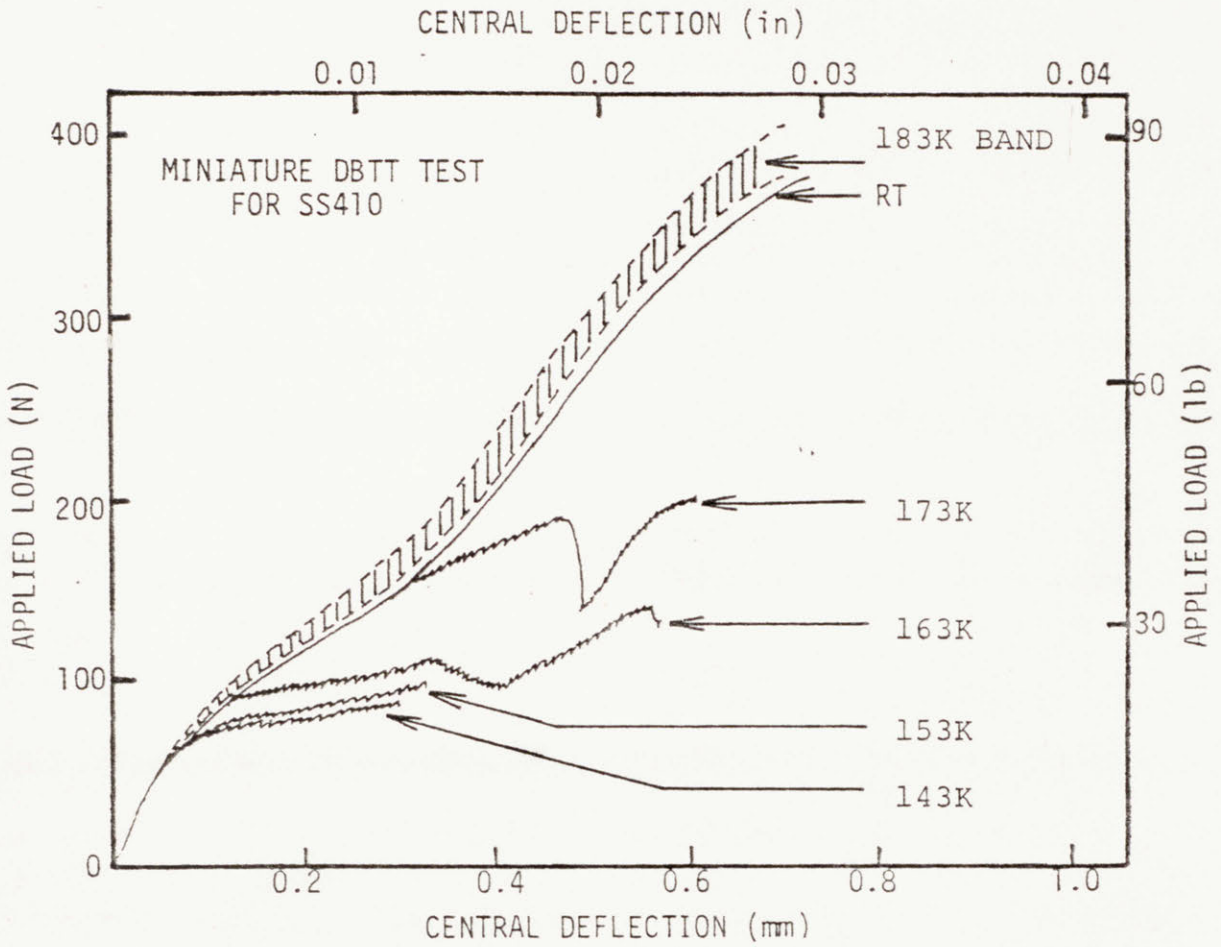


Figure 3.19 MDBT impact test curves showing ductile - brittle transition at about 173K.

reduction in the area under the curve, lower maximum load and earlier drop of the load. Fractographic evidence, as shown in Fig. 3.20, verifies dominantly brittle fracture at 173 K and dominantly ductile fracture at RT.

As expected, the miniaturization of the specimen shifted the transition temperature downward from the standard Charpy ductile-brittle transition temperature (DBTT) of about 343 K. In order to shift the measured transition temperture to higher temperature, the specimen disk was notched along the diameter to about 0.13 mm depth. Results of tests on notched disks are shown in Fig. 3.21 and indicate a higher transition temperature of about 223 K. Although these results are preliminary, they demonstrate the potential of MDBT to measure relative changes in DBTT.

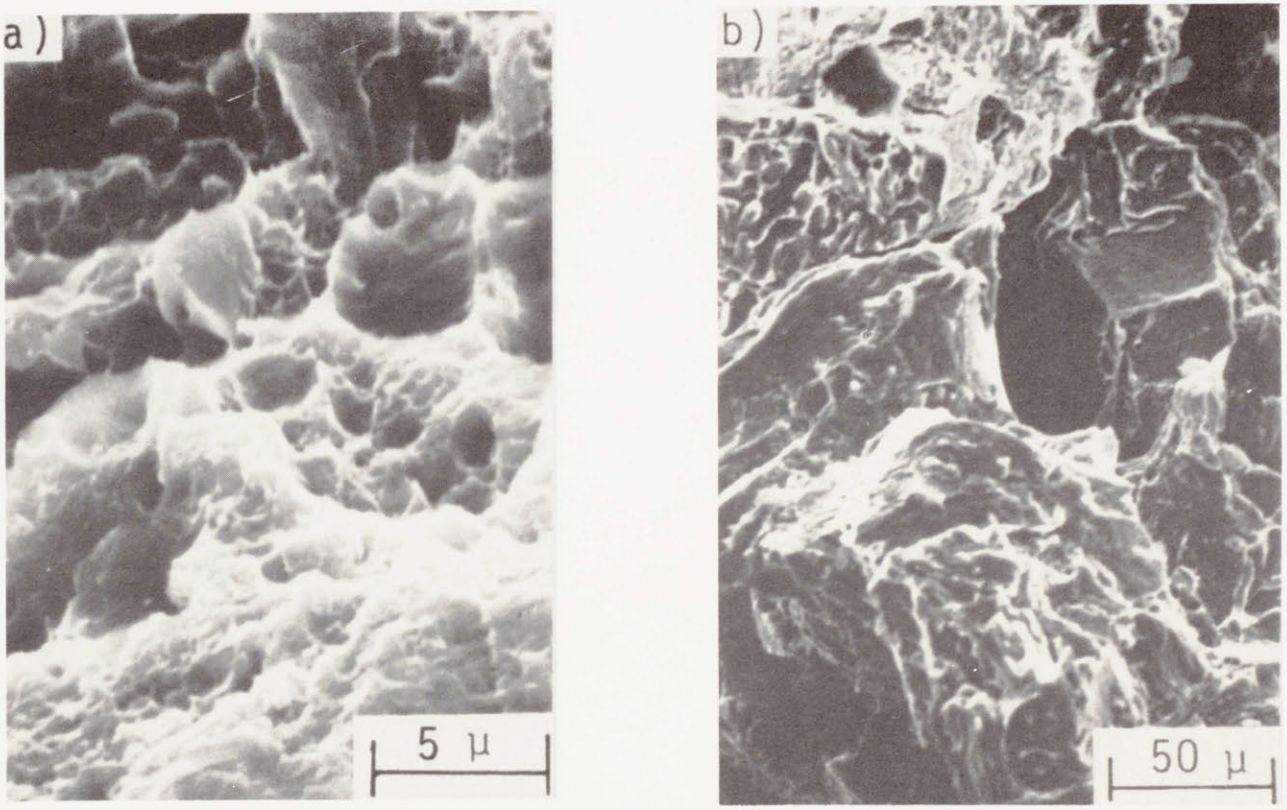


Figure 3.20 Fractographs of impact tested specimens, showing ductile fracture at room temperature (a) and predominantly brittle fracture at 173 K (b).

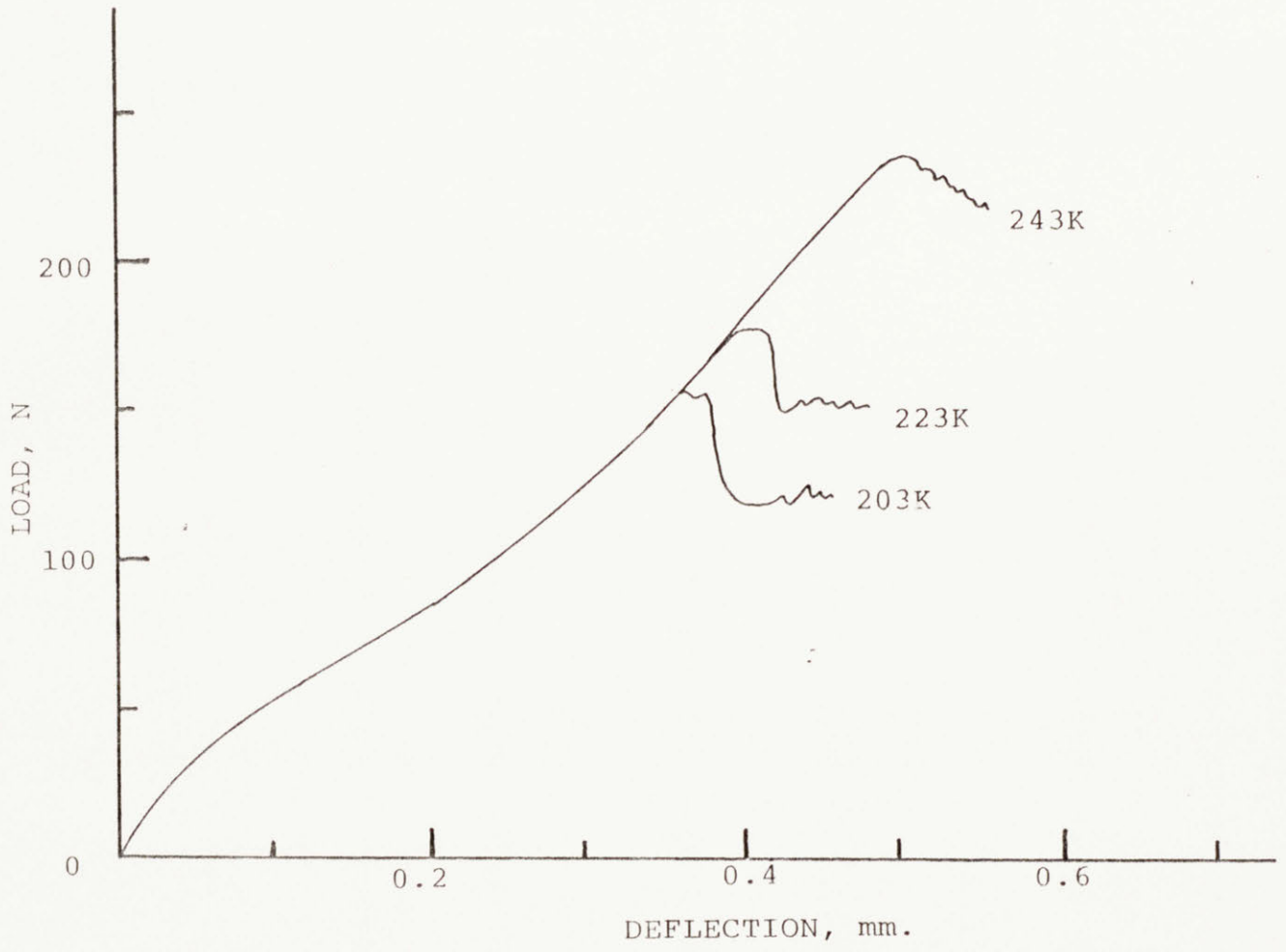


Figure 3.21 MDBT impact test curves of notched disk specimens, showing ductile - brittle transition at about 223K.

References for Chapter 3


3.1 N.F. Panayotou and E.K. Opperman, "Specimen Size Effect and Fusion Materials Research", DOE/ER-0045/8, pp 25-65

3.2 M.P. Manahan, "The Development of A Miniaturized Disk Bend Test for The Determination of Post-Irradiation Mechanical Behavior", Sc.D. Thesis, Dept. of Nucl. Eng., MIT, (May, 1982)

3.3 M.P. Manahan, A.S. Argon and O.K. Harling, J. Nucl. Matr., 103 & 104, (1981), pp 1545-1550

3.4 O.K. Harling, M. Lee, D-S Sohn, G. Kohse and C.W. Lau, "The MIT Miniaturized Disk Bend Test", presented at the ASTM Symposium on the Use of Nonstandard Subsized Specimens for Irradiation Testing, Albuquerque, N.M., Sept. 1983, to be published in an ASTM STP

3.5 O.K. Harling, M. Lee, D-S Sohn, G. Kohse and N.J. Grant, "Neutron Irradiated Mechanical Properties of Some Rapidly Solidified Austenitic Stainless Steels", submitted to the Twelfth Symposium on the Effects of Radiation on Materials, Williamsburg, Va, June, 1984, to be published in an ASTM STP

3.6 G.E. Kohse, "Ion Bombardment Effects on The Fatigue Life of Stainless Steel under Simulated Fusion First Wall Conditions", Ph.D. Thesis, Dept. of Nucl. Eng., MIT, (Feb., 1983)

3.7 Hibbitt, Karlson and Sorenson, "ABAQUS, User's Manual", Version 4, Jul. 1982, Hibbitt, Karlson and Sorenson Inc.

3.8 R.J. Roarke and W.C. Young, "Formulas for Stress and Strains", 5th ed McGraw-Hill Book Co., N.Y. (1975)

3.9 F.H. Huang, M.L. Hamilton and G.L. Wire, "Bend Testing for Miniature Disks", Nucl. Techn., Vol. 57, (May, 1982), p 234-242

3.10 M.L. Hamilton, Private Communication on July 18, 1984

3.11 E.J. Lavernia, "Liquid Dynamic Compaction of A Rapidly Solidified 7075 Aluminum Alloy Modified with 1% Ni and 1% Zr", M.S. Thesis, Dept. of Matr. Sci. and Eng., MIT, (Feb, 1984)

3.12 E.Y. Ting, "Atomization and Properties of A Modified 7075 Aluminum Alloy", Ph.D. Thesis, Dept. of Matr. Sci. and Eng., MIT, (May, 1984)

3.13 S.H. Kang, P. Domalavage and N.J. Grant, "Structure-Property Relationships for Rapidly Solidified, Modified Cupro-Nickel Alloys", Fianl Report to David Taylor Naval Ship Research and Development Center, Contract No. N000167-82-C-0131, Feb. 1984

3.14 V.K. Sikka, "Data Package on Modified 9Cr-1Mo Alloy for Review by ASTM Committee", ORNL

# CHAPTER 4 APPLICATION OF THE MDBT TO IRRADIATED MATERIALS

The MDBT method described in Chapter 3 was applied to irradiation testing of rapid solidification (RS) processed modified 316 stainless steel (SS) type developmental alloys. Type 316SS has been favorably considered as a candidate for several radiation application for its adequate strength up to moderately high temperature, reasonable swelling resistance, and possible retention of ductility after high levels of neutron exposure. The possible applications considered includes cladding material for fission reactor fuel elements and first wall material for controlled thermo-nuclear reactors. RS processing (RSP) has been the basis for a number of innovative materials developments and has shown the capacity of structural and compositional control as discussed in references 4.1 through 4.3. Highly refined grain size, considerably decreased segregation, elimination of coarse segregated phases, and high levels of solute supersaturation are some of the improvements and variations which have been demonstrated as beneficial effects on alloy properties. In order to reduce the harmful effects of irradiation on the mechanical properties, mainly embrittlement and swelling in this case, titanium was added to 316SS in stoichiometric composition to tie up the carbon content in the alloy as TiC. It was speculated that the TiC particles would provide nucleation sites for cavities and storage of helium. RSP produced a fine grain size (less than about 10 $\mu$m) and an ultrafine dispersion of fine carbides (less than about 150 Å). Titanium carbides of about 50 Å or smaller are indicated to be coherently bonded to the matrix and enhance the

strength of these alloys. However such fine TiC particles were found to be soluble at high temperatures and to coarsen and to be subject to recoil resolution under irradiation, at temperatures of about 773 K or less as described in reference 4.4. Another modification was tried with more stable refractory oxides such as $Y_2O_3$. Yttria has higher heat of formation than TiC and finely distributed small particles are very stable in the austenitic matrix to rather high temperatures. Such particles are not bonded to the matrix. Yttrium and oxygen have poor solubility and low diffusivity in the austenitic matrix. Therefore $Y_2O_3$ addition is expected to change the irradation response of the steel with respect to void formation, recoil resolution and helium precipitation and storage at the metal-oxide interface.

## 4.1 Specimen Preparation

Disk specimens of two alloy types were supplied for MDBT - titanium carbide modified and dispersion strengthened 316SS. Three different versions of TiC modified 316SS - PCA, PA1 and PA3 - were supplied. PCA and PA1 were modified to have 0.32 wt.-% Ti and 0.046 wt.-% C and PA3 to have 0.90 wt.-% Ti and 0.17 wt.-% C. PA1 was RS processed from PCA at a solidification rate of about $10^5$ K/s. $Y_2O_3$ strengthened alloy was produced from an ultra-low carbon and nitrogen SS by RSP to have 1.0 wt.-% Al and 4 vol.-% $Y_2O_3$. All the alloys except PA3 were irradiated in two conditions - annealed and cold worked. The cold worked condition was achieved by 20 % (PCA and PA1) or 25 % ($Y_2O_3$ strengthened version) reduction in area from the annealed condition. PA3 alloy was cold

worked to about 60 % reduction in area following hot extrusion and was aged for 30 minutes at 973 K to give a "recovered" microstructure. Detailed description of the processing of these materials can be found in reference 3.5. The materials were irradiated in the High Flux Isotope Reactor during irradiation CTR -30, -31, -32 (PCA,PA1) and CTR -42, -43 (PA3 rcvd) at the Oak Ridge National Laboratories. Table 4.1 summarizes the irradiation temperatures and damage levels and helium production for each material.

## 4.2 Results and Discussion

Irradiated disk specimens were bend tested at the irradiation temperatures and load/deflection curves were obtained. Unirradiated specimens were also tested at the same temperatures for comparison purpose for almost all the temperatures. The load/deflection curves of PCA-CW, as shown in Fig. 4.1, are a typical example of brittle (773 K) and ductile (873 K) curves after irradiation. Unirradiated curves are shown for comparison. It can be noted from the figure that the material retains about 70 % of the deflection at maximum load of the unirradiated material after 34 dpa irradiation at 573 K and thus indicates no drastic reduction of ductility. On the other hand, at 773 K the material shows a large decrease in the deflection at the maximum load after 34 dpa and thus indicates a drastic reduction in ductility. All the irradiated curves at 773 K at 8.5 dpa and at 573 and 673 K at 8.5 and 34 dpa show ductile type curves. All the 773 K curves except those of the low dose 8.5 dpa irradiation and all the 873 K curves show brittle type curves.

Table 4.1 Damage level in dpa (helium production in appm) for all the alloys used in the irradiation tests.

| Alloy | Irradiation Temperature, K | | | |
|---|---|---|---|---|
| | 573 | 673 | 773 | 873 |
| PCA-AN | —<br>34(3100) | —<br>34(3100) | 8.5(360)<br>34(3100) | 8.5(360)<br>34(3100) |
| PCA-CW | —<br>34(3100) | —<br>34(3100) | 8.5(360)<br>34(3100) | —<br>34(3100) |
| PA1-AN | —<br>34(3100) | —<br>— | 8.5(360)<br>34(3100) | —<br>34(3100) |
| PA1-CW | —<br>34(3100) | —<br>34(3100) | 8.5(360)<br>34(3100) | 8.5(360)<br>34(3100) |
| 316SS+$Y_2O_3$ -AN | — | — | 14(750) | 14(750) |
| 316SS+$Y_2O_3$ -CW | — | — | 14(750) | 14(750) |
| PA3-Revd | — | — | 14(750) | 14(750) |

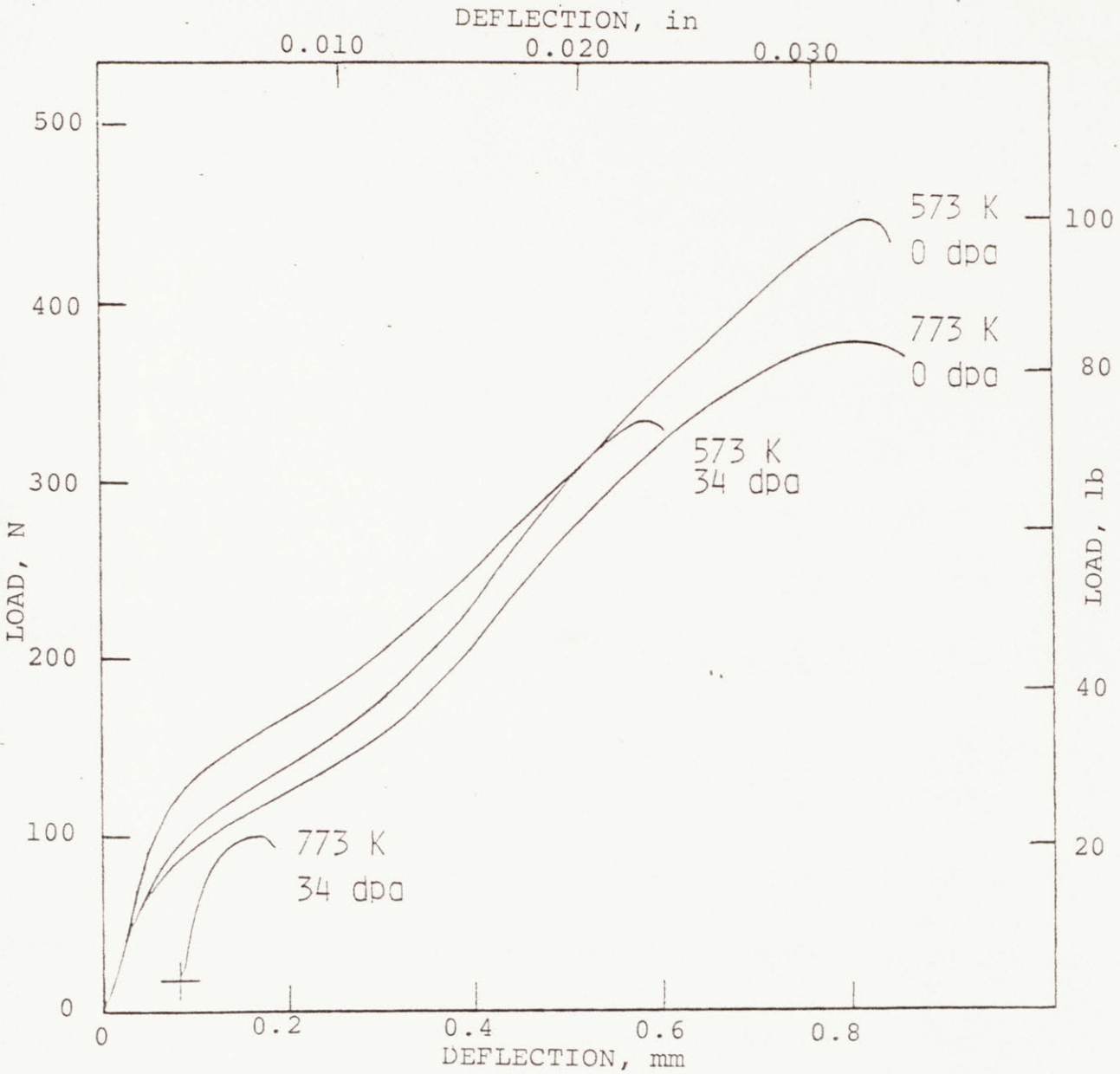


Figure 4.1 Typical example of brittle (773 K) and ductile (573 K) curves after irradiation, unirradiated curves shown for comparison.

Yield loads were obtained from the curves and the results are presented in Table 4.2. The MDBT load/deflection curves of PCA and PA1 were obtained before the installation of the filter and the digitizer, see Chapter 2 of this thesis, and thus showed comparatively greater noise and poorer resolution than those of 316SS + $Y_2O_3$ and PA3. The linear regions in the load/deflection curves for PCA-AN and PA1-AN before irradiation were so small that it was difficult to accurately measure their linear portion. Neverthless best efforts were made to obtain the yield load in a consistant way. But, the results should be used only for comparison. With the use of the electronic filter and the digitizer, better resolution and reduction of noise were achieved and load/deflection curves with about 10 N yield load or greater showed discernible linear regions.

For the computer analysis of the MDBT data of these modified 316SS type alloys, it is reasoned that they all have the same modulus of elasticity because they have almost the same composition as standard 316SS. Furthermore, it is assumed that the irradiation of the specimen does not change the elastic modulus. The values of the elastic modulus for type 316SS obtained from the Handbook of Stainless Steels (reference 4.6) are plotted as a function of of temperature in Fig. 4.2. A good linear relationship can be noticed. The elastic moduli at test temperatures were calculated from the interpolation or extrapolation of nearby data points and are indicated in the figure. ABAQUS code calculations were done for the highest and the lowest elastic moduli to obtain the sensitivity of yield load to different moduli in this range. The results are shown in Fig. 4.3 along with all the other calculation

Table 4.2 Measured yield loads in Newton. Each yield load represent a seperate specimen.

| Material | Dose dpa | Irradiation and/or Test Temperature., K | | | |
|---|---|---|---|---|---|
| | | 573 | 673 | 773 | 873 |
| PCA-CW | 0 | 43.4, 47.8 | 40.0, 39.4 | 36.0, 38.0 | 38.0, 37.4 |
| | 8.5 | | | 46.7, 52.0 | ——— |
| | 34 | 59.6, 60.0 | 45.4, 52.0 | 31.1, 35.7 | 32.0, 26.7 |
| PA1-CW | 0 | 40.0, 40.7, 40.7 | ——— | 38.0, 37.4 | 27.4, 29.4 |
| | 8.5 | | | 47.6, 50.3, 43.6 | 38.3, 40.0 |
| | 34 | 58.7, 54.7 | ——— | 35.4, 33.7 | 30.0 —— |
| PCA-AN | 0 | 11.3, 13.3 | 13.3, 13.3 | 10.7, 12.7, 10.7 | ——— |
| | 8.5 | | | 42.3, 42.3 | 40.0 —— |
| | 34 | 49.4, 47.4 | 46.7 —— | 35.4, 36.0 | 27.7, 28.4 |
| PA1-AN | 0 | 18.7, 20.0, 22.0 | ——— | 20.0, 19.3 | 18.7, 20.0 |
| | 8.5 | | | 40.0 —— | ——— |
| | 34 | 48.0, 46.7 | ——— | 32.0, 32.7 | 31.7 —— |
| PA3-Rcvd | 0 | | | 40.0, 41.8, 43.1 | 38.7, 40.0, 39.1 |
| | 14 | | | 46.3, 44.0 | 37.4, 38.3 |
| 316SS+$Y_2O_3$ CW | 0 | | | 47.6, 46.7, 48.5 | 36.5, 36.9 36.5 |
| | 14 | | | 59.6, 62.3 | 38.3, 38.3 |
| 316SS+$Y_2O_3$ AN | 0 | | | ——— | 37.4 —— |
| | 14 | | | 55.6, 59.6 | 35.6, 37.4 |

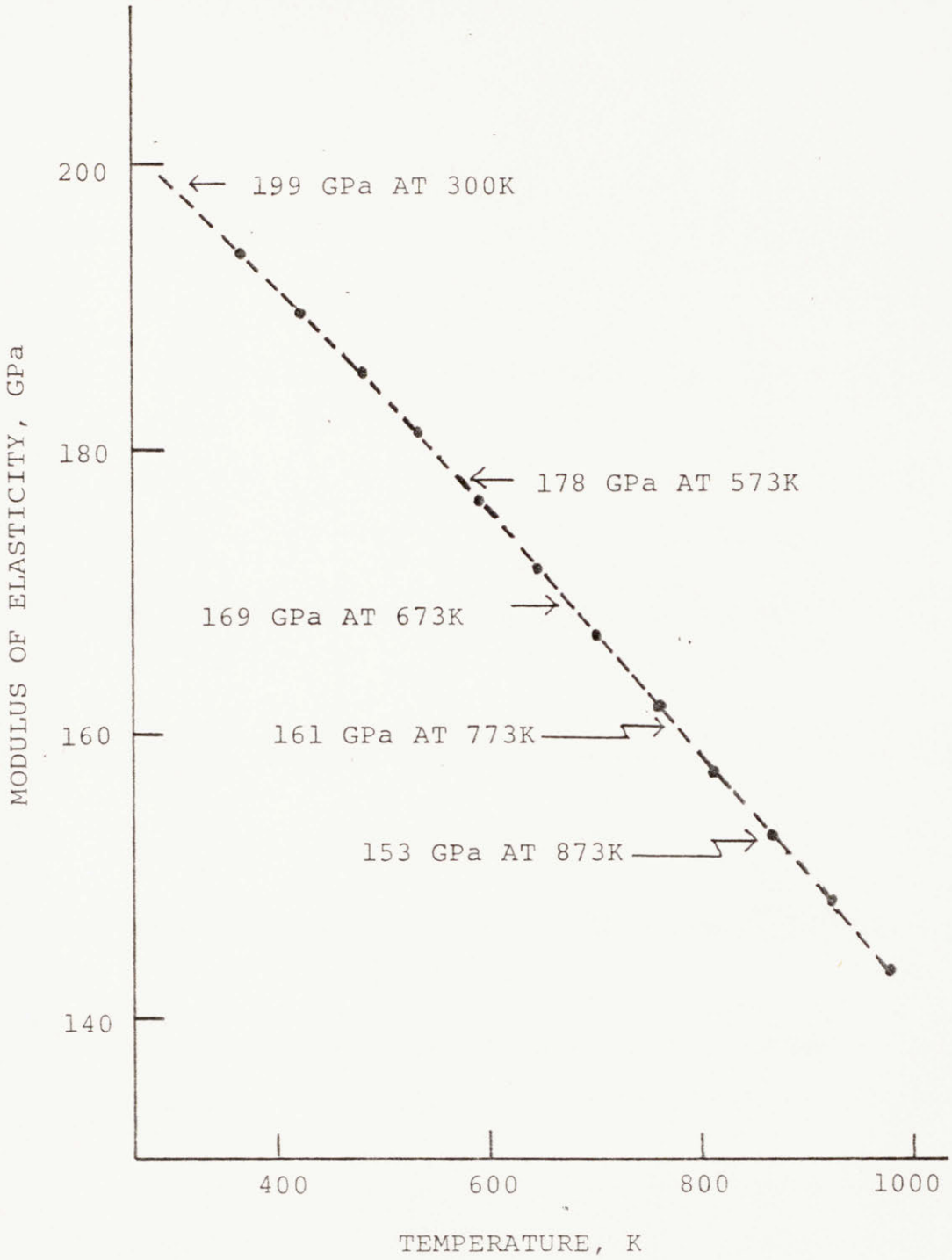


Figure 4.2 Modulus of elasticity as a function of temperature for type 316 stainless steel. Arrows indicate the moduli at test temperatures obtained from interpolation.

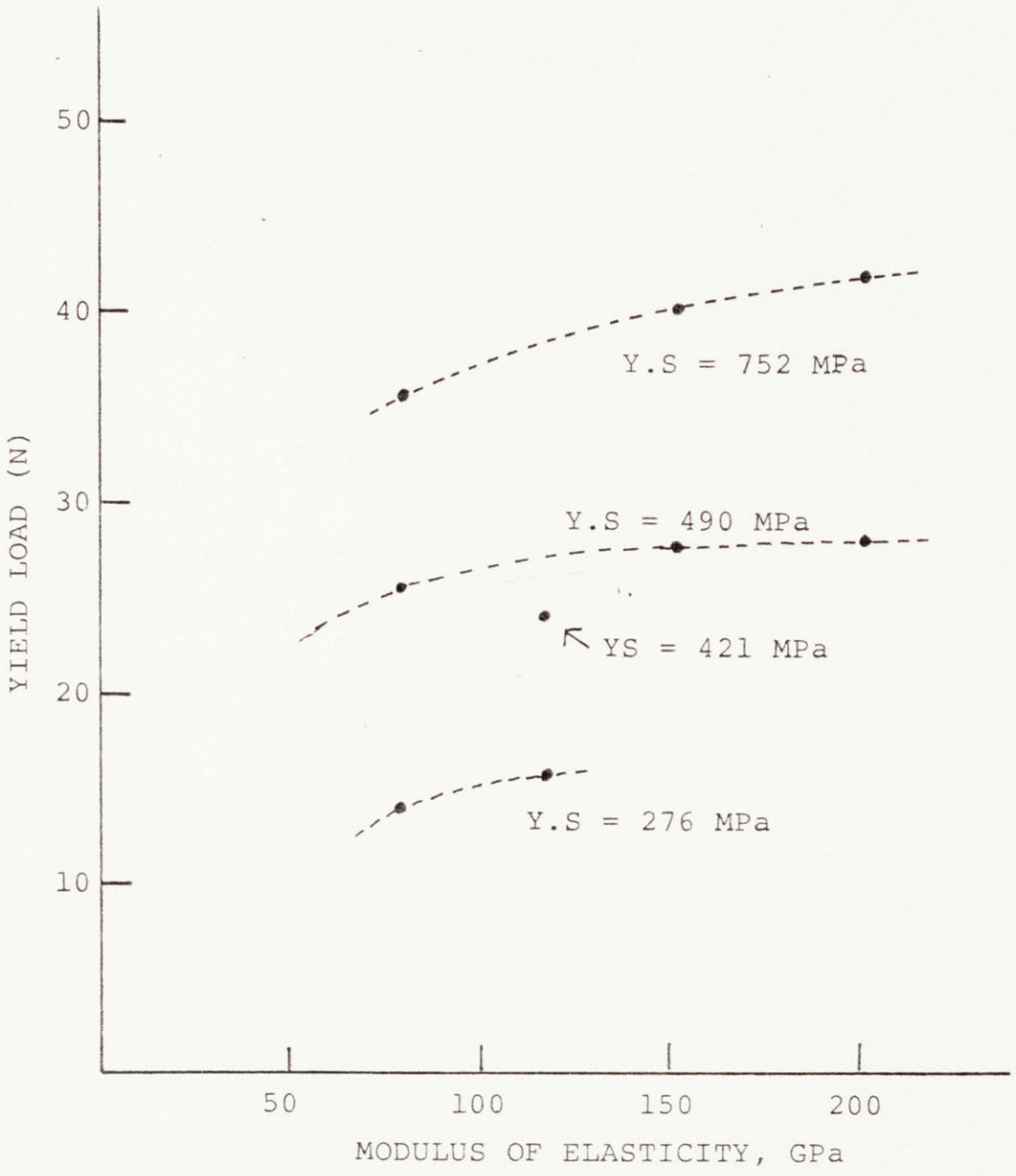


Figure 4.3 Sensitivity of yield load to the modulus of elasticity.

results. Note Fig. 4.3 can be used for the determinination of YS for unknown materials provided the YL is determined by the MDBT and a good estimate of the modulus is available. From the figure it can be seen that yield load is not very sensitive to elastic modulus in this modulus range. This weak sensitivity of yield load to elastic modulus makes it possible to interpolate between different moduli. Similarly interpolations of the yield load were made for materials with different yield strengths but with the same elastic modulus. Table 4.3 presents the input data for and the results of computer calculations for the analysis of the test data for modified 316SS type alloys. The result of yield strength estimations by the MDBT method are presented in Table 4.4 and in Fig. 4.4. Bend ductilities were calculated using Eq. 3.7 for the materials which show brittle type curves. The results are shown in Table 4.5 and in Fig. 4.5 as a function of irradiation dose.

As expected irradiation makes the alloys hardened at 573 and 673 K to show approximately the same yield strength for annealed and cold-worked materials by 34 dpa. The data at 773 and 873 K seem to show an initial hardening followed by gradual softening with increased dose. By 34 dpa all the alloys have about the same yield strength regardless of pre-irradiation strength for PCA and PAl. However, $Y_2O_3$ strengthened alloys seem to show somewhat higher yield strength and hardening at 14 dpa. Further irradiation data is needed to compare the general trends of 316SS+$Y_2O_3$ with other alloys. The absence of drastic reduction in ductility in all the alloys up to 34 dpa irradiation at lower tempertures, 573 and 673 K, seems to be in agreement with results for similar materials as reported in reference 4.7. The 773 and 873 K

Table 4.3 Input data for and the result of computer calculations for the analysis of modified 316 stainless steel type alloy test results.

| Case or Material | Input Data | | | Yield Load, N |
|---|---|---|---|---|
| | Yield Strength, MPa | Hardening Coefficient | Elastic Modulus, GPa | |
| UR | 752 | 0.04 | 199 | 41.8 |
| LR | 496 | 0.07 | 199 | 28.0 |
| U5 | 752 | 0.04 | 161 | 40.3 |
| Cu-Ni-5 | 496 | 0.05 | 161 | 27.6 |

Table 4.4 Estimated yield strength in MPa by the MDBT method for the irradiation test of modified 316 stainless steel type alloys.

| Material | Dose | Irradiation and/or Test Temperature, K. | | | | |
|---|---|---|---|---|---|---|
| | dpa | R.T. | 573 | 673 | 773 | 873 |
| PCA-CW | 0 | 965, 758 | 800, 903 | 738,724 | 669, 710 | 710, 696 |
| | 8.5 | ——— | ——— | ——— | 883, 986 | ——— |
| | 34 | ——— | 1110, 1124 | 834, 965 | 565, 662 | 586, 476 |
| PA1-CW | 0 | 869, 931 | 738, 745, 745 | ——— | 710, 696 | 490, 531 |
| | 8.5 | ——— | ——— | ——— | 899, 952, 819 | 710, 745 |
| | 34 | ——— | 1020, 1018 | ——— | 655, 621 | 545 |
| PCA-AN | 8.5 | ——— | ——— | ——— | 793, 793 | 745 |
| | 34 | ——— | 917, 876 | 862 | 655, 669 | 496, 510 |
| PA1-AN | 8.5 | ——— | ——— | ——— | 745 | ——— |
| | 34 | ——— | 889, 862 | ——— | 586, 600 | 579 |
| 316SS+$Y_2O_3$ | 0 | ——— | ——— | ——— | 896, 883,917 | 676, 683, 676 |
| -CW | 14 | ——— | ——— | ——— | 1138, 1193 | 710, 710 |
| 316SS+$Y_2O_3$ | 0 | ——— | ——— | ——— | ——— | 696 |
| -AN | 14 | ——— | ——— | ——— | 1062, 1138 | 655, 696 |
| PA3-Recd. | 0 | ——— | ——— | ——— | 745, 786,807 | 717, 745, 731 |
| | 14 | ——— | ——— | ——— | 876, 827 | 696, 710 |

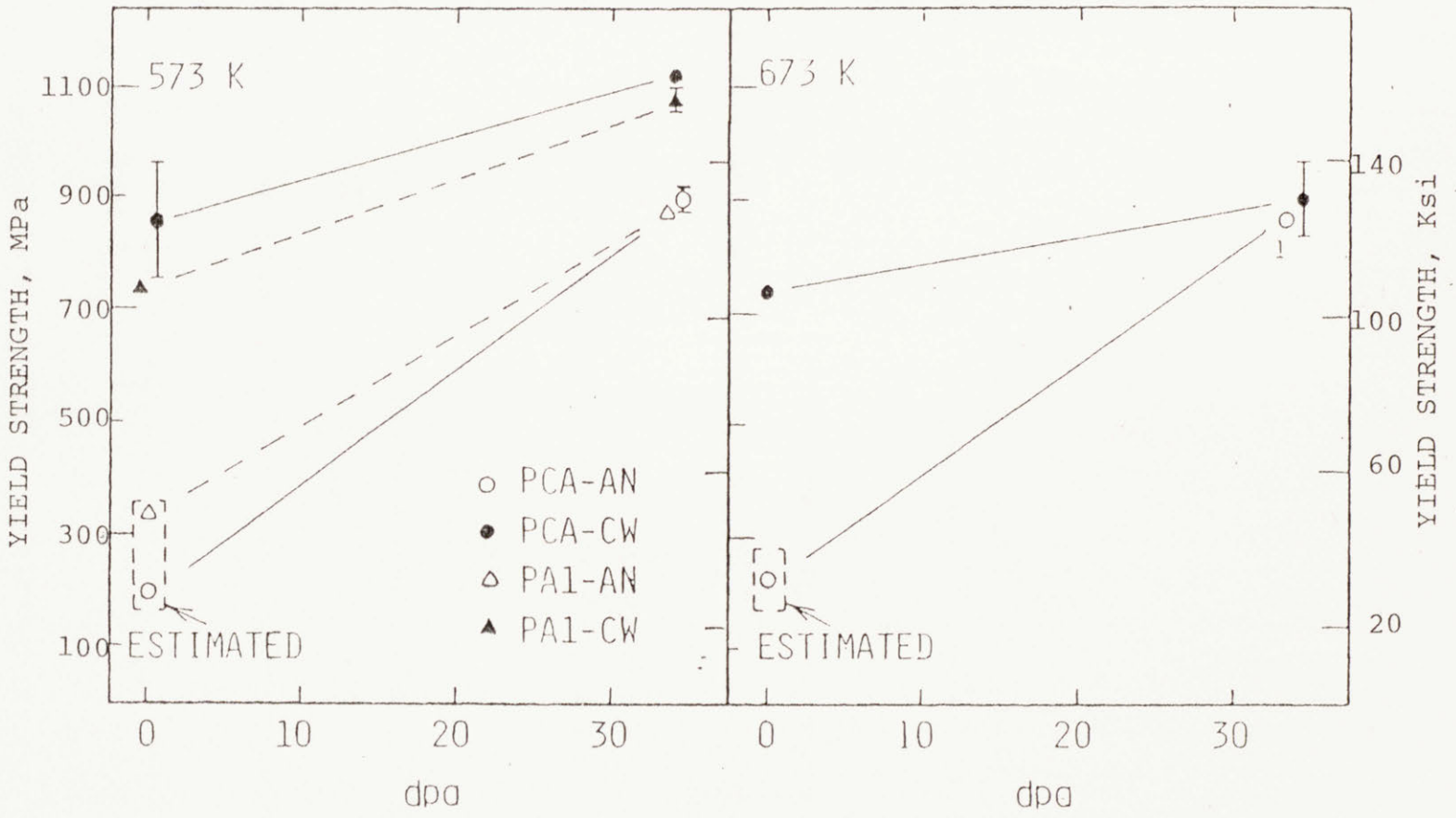


Figure 4.4-1 Yield strength of modified type 316 stainless steel, measured by the MDBT method, as a function of irradiation dose, 573 and 673 K data.

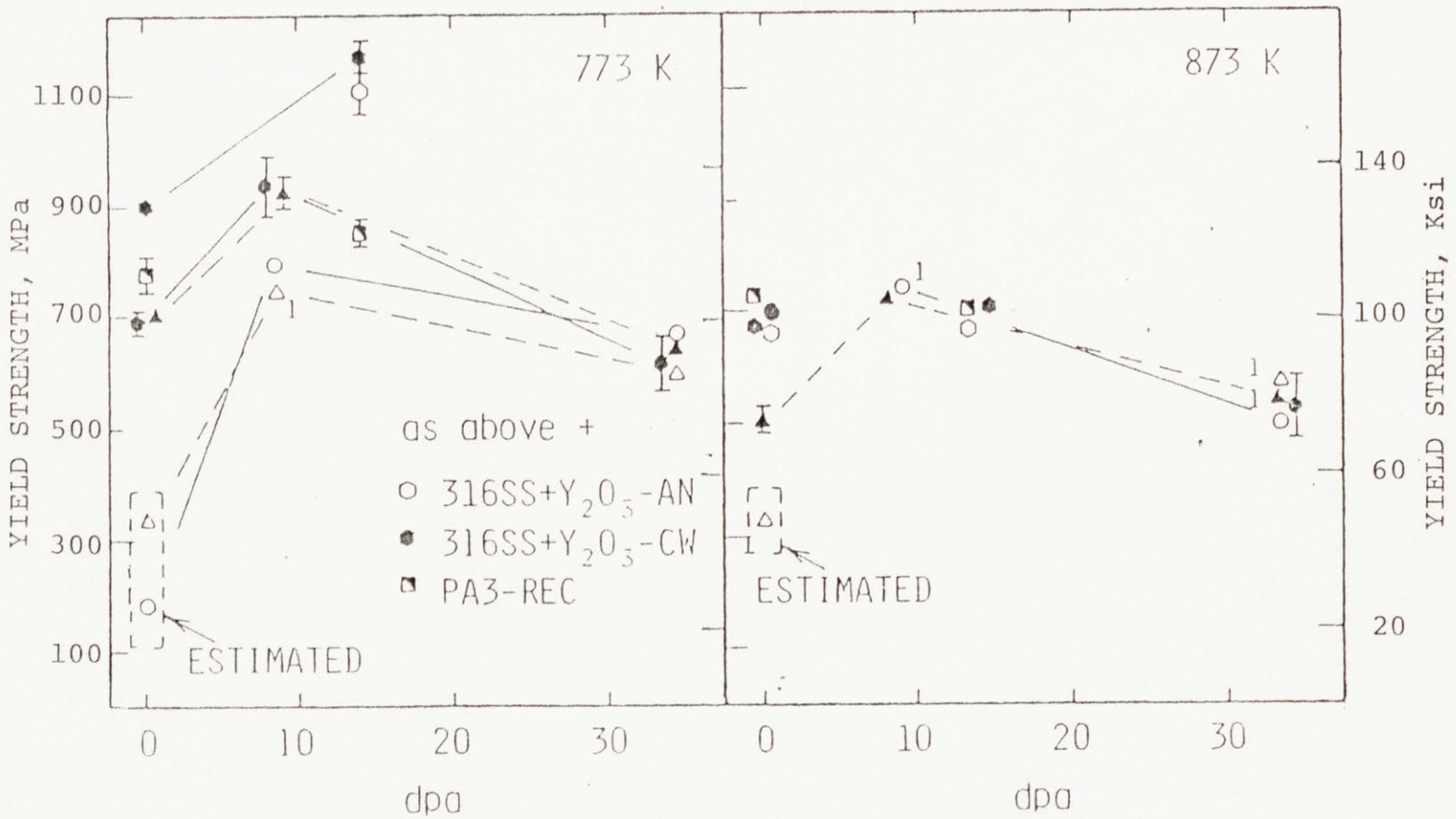


Figure 4.4-2 Yield strength of modified type 316 stainless steel measured by the MDBT method, as a function of irradiation dose, 773 and 873 K data.

Table 4.5 Result of ductility measurement for modified 316 stainless steel type alloys.

| Material | Dose dpa | Ductility, % | | | |
|---|---|---|---|---|---|
| | | 773 K | | 873 K | |
| PCA-CW | 34 | 0.9 | 1.3 | 0.8 | 0.5 |
| PCA-AN | 8.5 | ——— | | 3.1 | —— |
| | 34 | 1.5 | 1.0 | 0.7 | 0.6 |
| PA1-CW | 8.5 | ——— | | 3.3 | 1.5 |
| | 34 | 1.3 | 1.7 | 1.2 | 1.2 |
| PA1-AN | 34 | 2.1 | 1.6 | 0.7 | —— |
| PA3-Recd | 14 | 2.6 | 2.9 | 2.1 | 2.0 |
| 316SS+$Y_2O_3$, CW | 14 | 3.4 | 3.0 | 2.8 | 2.8 |
| AN | 14 | 3.3 | 2.8 | 1.9 | 2.6 |

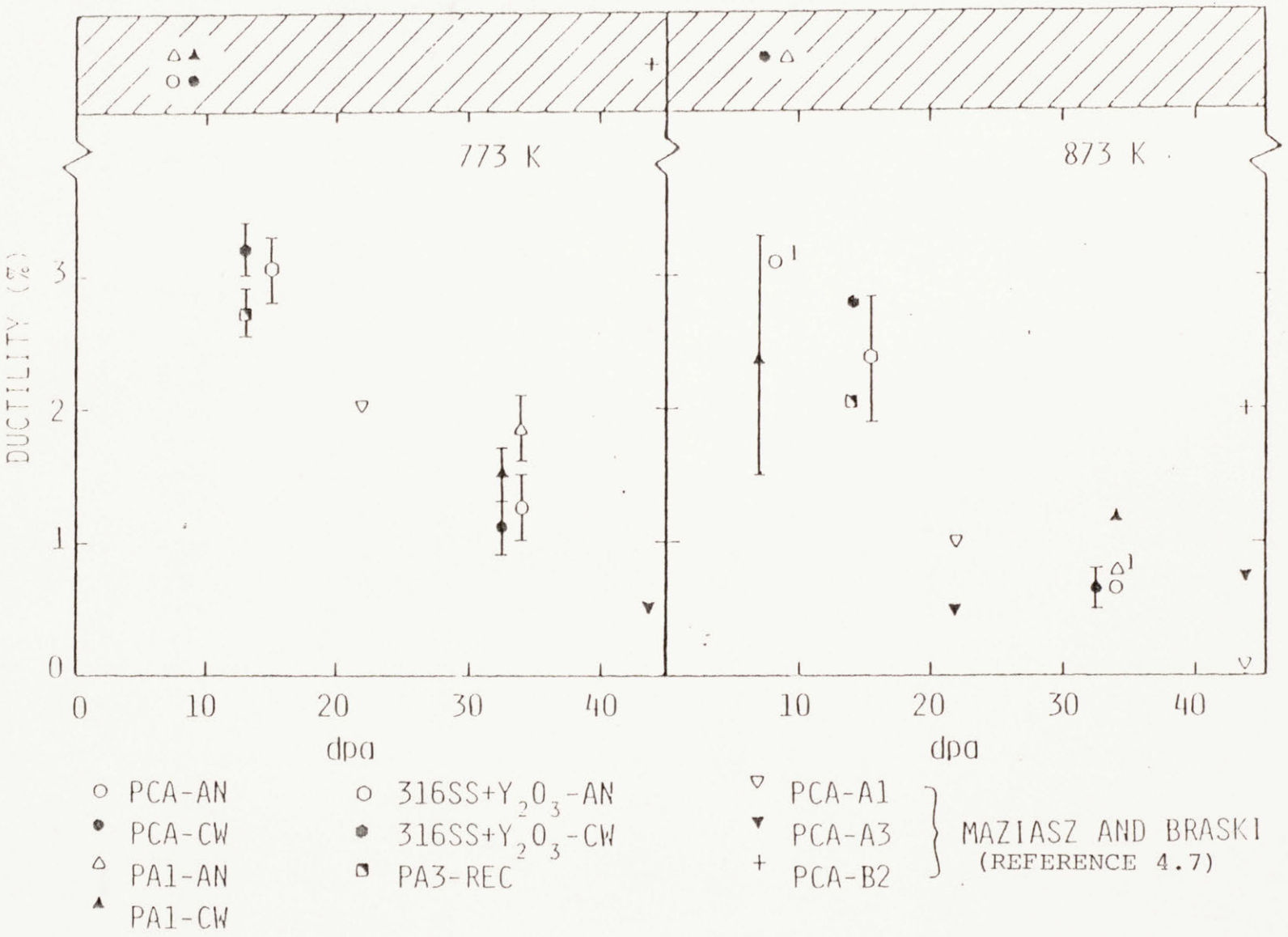


Figure 4.5 Ducitility of modified type 316 stainless steel, measured by the MDBT method, as a function of irradiation dose, 773 and 873 K data.

results indicate a great reduction in ductility at 14 and 34 dpa. The ductility results are compared with the results for similar materials (reference 4.7) in Fig. 4.5. They seem to show similar trend upon irradiation. Again, more irradiation tests are needed for 316SS+$Y_2O_3$ alloys to be compared with other alloys over the whole dose range.

## References for Chapter 4


4.1 P.K. Domalavage, N.J. Grant, and V. Gefen, "Structure and Properties of Rapidly Solidified 7075 P/M Aluminum Alloy Modified with Nickel and Zirconium", Met. Transactions A, 14A (1983), pp 1599-1606

4.2 E. Testart, J. Megusar, L. Arnberg, and N.J. Grant, "Mechanical Properties and Structure of Rapidly Solidified High Titanium Stabilized 316 Stainless Steel", J. Nucl. Matr., 103 & 104 (1981), pp 833-838

4.3 J. Megusar, L. Arnberg, J.B. Vander Sande and N.J. Grant, "Optimization of Structure and Properties of Path A Prime Candidate Alloy (PCA) by Rapid Solidification", J. Nucl. Matr., Vol 99, Nos. 2 and 3, (Sept., 1981), pp 190-202

4.4 H.J. Frost and K.C. Russel, "Particle Stability with Recoil Resolution", Acta Met., Vol. 30, (1982), pp 953-960

4.5 O.K. Harling, M. Lee, D-S. Sohn, G. Kohse and N.J. Grant, "Neutron Irradiated Mechanical Properties of Some Rapidly Solidified Austenitic Stainless Steel", Paper Submitted to the Twelfth Symposium on the Effects of Radiation on Materials, Williamsburg, Va, June, 1984

4.6 D. Peckner and I.M. Bernstein, Handbook of Stainless Steels, McGraw-Hill Book Co., 1977

4.7 P.J. Maziasz, and D.N. Braski, "Microstructural Design of PCA Austenitic Stainless Steel for Improved Resistance to Helium Embrittlement Under HFIR Irradiation", Proceedings of the Third Topical Meeting on Fusion Reactor Materials, Albuquerque, Sept. 1983

# CHAPTER 5 SUMMARY AND RECOMMENDATIONS

## 5.1 Summary of Results

This research involves the following:

1. the development of analysis methods in order to extract post-irradiation tensile properties
2. the verification of the these analysis methods by applying them to various alloys of known mechanical properties
3. the search for possible methods to measure the change of ductile-brittle transition temperature after irradiation using the MDBT approach.

The specimen disk behavior during deformation was closely examined and the deviation from linearity after the initial part of the MDBT load/deflection curve was found to be affected mainly by the yield strength of the material. Based on this observation, the load at the deviation point from linearity in the MDBT load/deflection curve (defined as the yield load) was correlated with the yield strength of the material. An iterative method, using the results of computer analysis of the MDBT by a finite element computer code, ABAQUS, to simulate the load/deflection response of the disk specimen up to the deviation point from linearity, was developed for the estimation of yield strength.

MDBT load/deflection curves for brittle disks show a sudden drop in load shortly after the point of deviation from linearity. This drop was found to be related to the onset of failure in the specimen. Based on

this observation, the ductility of the specimen was calculated from the deflection at maximum load using a simple analytical expression which was derived under the assumption of spherical cap geometry of the specimen during deformation.

The yield strengths and ductilities for several kinds of alloys measured by the MDBT, using the analysis methods developed in this research, were in good agreement with the reference values measured in conventional uniaxial tests. This agreement verifies these analysis methods at least in the range of the mechanical properties of the materials used in these verification tests.

In the impact test using the MDBT approach, a transition of the characteristic shape of the load/deflection curve, i.e., a sudden reduction of the area under the curve, lower maximum load and lower deflection at the load drop, was observed. These preliminary results showed the potential of the MDBT to measure changes in the ductile - brittle transition temperature.

The MDBT data analysis method developed in this research was applied to irradiation tests of several kinds of modified type 316 stainless steel in Chapter 4. Other unknown materials can be analyzed in a similar manner. The results showed expected material response after irradiation : hardening and embrittlement. Embrittlement was more pronounced after irradiation at 773 and 873 K than after irradation at 573 and 673 K.

## 5.2 Recommendations for Future Work

The following is a list of recommendations for future work :

1. Expand the MDBT application range by testing more materials with higher and lower yield strength and/or elastic moduli.

2. Perform a sensitivity analysis on the punch tip radius to determine the optimum size of the punch tip radius. A larger punch tip radius would improve the precision of the yield load determination but could limit the testing of ductile material.

3. Consider the use of a more precise load cell to improve the accuracy of load measurement and the stability of the load cell under temperature change.

4. Perform more ductility tests with materials of wider range of ductilities so that the range of validity of this simple spherical cap geometry deformation assumption in the MIT test geometry can be more accurately determined.

# APPENDIX A

## DESIGN DRAWINGS

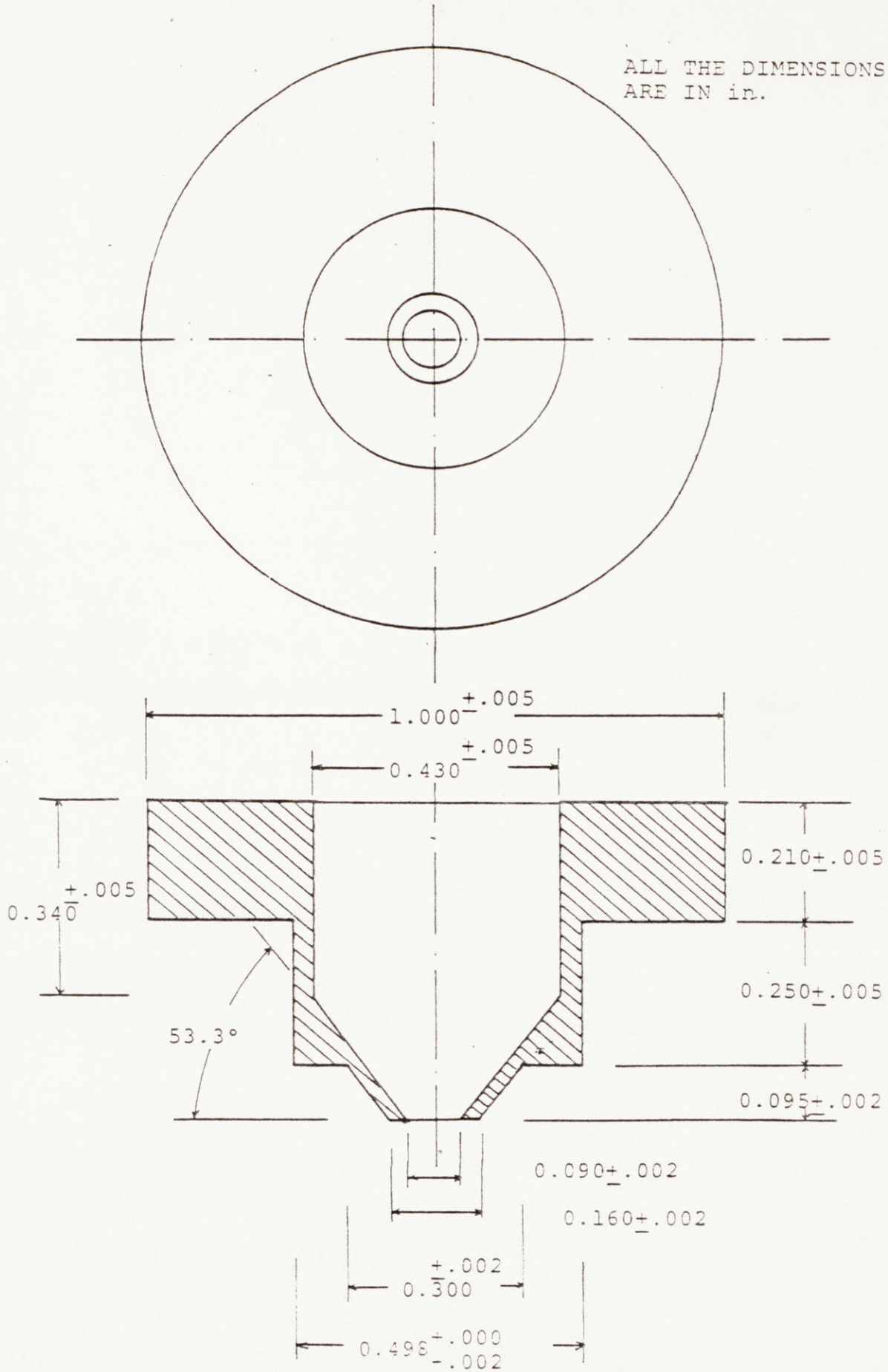


Figure A.1 Design drawing for specimen remover. Material-304SS

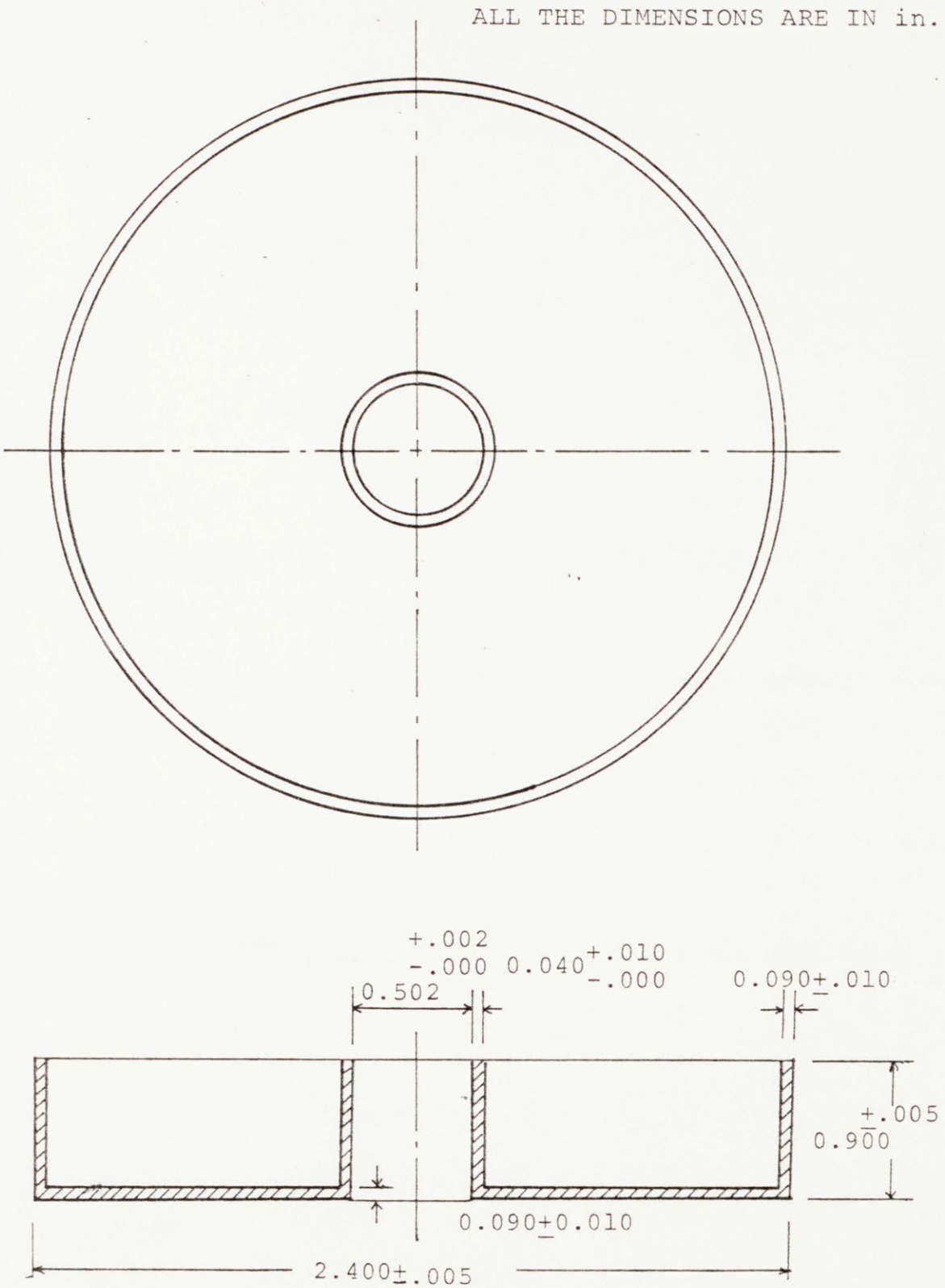


Figure A.2 Design drawing for the cooling cup. Material-copper

# APPENDIX B

## SAMPLE INPUT DATA LIST

## FOR

## ABAQUS ANALYSIS OF THE MDBT

This appendix provides a listing of the ABAQUS finite element code input for the fine element mesh (63 element mesh) used in the analysis of the reference test results to verify the analysis methods developed in this thesis. The same fine element mesh was used in all the subsequent computer analyses of the MDBT results.

```
*HEADING
RUN FOR CU-NI-5 WITH DSS9 63 ELEMENT FINE MESH, MU=0.6
, BOTH MPC'S ARE USED
*NODE
100, ,.0100002
1, ,
801, ,.010
13,.006,
813,.006,.010
27,.0445,
827,.0445,.010
43,.0525,
843,.0525,.010
47,.059,
847,.059,.010
251,.00025,.00875
351,.00025,.010
258,.00375,.00875
358,.00375,.010
271,.04675,
371,.04675,.00125
278,.05025,
378,.05025,.00125
916, ,
988, ,
919,-1.7624230E-6,
921,-6.4489610E-6,
923,-1.4257419E-5,
925,-2.5184145E-5,
927,-3.9224038E-5,
929,-5.6370560E-5,
931,-7.6615752E-5,
933,-9.9950250E-5,
935,-1.2363310E-4,
937,-1.5584283E-4,
939,-1.8837537E-4,
941,-2.2394620E-4,
943,-2.6253933E-4,
945,-3.0413751E-4,
947,-3.4872232E-4,
949,-3.9627417E-4,
915,-5.0019512E-4,
917,-6.1572216E-4,
951,1.6552506E-4,
953,1.2693284E-4,
955,9.3886622E-5,
957,6.4928512E-5,
959,4.1594579E-5,
961,2.3414656E-5,
963,1.0412149E-5,
965,2.6038840E-6,
967,2.E-7,
```

```
987,2.E-7,
*NGEN
1,801,100
601,801,50
13,813,100
1,13,2
101,113,4
201,213,2
301,313,4
401,413,2
501,513,4
601,613,1
701,713,1
801,813,1
609,809,50
651,659,2
751,759,1
251,258,1
351,358,1
27,827,100
13,27,1
213,227,2
413,427,1
613,627,2
813,827,1
43,843,100
27,43,
127,143,
227,243,
327,343,4
427,443,2
627,643,4
827,843,2
31,231,50
39,239,50
81,89,
181,189,2
271,278,
371,378,
47,847,200
43,47,
243,247,2
443,447,
643,647,2
843,847,
916,988,2
967,987,2
*ELEMENT,TYPE=CAX8R
1,701,702,802,801,251,752,351,751
3,601,603,703,701,602,653,702,651
7,401,405,605,601,403,505,603,501
19,609,611,811,809,610,711,810,709
```

```
24,413,415,815,813,414,615,814,613
38,427,431,831,827,429,631,829,627
39,227,231,431,427,229,331,429,327
43,131,133,233,231,132,183,232,181
44,31,32,132,131,271,82,371,81
60,443,445,845,843,444,645,844,643
*ELGEN,ELSET=ALL
1,2,1,1
2,2,1,2
4,2,1,1
5,2,1,5
10,2,1,1
11,2,1,2
13,2,1,1
3,2,2,3
6,2,2,6
12,2,2,3
7,3,-200,1
7,2,4,9
16,2,4,5
16,3,-200,1
21,3,-200,1
19,2,2,1
24,2,-400,1
24,7,2,2
25,7,2,2
38,2,4,3
41,3,4,8
39,2,-200,1
39,2,4,3
42,3,4,8
58,2,-200,1
43,2,2,3
46,2,2,5
51,2,2,3
44,2,1,1
45,2,1,2
47,2,1,1
48,2,1,4
52,2,1,1
53,2,1,2
55,2,1,1
60,2,2,2
60,2,-400,1
62,2,-400,1
*ELSET,ELSET=ONE
9
*NSET,NSET=BCEN
1,101,201,301,401,501,601,651,701,751,801
*NSET,NSET=FIXD,GENERATE
916,988,2
*NSET,NSET=DFLN
```

```
100,801,601,401,201,1,961,963,274,965,35,967,275,969,971
*NSET,NSET=FOS
100,801,966,968,970,972
*MATERIAL,ELSET=ALL
*ELASTIC
22.0E6,0.30
*PLASTIC
** CU-NI-5 FROM PROF. N. J. GRANT
7.20E4,0.000,
7.47E4,0.002,
7.72E4,0.006,
7.89E4,0.010,
8.08E4,0.018,
8.48E4,0.048,
8.76E4,0.098,
9.51E4,0.498,
9.82E4,0.998
*BOUNDARY
BCEN,1
FIXD,1,2
100,1
*GAP,TYPE=UNI,PLANAR
919,920,1.7624230E-6,1.0,0.0,0.0,0.0,.6,1.E7
921,922,6.4489610E-6,1.0,0.0,0.0,0.0,.6,1.E7
923,924,1.4257419E-5,1.0,0.0,0.0,0.0,.6,1.E7
925,926,2.5184145E-5,1.0,0.0,0.0,0.0,.6,1.E7
927,928,3.9224038E-5,1.0,0.0,0.0,0.0,.6,1.E7
929,930,5.6370560E-5,1.0,0.0,0.0,0.0,.6,1.E7
931,932,7.6615752E-5,1.0,0.0,0.0,0.0,.6,1.E7
933,934,9.9950250E-5,1.0,0.0,0.0,0.0,.6,1.E7
935,936,1.2636331E-4,1.0,0.0,0.0,0.0,.6,1.E7
937,938,1.5584283E-4,1.0,0.0,0.0,0.0,.6,1.E7
939,940,1.8837537E-4,1.0,0.0,0.0,0.0,.6,1.E7
941,942,2.2394620E-4,1.0,0.0,0.0,0.0,.6,1.E7
943,944,2.6253933E-4,1.0,0.0,0.0,0.0,.6,1.E7
945,946,3.0413751E-4,1.0,0.0,0.0,0.0,.6,1.E7
947,948,3.4872232E-4,1.0,0.0,0.0,0.0,.6,1.E7
949,950,3.9627417E-4,1.0,0.0,0.0,0.0,.6,1.E7
915,916,5.0019512E-4,1.0,0.0,0.0,0.0,.6,1.E7
917,918,6.1572216E-4,1.0,0.0,0.0,0.0,.6,1.E7
951,952,1.6552506E-4,-1.0,0.0,0.0,0.0,.6,1.E7
953,954,1.2693284E-4,-1.0,0.0,0.0,0.0,.6,1.E7
955,956,9.3386622E-5,-1.0,0.0,0.0,0.0,.6,1.E7
957,958,6.4928512E-5,-1.0,0.0,0.0,0.0,.6,1.E7
959,960,4.1594579E-5,-1.0,0.0,0.0,0.0,.6,1.E7
961,962,2.3414656E-5,-1.0,0.0,0.0,0.0,.6,1.E7
963,964,1.0412149E-5,-1.0,0.0,0.0,0.0,.6,1.E7
965,966,2.6038840E-6,-1.0,0.0,0.0,0.0,.6,1.E7
967,968,2.E-7,-1.0,0.0,0.0,0.0,.6,1.E7
969,970,2.E-7,-1.0,0.0,0.0,0.0,.6,1.E7
971,972,2.E-7,-1.0,0.0,0.0,0.0,.6,1.E7
973,974,2.E-7,-1.0,0.0,0.0,0.0,.6,1.E7
```

```
975,976,2.E-7,-1.0,0.0,0.0,.6,1.E7
977,978,2.E-7,-1.0,0.0,0.0,.6,1.E7
979,980,2.E-7,-1.0,0.0,0.0,.6,1.E7
981,982,2.E-7,-1.0,0.0,0.0,.6,1.E7
983,984,2.E-7,-1.0,0.0,0.0,.6,1.E7
985,986,2.E-7,-1.0,0.0,0.0,.6,1.E7
987,988,2.E-7,-1.0,0.0,0.0,.6,1.E7
*GAP,TYPE=UNI
100,801,2.E-7,0.0,-1.0,0.0
*MPC
2,251,701,702,703
2,252,701,702,703
2,253,703,704,705
2,254,703,704,705
2,255,705,706,707
2,256,705,706,707
2,257,707,708,709
2,258,707,708,709
2,602,601,603,605
2,604,601,603,605
2,606,605,607,609
2,608,605,607,609
2,610,609,611,613
2,612,609,611,613
2,759,809,709,609
2,659,809,709,609
2,713,813,613,413
2,513,813,613,413
2,313,413,213,13
2,113,413,213,13
2,327,427,227,27
2,127,427,227,27
2,181,231,131,31
2,81,231,131,31
2,232,231,233,235
2,234,231,233,235
2,236,235,237,239
2,238,235,237,239
2,371,131,132,133
2,372,131,132,133
2,373,133,134,135
2,374,133,134,135
2,375,135,136,137
2,376,135,136,137
2,377,137,138,139
2,378,137,138,139
2,189,239,139,39
2,89,239,139,39
2,343,443,243,43
2,143,443,243,43
*MPC,USER
3,919,351,351,100
```

4,919,351,351,100
3,921,802,802,100
4,921,802,802,100
3,923,352,352,100
4,923,352,352,100
3,925,803,803,100
4,925,803,803,100
3,927,353,353,100
4,927,353,353,100
3,929,804,804,100
4,929,804,804,100
3,931,354,354,100
4,931,354,354,100
3,933,805,805,100
4,933,805,805,100
3,935,355,355,100
4,935,355,355,100
3,937,806,806,100
4,937,806,806,100
3,939,356,356,100
4,939,356,356,100
3,941,807,807,100
4,941,807,807,100
3,943,357,357,100
4,943,357,357,100
3,945,808,808,100
4,945,808,808,100
3,947,358,358,100
4,947,358,358,100
3,949,809,809,100
4,949,809,809,100
3,915,810,810,100
4,915,810,810,100
3,917,811,811,100
4,917,811,811,100
1,951,31,31
2,951,31,31
1,953,271,271
2,953,271,271
1,955,32,32
2,955,32,32
1,957,272,272
2,957,272,272
1,959,33,33
2,959,33,33
1,961,273,273
2,961,273,273
1,963,34,34
2,963,34,34
1,965,274,274
2,965,274,274
1,967,35,35

```
2,967,35,35
1,969,275,275
2,969,275,275
1,971,36,36
2,971,36,36
1,973,276,276
2,973,276,276
1,975,37,37
2,975,37,37
1,977,277,277
2,977,277,277
1,979,38,38
2,979,38,38
1,981,278,278
2,981,278,278
1,983,39,39
2,983,39,39
1,985,41,41
2,985,41,41
1,987,43,43
2,987,43,43
***PLOT
**UNDEFORMED MESH/ DSS VERSION 9, 5/12/84
** , ,9.,4.,.5,2.5,4,1, , ,
***DRAW,ELNUM
***PLOT
**UNDEFORMED MESH, DETAIL/DSS VERSION 9
** , , , , , , , , , ,
***DETAIL
**.0000,.0075, ,.006,.010,
***DRAW,ELNUM
***DETAIL
**.0000,.0075, ,.006,.010,
***DRAW,NODENUM
***DETAIL
**.0445,.0000, ,.0525,.0025,
***DRAW,ELNUM
***DETAIL
**.0445,.0000, ,.0525,.0025,
***DRAW,NODENUM
*RESTART,WRITE,FREQ=500
*STEP,NLGEOM,INC=100
*STATIC,PTOL=.0001
1.0,1.0,0.001
*BOUNDARY
100,2,,-2.00E-7
*PRINT, RESIDUAL=NO
*LIST PRINT,FREQ=2
*NODE PRINT,NSET=DFLN,FREQ=2
2,1,1,1,1,1,1,
*NODE PRINT,NSET=FOS,FREQ=2
1,1,1,1,2,2,1,
```

```
*ELPRINT,FREQ=500,ELSET=ONE(POINT=1,POINT=3)
2,2,1,1,1
2,1,2,1,1
*END STEP
*STEP,NLGEOM,INC=100
*STATIC,PTOL=.050
1.0,1.0,0.001
*BOUNDARY
100,2,,-5.2E-6
*END STEP
*STEP,NLGEOM,INC=100
*STATIC,PTOL=.050
1.0,1.0,0.001
*BOUNDARY
100,2,,-2.02E-5
*END STEP
*STEP,NLGEOM,INC=100
*STATIC,PTOL=.050
1.0,1.0,0.001
*BOUNDARY
100,2,,-5.02E-5
*END STEP
*STEP,NLGEOM,INC=100
*STATIC,PTOL=.050
1.0,1.0,0.001
*BOUNDARY
100,2,,-1.002E-4
*END STEP
*STEP,NLGEOM,INC=100
*STATIC,PTOL=.050
1.0,1.0,0.001
*BOUNDARY
100,2,,-1.502E-4
*END STEP
*STEP,NLGEOM,INC=100
*STATIC,PTOL=.050
0.25,1.0,0.0001
*BOUNDARY
100,2,,-2.002E-4
*END STEP
*STEP,NLGEOM,INC=100
*STATIC,PTOL=.050
1.0,1.0,0.001
*BOUNDARY
100,2,,-2.602E-4
*END STEP
*STEP,NLGEOM,INC=100
*STATIC,PTOL=.050
1.0,1.0,0.0001
*BOUNDARY
100,2,,-3.002E-4
*END STEP
```

```
*STEP,NLGEOM,INC=100
*STATIC,PTOL=.050
1.0,1.0,0.001
*BOUNDARY
100,2,,-4.002E-4
*END STEP
*STEP,NLGEOM,INC=100
*STATIC,PTOL=.050
1.0,1.0,0.001
*BOUNDARY
100,2,,-5.002E-4
*END STEP
*STEP,NLGEOM,INC=100
*STATIC,PTOL=.050
1.0,1.0,0.001
*BOUNDARY
100,2,,-6.002E-4
*END STEP
*STEP,NLGEOM,INC=100
*STATIC,PTOL=.050
0.25,1.0,0.001
*BOUNDARY
100,2,,-7.002E-4
*END STEP
*STEP,NLGEOM,INC=100
*STATIC,PTOL=.050
0.25,1.0,0.0001
*BOUNDARY
100,2,,-8.002E-4
*END STEP
*STEP,NLGEOM,INC=100
*STATIC,PTOL=.050
1.0,1.0,0.001
*BOUNDARY
100,2,,-9.002E-4
*END STEP
*STEP,NLGEOM,INC=100
*STATIC,PTOL=.050
1.0,1.0,0.001
*BOUNDARY
100,2,,-10.002E-4
*END STEP
*STEP,NLGEOM,INC=100
*STATIC,PTOL=.050
1.0,1.0,0.001
*BOUNDARY
100,2,,-11.002E-4
*END STEP
*STEP,NLGEOM,INC=100
*STATIC,PTOL=.050
1.0,1.0,0.001
*BOUNDARY
```

```
100,2,,-12.002E-4
*END STEP
```

# APPENDIX C

## ELEMENT MESH DATA
## USED IN THIS THESIS

This appendix provides element/nodal numbering informations. Figures C.1 through C.3 present the fine element mesh and Figures C.4 through C.8 show the ultra-fine element mesh.

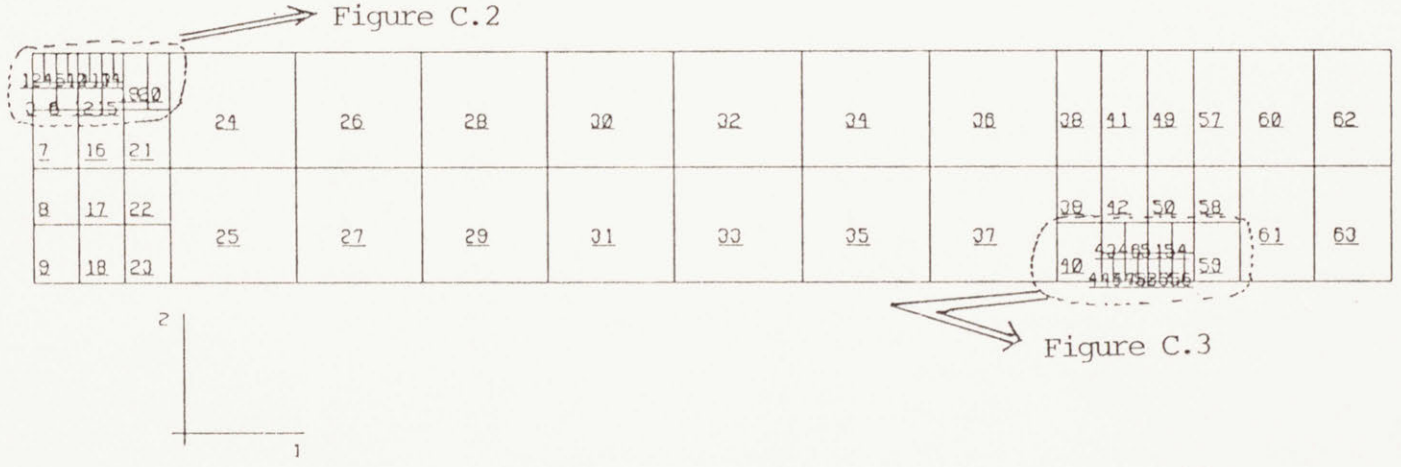


Figure C.1 Fine mesh element numbering

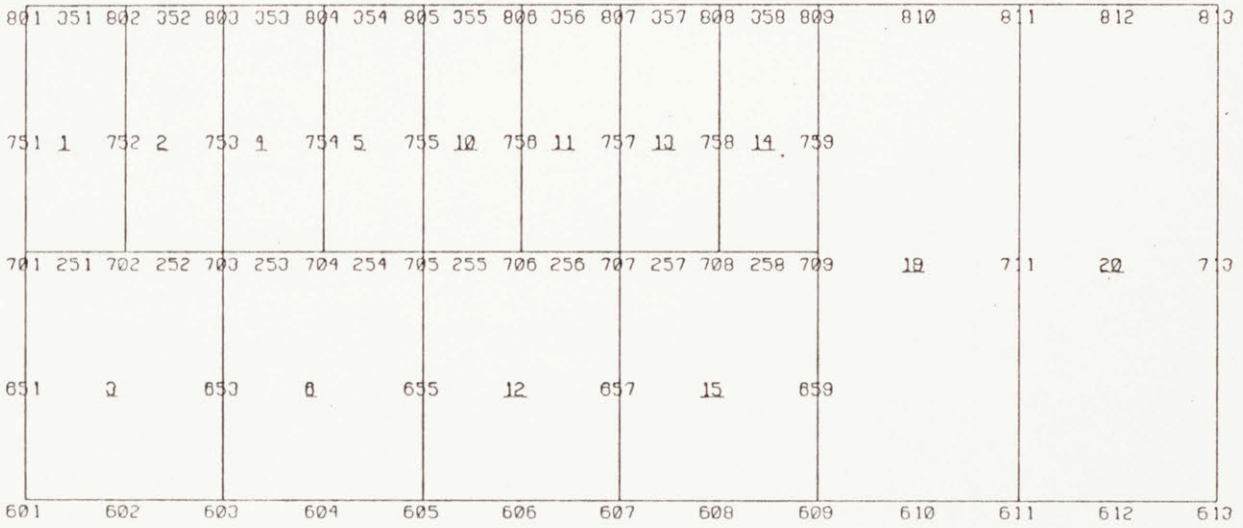


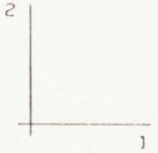


DETAILED ELEMENT MESH PLOT OF FINE MESH

Figure C.2 Detailed nodal/element numbering of the fine mesh

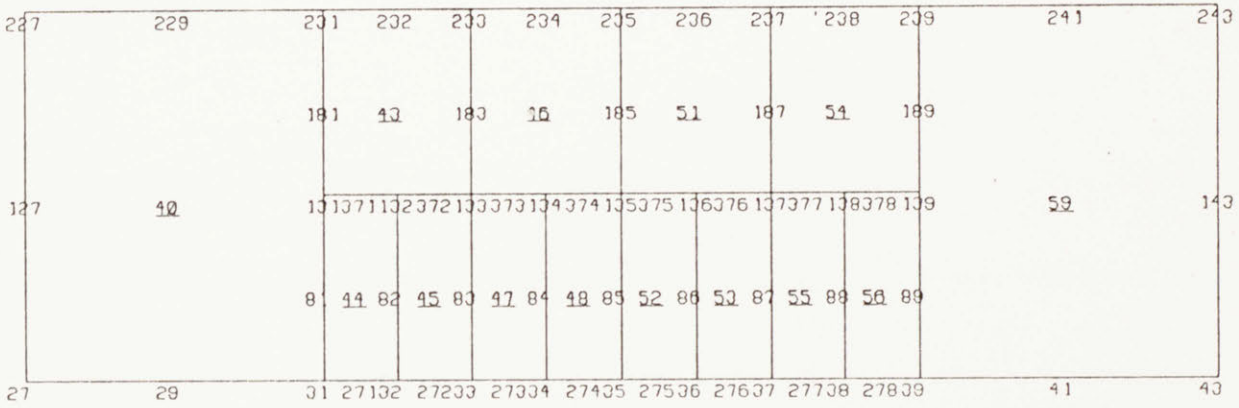



DETAILED ELEMENT MESH PLOT OF FINE MESH

Figure C.3 Detailed nodal/element numbering of the fine mesh, support contacting portion

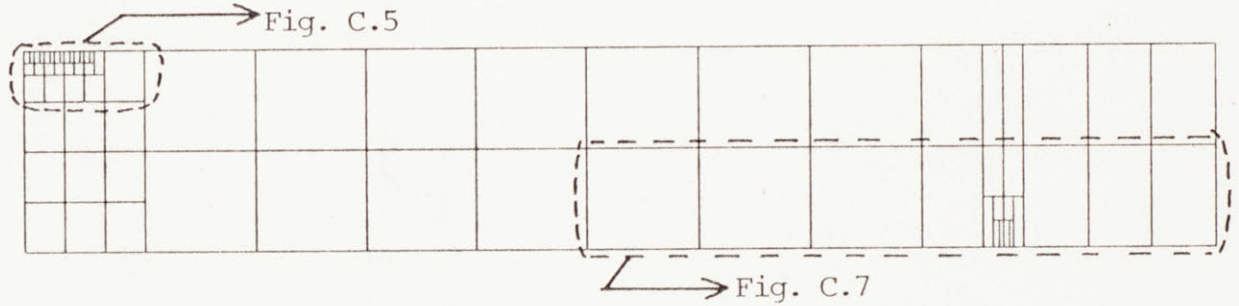



ELEMENT MESH PLOT OF ULTRA FINE MESH

Figure C.4 Ultra-fine element mesh (70 elements)

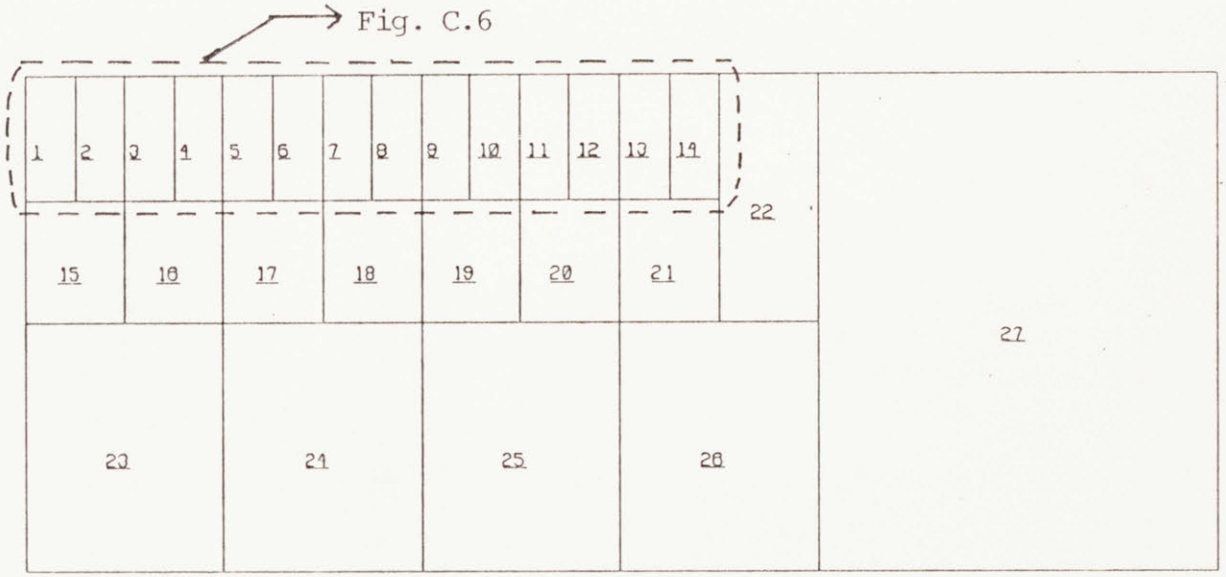


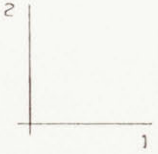


DETAILED ELEMENT MESH PLOT OF ULTRA FINE MESH

Figure C.5 Detailed element numbering of the ultra-fine mesh, punch contacting region


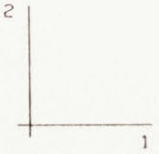


DETAILED ELEMENT MESH PLOT OF ULTRA FINE MESH

Figure C.6 Detailed nodal/element numbering of the ultra-fine mesh, punch contacting region

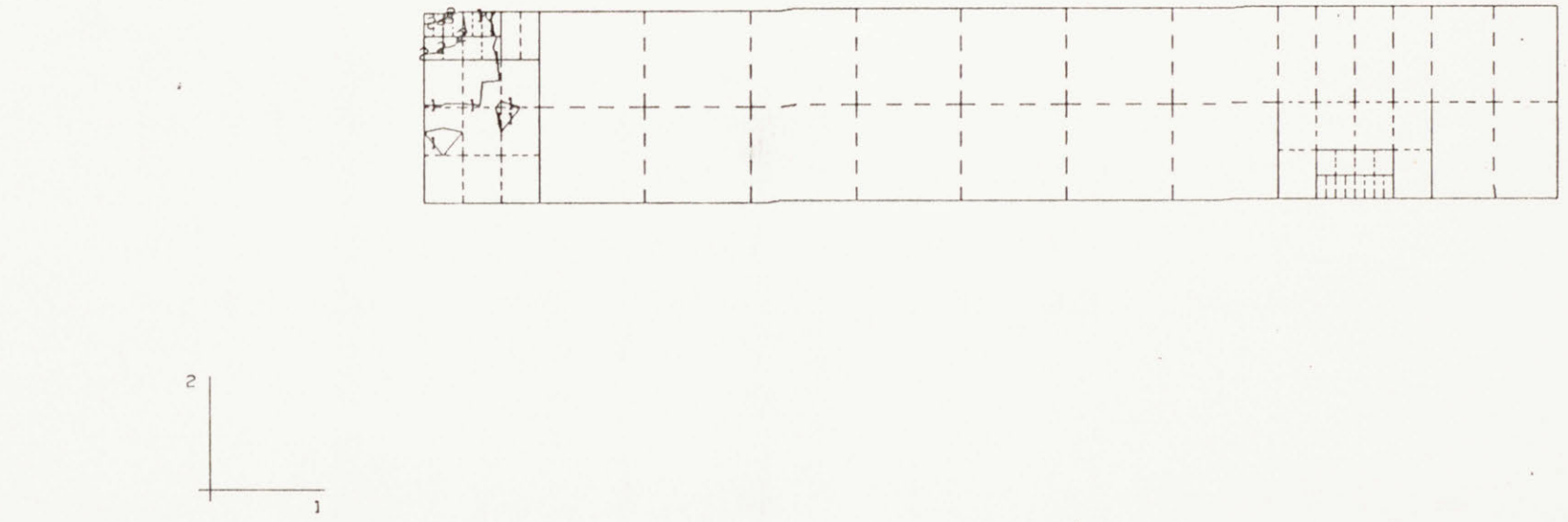


Figure D.11 Equivalent total plastic strain contours for punch displacement of 0.0076 mm

DISPL.
MAG. FACTOR = +1.0E+00
SOLID LINES - DISPLACED MESH
DASHED LINES - ORIGINAL MESH

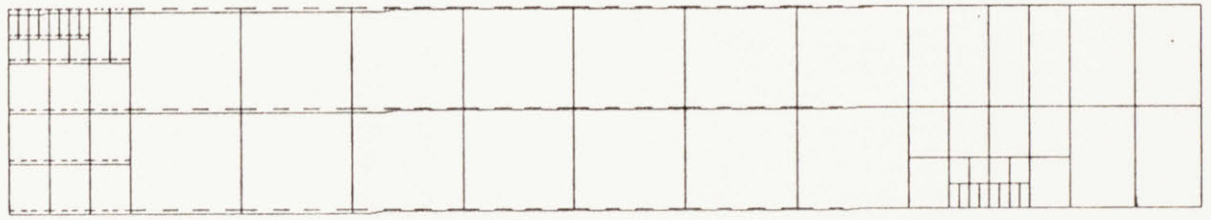


DEFORMED CONFIGURATION, CU-NI-5 (DSS9)

STEP 13 INCREMENT 9

Figure D.12 Deformed configuration for punch displacement of 0.0076 mm

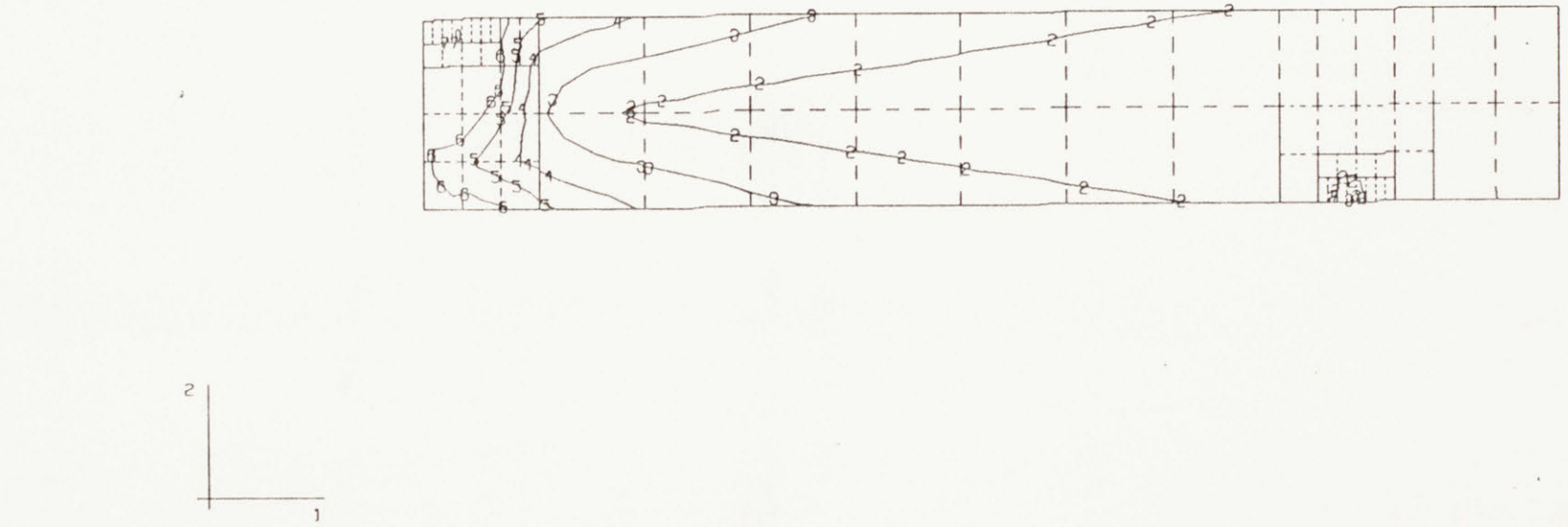


Figure D.13 Mises equivalent stress contours for punch displacement of 0.0102 mm

EQUIV. PLASTIC STRAIN
I.D. VALUE
1 +1.00E-10
2 +2.50E-02
3 +5.00E-02
4 +7.50E-02
5 +1.00E-01
6 +1.25E-01
7 +1.50E-01
8 +1.75E-01
9 +2.00E-01
10 +2.25E-01
11 +2.50E-01

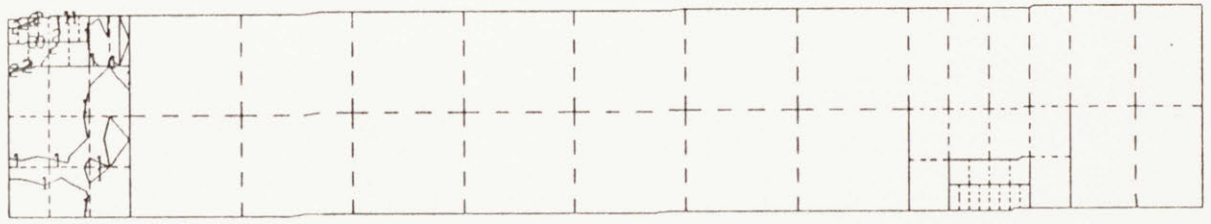


STRAIN CONTOURS, CU-NI-5 (DSS9)

STEP 15 INCREMENT 2

Figure D.14 Equivalent total plastic strain contours for punch displacement of 0.0102 mm

DISPL.
MAG. FACTOR = +1.0E+00
SOLID LINES - DISPLACED MESH
DASHED LINES - ORIGINAL MESH

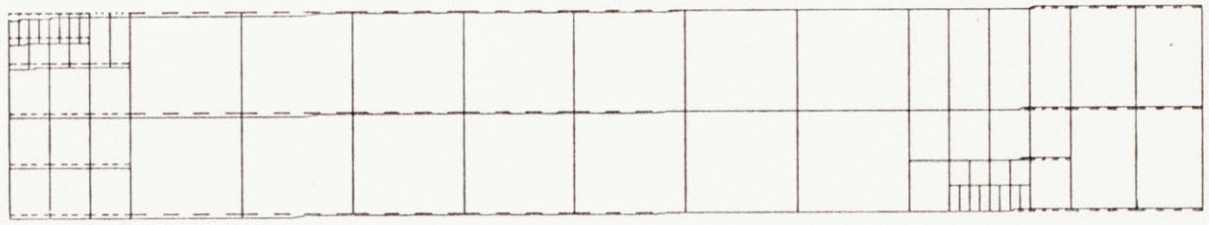


DEFORMED CONFIGURATION, CU-NI-5 (DSS9)

STEP 15 INCREMENT 2

Figure D.15 Deformed configuration for punch displacement of 0.0102 mm

MISES EQUIV. STRESS
I.D. VALUE
1 +1.00E-10
2 +1.42E+04
3 +2.84E+04
4 +4.26E+04
5 +5.68E+04
6 +7.10E+04
7 +8.52E+04
8 +9.94E+04
9 +1.13E+05
10 +1.27E+05
11 +1.42E+05

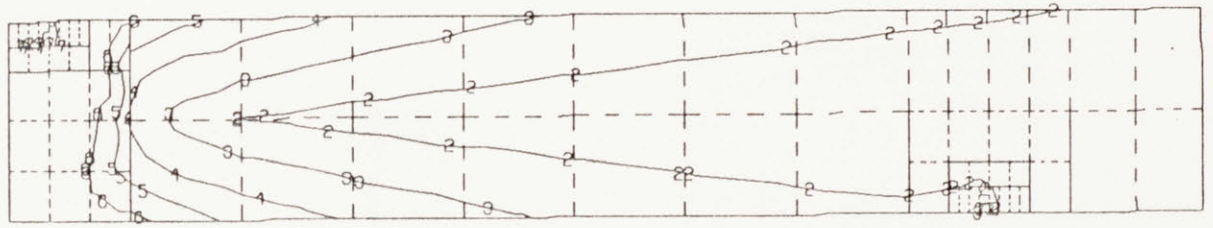

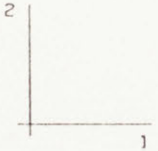


STRESS CONTOURS, CU-NI-5 (DSS9)

STEP 16 INCREMENT 15

Figure D.16 Mises equivalent stress contours for punch displacement of 0.0127 mm

EQUIV. PLASTIC STRAIN
I.D. VALUE
1 +1.00E-10
2 +2.50E-02
3 +5.00E-02
4 +7.50E-02
5 +1.00E-01
6 +1.25E-01
7 +1.50E-01
8 +1.75E-01
9 +2.00E-01
10 +2.25E-01
11 +2.50E-01

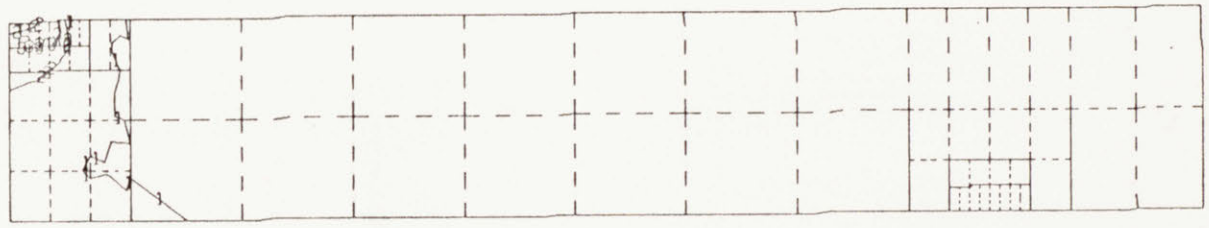


STRAIN CONTOURS, CU-NI-5 (DSS9)

STEP 18 INCREMENT 15

Figure D.17 Equivalent total plastic strain contours for punch displacement of 0.0127 mm

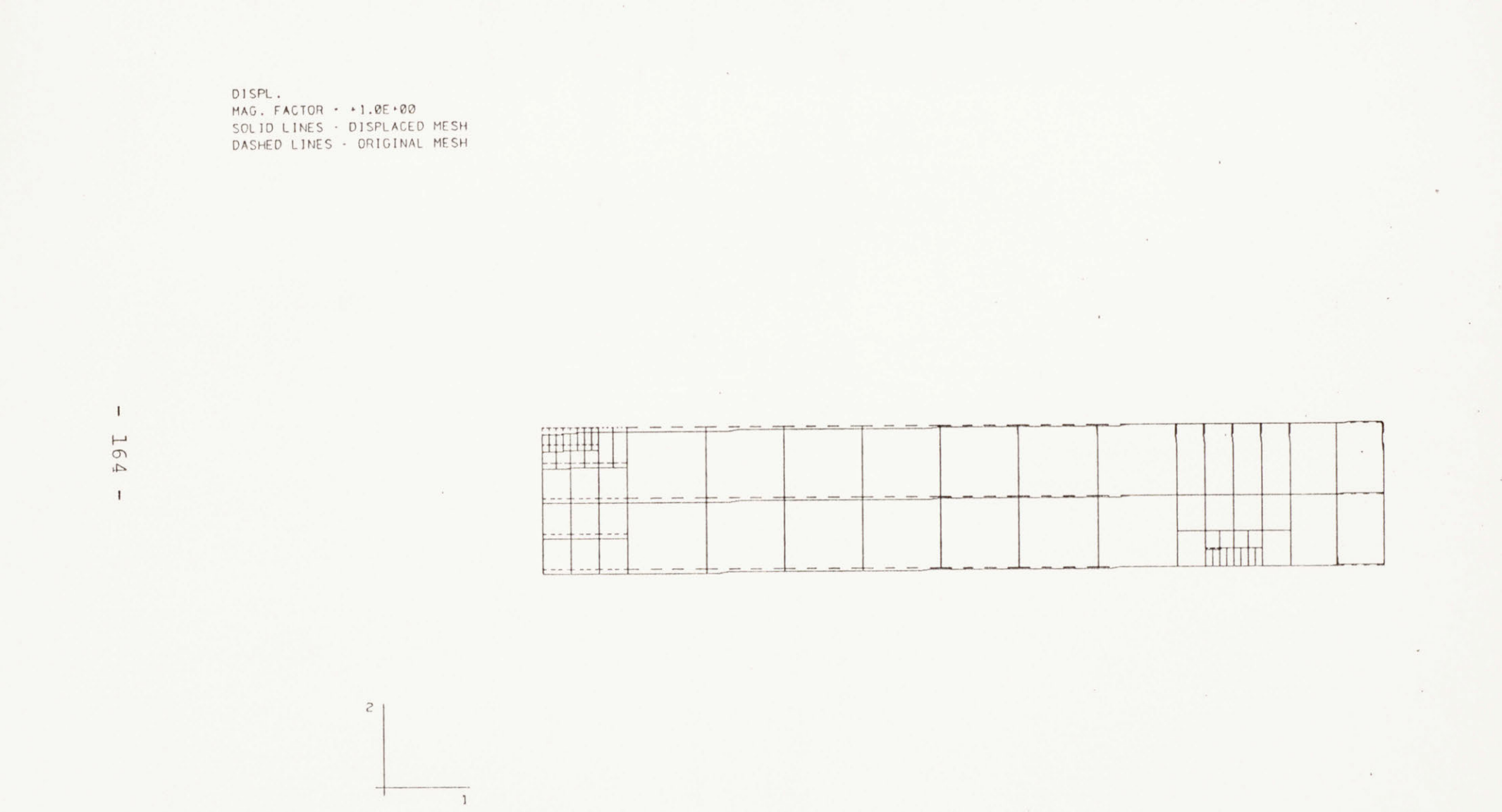


Figure D.18 Deformed configuration for punch displacement of 0.0127 mm

MISES EQUIV. STRESS
I.D. VALUE
1 +1.00E-10
2 +1.42E+09
3 +2.84E+09
4 +4.26E+09
5 +5.68E+09
6 +7.10E+09
7 +8.52E+09
8 +9.94E+09
9 +1.13E+05
10 +1.27E+05
11 +1.42E+05

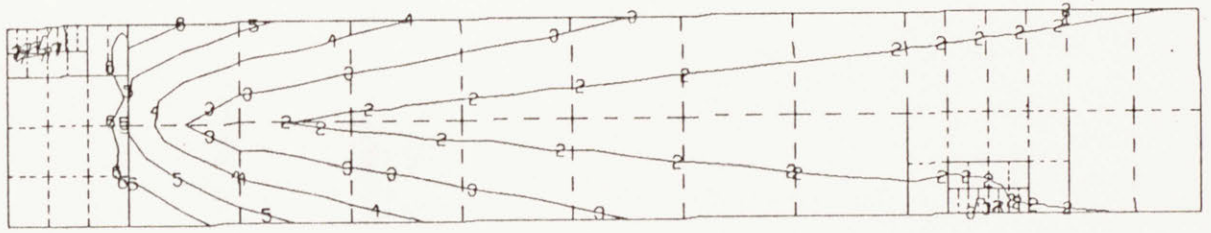

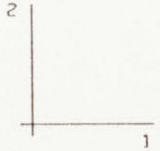


STRESS CONTOURS, CU-NI-5 (DSS9)

STEP 17 INCREMENT 9

Figure D.19 Mises equivalent stress contours for punch displacement of 0.0152 mm

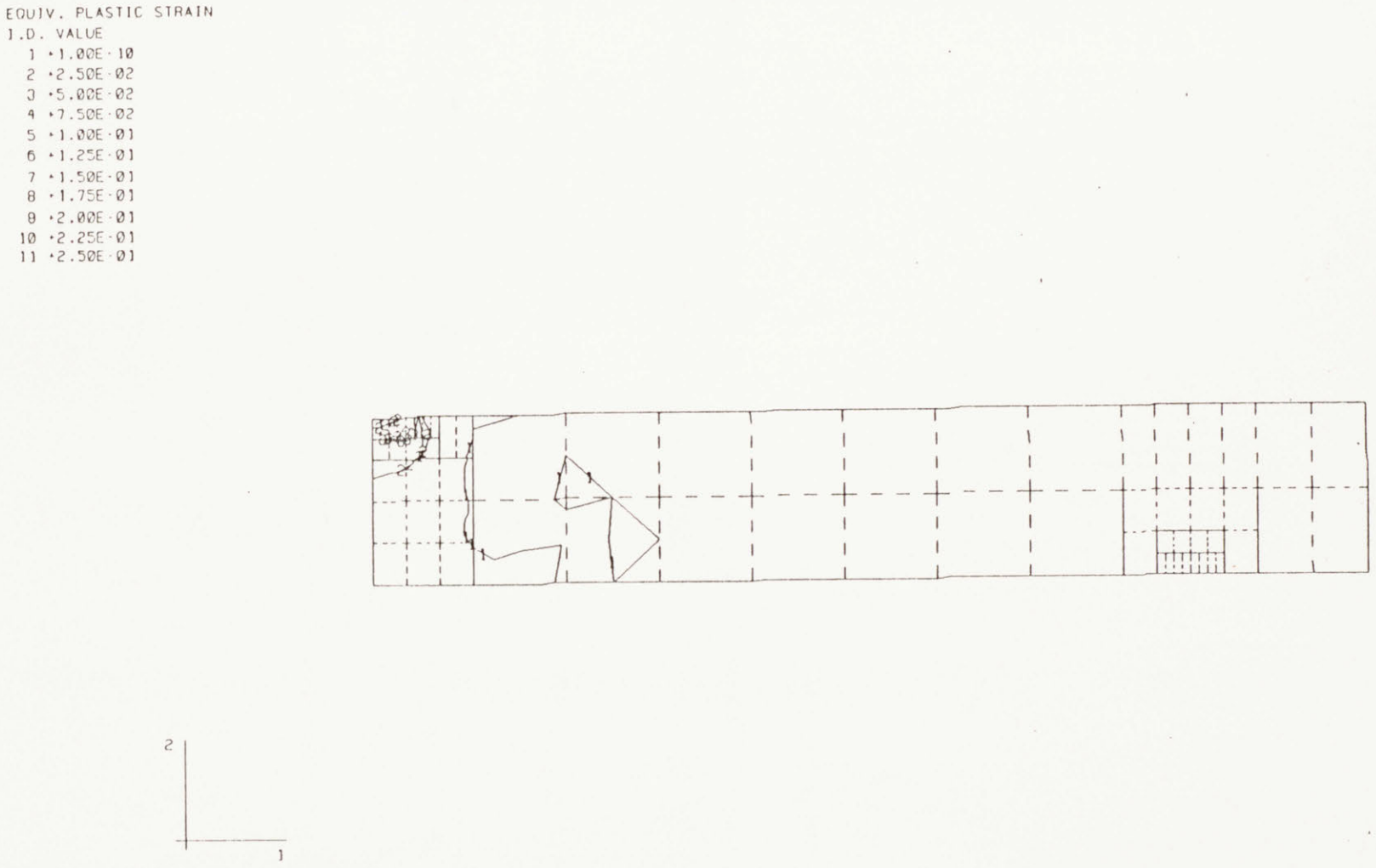


Figure D.20 Equivalent total plastic strain contours for punch displacement of 0,0152 mm

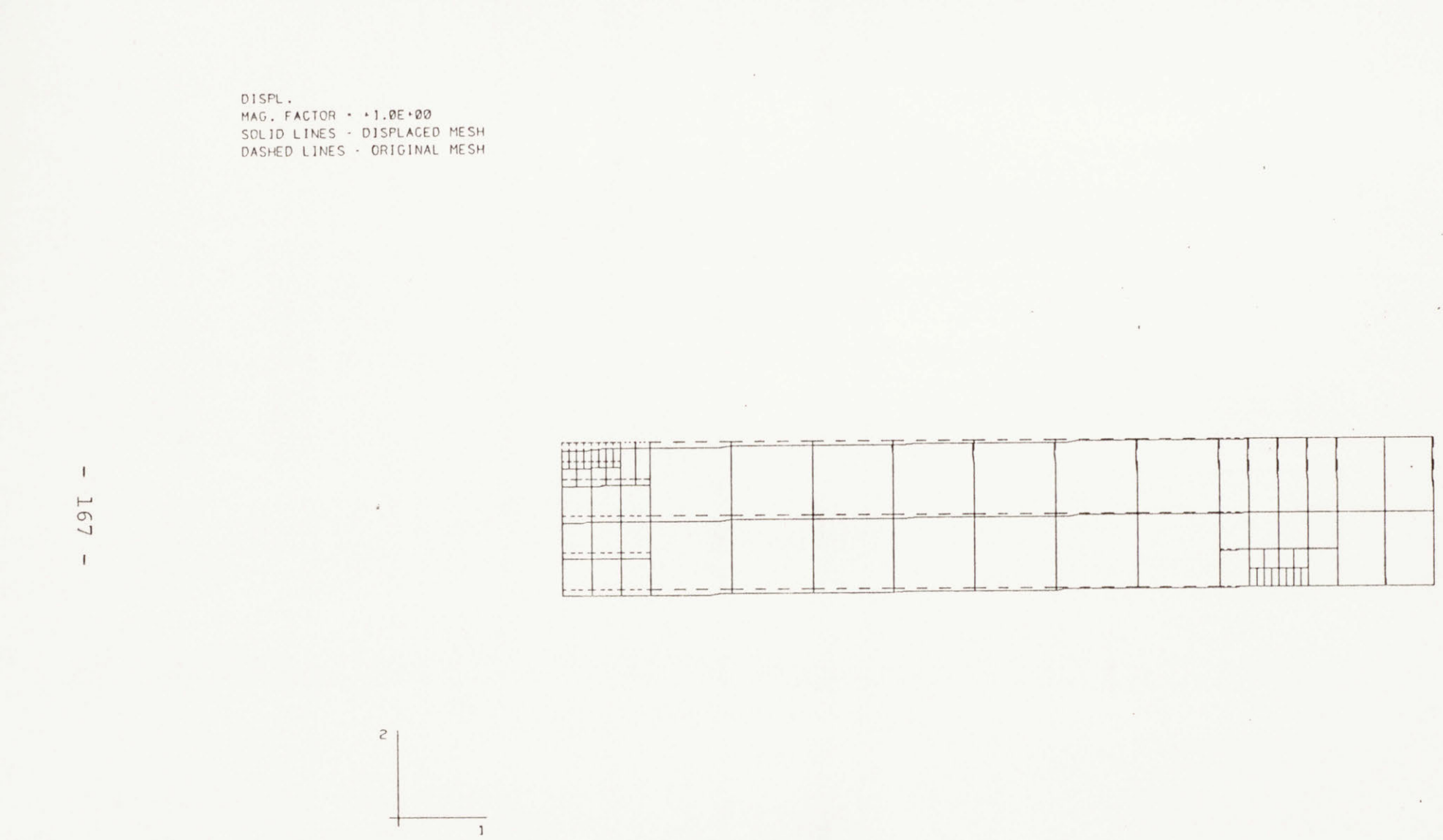


Figure D.21 Deformed configuration for punch displacement of 0.0152 mm

MISES EQUIV. STRESS
I.D. VALUE
1 +1.00E-10
2 +1.42E+04
3 +2.84E+04
4 +4.26E+04
5 +5.68E+04
6 +7.10E+04
7 +8.52E+04
8 +9.94E+04
9 +1.13E+05
10 +1.27E+05
11 +1.42E+05

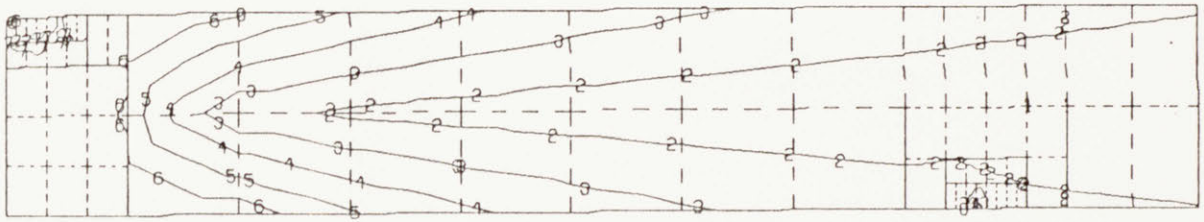


STRESS CONTOURS, CU-NI-5 (DSS9)

STEP 19 INCREMENT 7

Figure D.22 Mises equivalent stress contours for punch displacement of 0.0178 mm

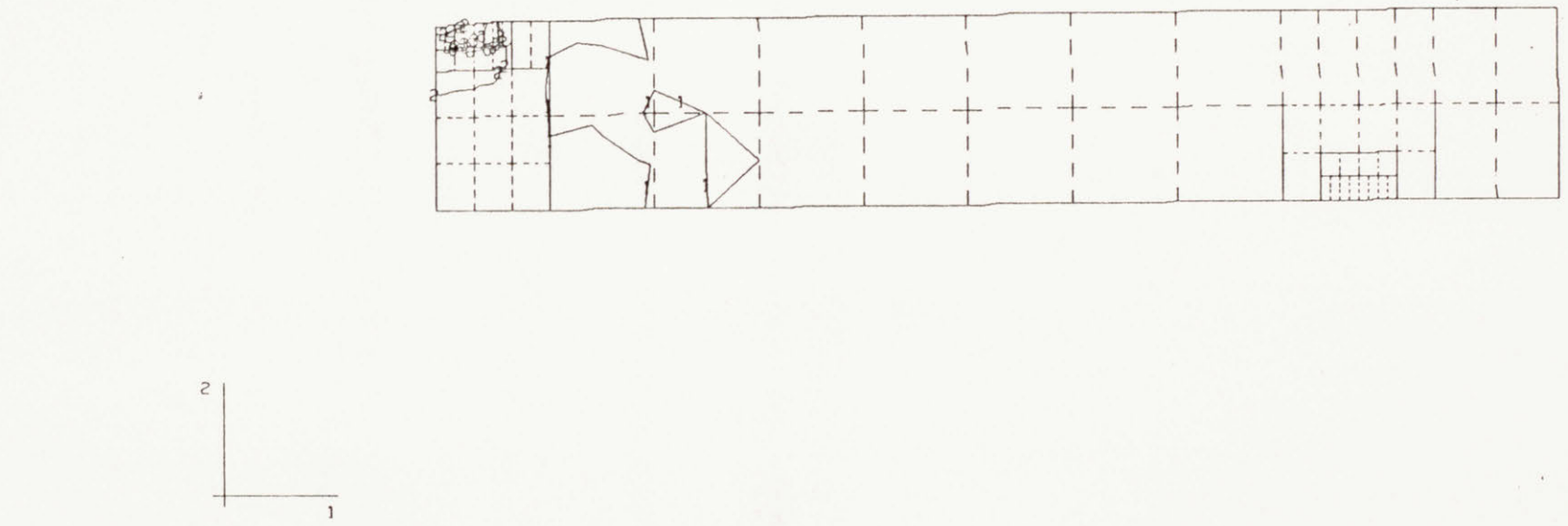


Figure D.23 Equivalent total plastic strain contours for punch displacement of 0.0178 mm

DISPL.
MAG. FACTOR = +1.0E+00
SOLID LINES - DISPLACED MESH
DASHED LINES - ORIGINAL MESH

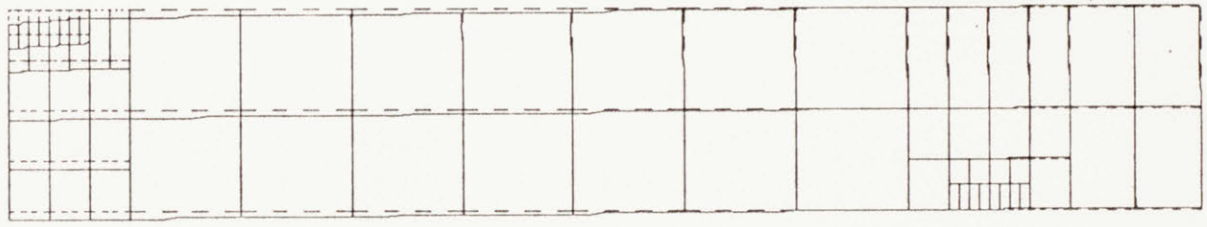


DEFORMED CONFIGURATION, CU-NI-5 (DSS9)

STEP 19 INCREMENT 7

Figure D.24 Deformed configuration for punch displacement of 0.0178 mm

MISES EQUIV. STRESS
I.D. VALUE
1 +1.00E-10
2 +1.42E+04
3 +2.84E+04
4 +4.26E+04
5 +5.68E+04
6 +7.10E+04
7 +8.52E+04
8 +9.94E+04
9 +1.13E+05
10 +1.27E+05
11 +1.42E+03

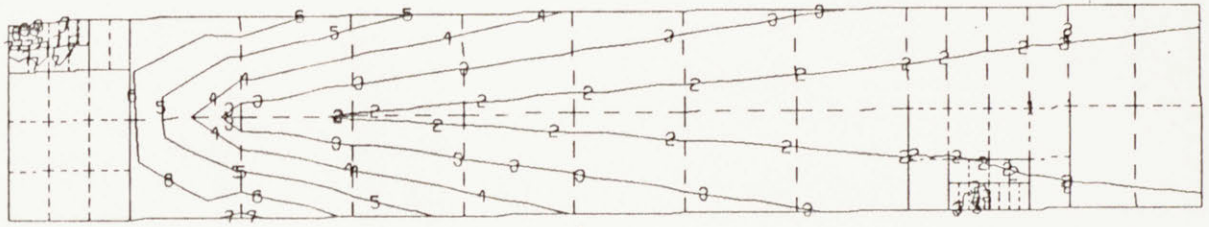


STRESS CONTOURS, CU-NI-5 (DSS9)

STEP 21 INCREMENT 4

Figure D.25 Mises equivalent stress contours for punch displacement of 0.0203 mm

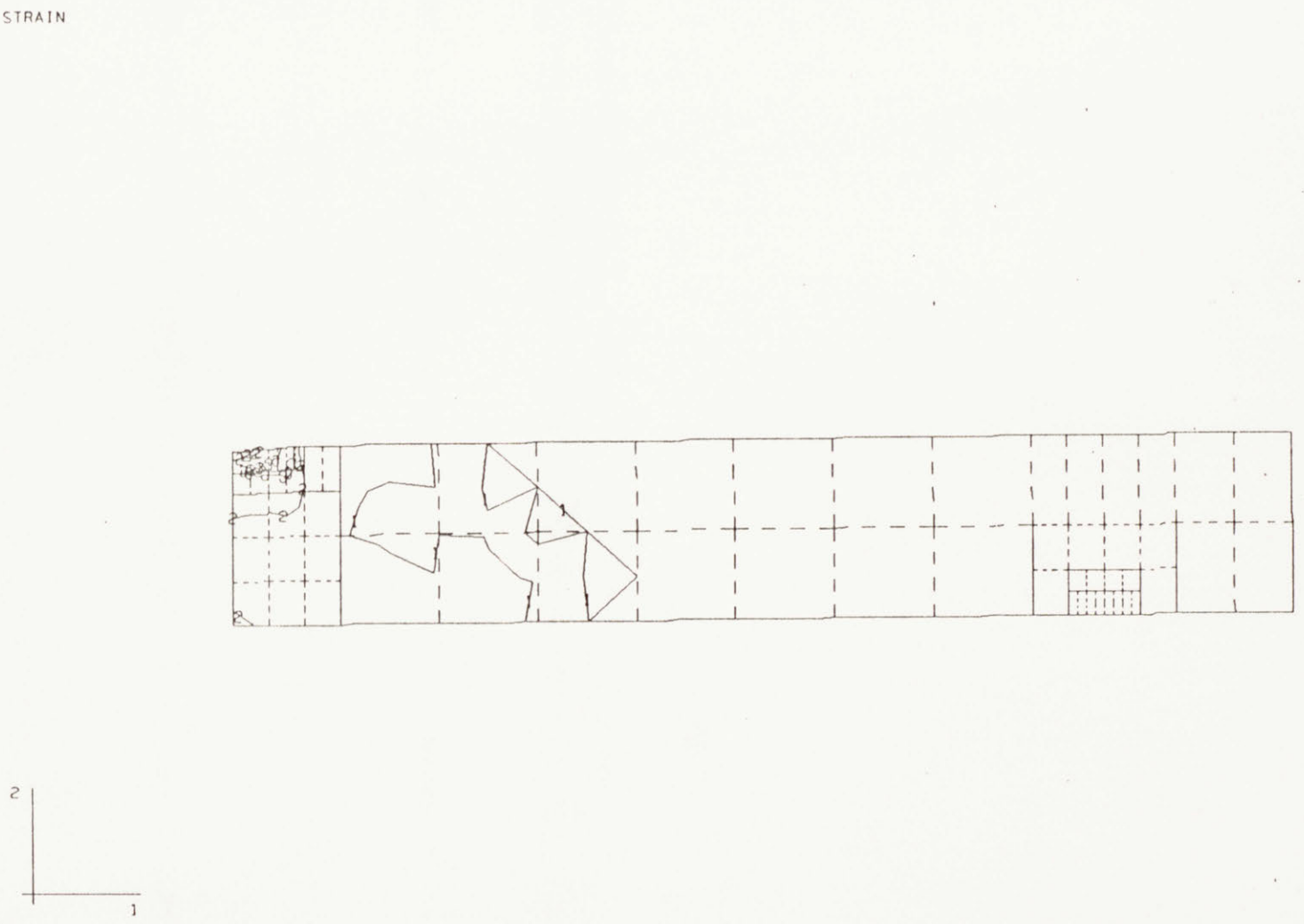


Figure D.26 Equivalent total plastic strain contour for punch displacement of 0.0203 mm


Figure D.27 Deformed configuration for punch displacement of 0.0203 mm